

LONG TERM IMPACT OF BIOMINERALIZATION IN ARSENIC FATE UNDER SIMULATED
LANDFILL CONDITIONS

BY

Sahar Fathordoobadi

A Dissertation Submitted to the Faculty of the
DEPARTMENT OF CHEMICAL AND ENVIRONMENTAL ENGINEERING

In Partial Fulfillment of the Requirements
For the Degree of

DOCTOR OF PHILOSOPHY
WITH A MAJOR IN ENVIRONMENTAL ENGINEERING

In the Graduate College
THE UNIVERSITY OF ARIZONA

2014

THE UNIVERSITY OF ARIZONA
GRADUATE COLLEGE

As members of the Dissertation Committee, we certify that we have read the dissertation prepared by Sahar Fathordoobadi entitled LONG TERM IMPACT OF BIOMINERALIZATION IN ARSENIC FATE UNDER SIMULATED LANDFILL CONDITIONS and recommend that it be accepted as fulfilling the dissertation requirement for the Degree of Doctor of Philosophy.

Wendell P. Ela

Date: 4th August 2014

A. Eduardo Saez

Date: 4th August 2014

Robert G. Arnold

Date: 4th August 2014

Jonathan D. Chorover

Date: 4th August 2014

Final approval and acceptance of this dissertation is contingent upon the candidate's submission of the final copies of the dissertation to the Graduate College.

I hereby certify that I have read this dissertation prepared under my direction and recommend that it be accepted as fulfilling the dissertation requirement.

Dissertation Director: Wendell P. Ela

Date: 4th August 2014

STATEMENT BY AUTHOR

This dissertation has been submitted in partial fulfillment of requirements for an advanced degree at the University of Arizona and is deposited in the University Library to be made available to borrowers under rules of the Library.

Brief quotations from this dissertation are allowable without special permission, provided that accurate acknowledgement of source is made. Requests for permission for extended quotation from or reproduction of this manuscript in whole or in part may be granted by the head of the major department or the Dean of the Graduate College when in his or her judgment the proposed use of the material is in the interests of scholarship. In all other instances, however, permission must be obtained from the author.

Signed: Sahar Fathordoobadi

ACKNOWLEDGEMENTS

The writing of this dissertation has been one of the most significant academic challenges I have ever had to face which would have not been possible without the help, support and encouragement of so many people in many ways.

First of all I wish to express my sincere and deepest gratitude to my amazing advisors, Drs. Wendell Ela and Eduardo Sáez for their guidance, patience, encouragement, and providing me with an excellent atmosphere for doing research and above all believing in me. Such a great privilege to have the chance to work and learn under their mentorship. I admire them as Scientists/Engineers and individuals and will remain in their dept for the rest of my life.

This dissertation would not have been possible without the aid, support and guidance of each of my professors and staff at the Department of Chemical and Environmental Engineering specially Christopher Olivares who has contributed a lot to keep my experiments running, Dr. Fernando Alday with all his guidance and training on this project, and Dr. Madhumitha Raghav for always being there for me. I would like to acknowledge Patricia Gonzales for her contribution in chapter 2 of this work. Also, many thanks to my Minor advisor, Dr. Jonathan Chorover and to Dr. Rot Root from the Department of Soil, Water and Environmental Science for all their guidance and collaboration with this project and performance of Micro-focused XRF mapping and XAS analyses in the Stanford Synchrotron Radiation Lightsource (SSRL) in Menlo Park, CA.

I would like to express my deepest thanks to my parents Parvin and Saeed for their presence and encouragement during all this time. Lots of love and thanks to my dearest sister Sanaz for always being there for me and believing in me. I adore you.

To my invaluable network of supportive, patient, forgiving, generous and loving friends, without whom I could not have survived the process and whom provided me unflinching encouragement in various ways, including: Sahra, Mohammad, Maziar, Sara, Andrea, Umur, Vicky, Lucia, Erin, Anita, Shahrzad, Baran, all my lovely friends here in Tucson who filled my life with so much love, motivation, and energy. I love you all so much.

I would like to acknowledge the financial support for this research project from the National Institute of Environmental Health Sciences (NIEHS) supported Superfund Research Program (Grant 2 P42 ES04940-11).

DEDICATION

To my extraordinary grandfathers: Rahim Fathordoobadi, who I dearly miss his present in my life and Karim Fathordoobadi, who put the fundament of my learning character and to my beloved uncle, Manoochehr Taleshi, who left fingerprint of grace on my life.

TABLE OF CONTENTS

LIST OF FIGURES	10
LIST OF TABLES	14
ABSTRACT.....	16
CHAPTER 1- INTRODUCTION AND OVERVIEW	18
1. Background	18
<i>1.1. Iron/Arsenic Fate in Anaerobic Environment.....</i>	<i>22</i>
<i>1.2. Biomineralization in Landfill.....</i>	<i>29</i>
2. Objectives	31
3. Dissertation Overview	34
CHAPTER 2 - FERROUS BIOMINERAL FORMATION AND ITS AFFINITY FOR ARSENIC SEQUESTRATION UNDER SIMULATED LANDFILL CONDITIONS...	37
1. Introduction.....	37
2. Materials and Methods.....	42
2.1. <i>Column Experiments</i>	<i>42</i>
2.1.2. Column Characteristics	44
2.1.3. Solid Phase Characterization	47
2.2. <i>Batch Adsorption/Co-precipitation Experiments.....</i>	<i>47</i>
2.2.1. Arsenic Stock Solutions.....	48
2.2.2. Vivianite Synthesis	48
2.2.3. Siderite Synthesis.....	49
2.2.4. Batch Vivianite Adsorption	49
2.2.5. Batch Siderite Adsorption.....	50
2.2.6. Vivianite Co-precipitation	50
2.2.7. Siderite Co-precipitation.....	52
3. Results and Discussions.....	53
3.1. <i>Column Study</i>	<i>53</i>
3.2. <i>Batch Adsorption/Co-precipitation Study.....</i>	<i>60</i>
3.2.1 Effect of Contact Time on Siderite Adsorption	61
3.2.2. Effect of Contact Time on Siderite Co-precipitation.....	62
3.2.3. Siderite Adsorption Isotherm.....	63
3.2.4. Siderite Co-precipitation Isotherm.....	65
3.2.5. Synthesized Vivianite Characterization.....	67
3.2.6. Vivianite Sorption/Co-precipitation Isotherms.....	68
4. Conclusions.....	72

TABLE OF CONTENTS-Continued

CHAPTER 3 - BIOMINERALIZATION CONTROLS ARSENIC MOBILITY IN MATURE LANDFILL CONDITIONS.....	75
1.Introduction.....	75
2. Materials and Methods.....	80
2.1. <i>Sludge Preparation</i>	80
2.2. <i>AFH Characteristics</i>	81
2.3. <i>Solid Phase Characterization</i>	83
3. Results and Discussion	85
3.1. <i>Arsenic and Iron Leaching Trends</i>	85
3.2. <i>Mobilized As Concentration</i>	86
3.3. <i>Fe/As Leaching Stoichiometry</i>	88
3.4. <i>Secondary Mineral AsSorption</i>	91
CHAPTER 4 - MICROSCALE SPECIATION OF ARSENIC AND IRON IN FERRIC-BASED SORBENTS SUBJECTED TO SIMULATED LANDFILL CONDITIONS ...	99
1. Introduction.....	100
2. Materials and Methods.....	103
2.1. <i>Column Design</i>	103
2.2. <i>X-ray Spectroscopy</i>	104
2.3 <i>XRF Imaging Collection and Analysis</i>	105
3. Results.....	107
3.1. <i>Column leachate aqueous chemistry</i>	107
3.2. <i>As Speciation by Bulk XAS</i>	108
3.3. <i>Fe Speciation by bulk XAS</i>	111
3.4. <i>X-ray Fluorescence</i>	114
3.4.1. <i>Low Sulfate Column</i>	114
3.4.2. <i>High Sulfate Column</i>	114
4. Discussion.....	116
4.1. <i>As and Fe Speciation in Low Sulfate Column</i>	117
4.2. <i>Arsenic and Iron Speciation at High Sulfate Activity</i>	118
4.3. <i>Fe-S-As Reactions in Sulfidic Environments</i>	120
CHAPTER 5 - HOW SULFUR REDOX CYCLE AND CONCENTRATION IMPACTS ABSRs FATE IN LANDFILLS	124
1. Introduction.....	124

TABLE OF CONTENTS-Continued

2.Objectives	128
3. Materials and methods	129
3.1. <i>Sludge preparation</i>	129
3.2. <i>Sludge Characteristics</i>	130
3.3. <i>Columns Experiments</i>	131
3.4. <i>Solid Phase Characterization</i>	132
4. Results and Discussions	133
4.1. <i>Arsenic and Iron Leaching Patterns</i>	133
4.2. <i>Sulfate Consumption Rate</i>	137
4.3. <i>Solid Phase Biomineralization</i>	139
4.4. <i>Electron Consumption Model</i>	144
4.5. <i>Possible Reaction Pathways and Mechanisms</i>	148
4.6. <i>Thermodynamic Favorability Diagram of Pertinent Reactions</i>	154
6. Conclusions.....	157
CHAPTER 6 - CONCLUSIONS AND FUTURE WORK	158
APPENDIX A - CHAPTER 2 SUPPLEMENTARY INFORMATION	164
APPENDIX B - CHAPTER 4 SUPPLEMENTARY INFORMATION	165
1. XAS data collection and processing	165
1.1. <i>Arsenic</i>	166
1.2. <i>Iron</i>	167
2. XRF data collection	167
3. Details of column experiment.....	168
APPENDIX C - TIME DEPENDENT ARSENIC RELEASE FROM ARSENIC BEARING SOLID RESIDUALS UNDER SIMULATED LANDFILL CONDITIONS	177
1. Introduction.....	177
2. Material and Methods	180
2.1. <i>Ferrihydrite Sludge Preparation</i>	180
2.2. <i>Column Characteristics</i>	182
2.3. <i>Solid Phase Characterization</i>	183
3. Results and Discussion	184
3.1. <i>Arsenic and Iron Leaching Trends</i>	184
3.2. <i>Incongruent Fe/As release Effect</i>	191

TABLE OF CONTENTS-*Continued*

3.3. <i>BiomineralTransformation/Characterization</i>	193
4. Conclusions.....	196
REFERENCES	198

LIST OF FIGURES

Figure 2.1. The primary routes of iron and sulfate reduction in landfills are microbially mediated and secondary mineral formation is a common by-product. Biomineralization plays a key role in determining whether or not desorbed As will be sequestered under landfill conditions. SRB: Sulfate reducing bacteria; B: Biomineral; A: Arsenic.	41
Figure 2.2. Experimental Set-up; Up-flow bench-scale column, packed with laboratory synthesized Fe/As sludge of 20:1 molar ratio mixed with glass beads and inoculated with anaerobic digester sludge obtained from Ina Road wastewater treatment plant. The feed contains lactate as the carbon source and primary electron donor (5.5 mM), and ferric iron and arsenate as primary electron acceptors.	46
Figure 2.3. Column effluent total arsenic and speciation shows As(V) being dominant during the first half of column life and As(III) being major species from 319 days to the end of column's life. Almost all of the initial arsenic mass (~100%) leached out of the column after 665 days.	54
Figure 2.4. Column effluent total iron concentrations. <1% of the iron initially loaded into both columns leached over the duration of the experiment.	55
Figure 2.5. Fe/As molar ratio in the effluent: As/Fe non-stoichiometric release was evident since the initial loading Fe/As molar ratio was 22:1.	56
Figure 2.6. Powder-XRD pattern of synthesized mineral and match to siderite pattern.	60
Figure 2.7. Effect of contact time on As concentration in the sorbent (qe) from As(V) and As(III) solutions by siderite. Conditions: Adsorbent dosage = 10 gL ⁻¹ , initial As concentration = 100 mgL ⁻¹ . For both As(V) and As(III), adsorption capacity increase over time for the first 2 weeks of the experiment after which it reached equilibrium to the termination of the experiment.	62
Figure 2.8. Effect of contact time on As co-precipitation from As(V) and As(III) solutions by siderite, with reaction conditions: solid produced = 80 gL ⁻¹ , initial As concentration = 100 mgL ⁻¹ . There was not a considerable removal difference in As(III) within duration of experiment, however, 30% removal decrease was observed in As (V) at the end which was still 20% higher than that of As(III).	63
Figure 2.9. Freundlich plots for As adsorption from As(V) and As(III) solutions on siderite, with reaction conditions: adsorbent dosage = 10 gL ⁻¹ ; initial concentrations = 0.2–100 mgL ⁻¹ ; contact time = 2 weeks	65
Figure 2.10. Freundlich plots for As co-precipitation from As(V) and As(III) solutions on siderite, with reaction conditions: Solid mass produced = 80 gL ⁻¹ ; initial concentrations = 0.2–3500 mgL ⁻¹ ; contact time = 24 h.	66
Figure 2.11. Powder-XRD pattern of synthesized mineral and match to vivianite pattern.	68
Figure 3.1. The primary routes of iron and sulfate reduction in landfills are microbially mediated and secondary mineral formation is a common by-product. Biomineralization plays a key role in determining whether or not desorbed As will be sequestered under landfill conditions.	78
Figure 3.2. Arsenic leaching from all columns followed the same asymmetric bell curve, including an approximately 60 day lag phase, a rapid increase to a effluent concentration greater than 200 mM, and a slow tapering decline.	88

Figure 3.3. The lower Fe:As molar ratio in the effluent than the initial ABSR Fe:As molar ratio of greater than 22:1 demonstrates decoupling of iron from arsenic leaching in all trials. In addition, the lag phase ratio was greater than 6 times more than the post-lag phase ratio for any given column..... 90

Figure 3.4. Final Fe (a) and As (b) mass distribution in LS and HS columns. More than 100% of the initial Fe mass present for the LS and HS cases relocated to the top two quadrants. Arsenic was retained mainly in the Q4 and Q3 of both LS and HS cases. 94

Figure 4.1. As K-edge XAS of AFH from the synthetic landfill column experiments; LS column (a) XANES (b)unfiltered k^3 weighted EXAFS, and (c) uncorrected for phase shift Fourier transformed EXAFS (FT); HS column in shaded panels d) XANES (e) EXAFS, and (f) FT. Collected experimental spectra (black) and model reference spectra (gray = As(V)=Fh, blue = As(III)-Fh, red = realgar) together with calculated best fits to the data (stippled red). The vertical lines in a) show reference AsS (red), As(III) (blue), and As(V) (gray); vertical lines and arrows in c and f) highlight the structural features corresponding to the calculated coordination and distance, shown with inset schematic, and explained in the text; numerical fit parameters are given in Table SI4. 110

Figure 4.2. Normalized first derivative Fe K-edge XANES collected at 8-15K for a) LS and b) HS. Fe K-edge c) EXAFS and d) uncorrected for phase shift Fourier transformed EXAFS (FT). Solid lines are data, stippled lines are best fits, shaded regions in d) are mackinawite FeS (black) and green rust GR₁CO₃ (green) with Fe-backscatterer pair labeled; all numerical fit parameters are given Table 4.1 112

Figure 4.3. Multiple energy μ -XRF maps for the low sulfate (LS: a-d) column experiments after 300 days of bioreduction in inoculated synthetic landfill leachate, and high sulfate (HS: e-h) after 331 days of bioreduction in inoculated synthetic landfill leachate. The top panels show total Fe (a) and As (b) intensity for LS according to the color-scale shown, c.) ternary Fe speciation for LS, ferrihydrite shown in red, carbonate green rust (GR₁CO₃) in green, and siderite in blue, and d.) binary distribution of As species for LS with As(III) in red and As(V) in blue, with color intensity corresponding to concentration. The bottom panels show total Fe (e) and As (f) for HS columns, g.) ternary Fe speciation for LS, with FeS shown in red, GR₁CO₃ in green, and siderite in blue, and h.) binary As speciation with As sulfide and As(III) in blue. The white dashed lines delineate the edges of glass beads, and color intensity corresponds to the molar concentration of each chemical species per volume in each pixel, mapped at $3\mu\text{m}^2$ and $2.5\mu\text{m}^2$ for LS and HS respectively. 116

Figure 5.1. Medium sulfate column (MS) arsenic speciation with As(V) being dominant during the course of the experiment. 35% of the initial arsenic mass leached out of the reactor after 331 days..... 135

Figure 5.2. High sulfate Column (HS) arsenic speciation with As(III) being dominant during the course of the experiment. 45% of the initial arsenic mass leached out of the reactor after 551 days..... 136

Figure 5.3. Arsenic leaching trend in both simulated landfill columns follows same pattern with different total As mass released; 35% fromMSand 45% fromHS column. 136

Figure 5.4. Cumulative arsenic leaching trend in medium sulfate column A and high sulfate column B. After 331 days 35% of the loaded As leached out of MS column compare to 22.85% of total As that was released from HS reactor after the same period of time.	137
Figure 5.5. Sulfate consumption pattern in MS column. Within the first month of operation almost 50% of the input sulfate was consumed after which effluent sulfate concentration reduced to less than 10% of its influent concentration to the end of the run.	138
Figure 5.6. Sulfate consumption pattern in HS column. Within the first month of operation almost 25% of the input sulfate was consumed after which effluent sulfate concentration kept increasing back to about 75% of its influent concentration to the end of the run.	138
Figure 5.7. XRD patterns for biominerals formed in MS column. The XRD patterns compared to the database show FeS and siderite as the main species in the bottom and top sections of the column, respectively. Goethite was also detected but with weaker peaks than the reduced Fe minerals	141
Figure 5.8. First derivative As XANES spectra for standard reference species compared to spectra for experimental samples collected from MS column at the completion of the 331 day advective flow experiment. The vertical dashed lines highlight the first-derivative peak energy of arsenite reference species. Mineral fit to samples from bottom and the top two sections confirm presence of As(III) as the only arsenic speciation in the solid phase.	142
Figure 5.9. Normalized and First derivative Fe XANES spectra for standard reference species compared to spectra for experimental samples collected from MS column at the completion of the 331 day advective flow experiment. Mineral fit to samples from bottom and the top two sections confirm presence of ferrous solid phase as the main Fe oxidation state in the MS column.	143
Figure 5.10. Electron consumption model for MS column. At sulfate concentration of 2.08 mM, lactate (5.5mM) provide sufficient reducing power to reduce sulfate, iron, and arsenic completely in the column in a period of less than a month.	147
Figure 5.11. Electron consumption model for HS column. At sulfate concentration of 20.8 mM, lactate (5.5mM) is only able of partial reduction of sulfate and iron close to inlet. Reduced sulfur move up in the direction of flow where only oxidized state of iron and arsenic exist.	148
Figure 5.12. Influent sulfate concentration dictates possible biotic/abiotic reactions and pathways occurring in MS and HS reactors, resulting in diverse mineral phases and different arsenic speciation between the two columns.	154
Figure 5.13. Standard state Gibbs free energy for pertinent reactions using lactate as organic electron donor. Adopted from Kocar et al, 2009.	156
Figure 5.14. Thermodynamic favorability of pertinent redox reactions in a simulated landfill column. ΔG_{rxn} are calculated using concentration measured in the effluent of our columns.	156

Figure 1. As(V) and As(III) adsorption (plots a and b) as well as co-precipitation (plots c and d) isotherms. Adsorption experiments were run at arsenic concentration: 0.2-100 mgL ⁻¹ and co-precipitation experiments were run at arsenic concentration: 0.2-3500 mgL ⁻¹	164
Figure 2. Pixel by pixel comparison from Fig. 3d (LS) of arsenic species in XRF image, showing intensity counts for AsIII and AsV.....	175
Figure 3. Light microscope micrographs of a) LS under backlit- transmitted light, and b) HS under reflected light with the mapped area by XRF indicated with the dashed box. The images show the reacted AFH solids in the space between glass beads with relatively more solids in the LS v HS column.	176
Figure 1. .Effluent arsenic concentration profile at phase I, II, and III in LS set. Total arsenic leached at each phase is 1.45%, 3.48%, and 45.78% after 93,226, and 476 days, respectively.	185
Figure 2. Effluent arsenic concentration profile at phase I, II, and III in MS set. Total arsenic leached at each phase is 4.07%, 21.64%, and 49.81% after 93,219, and 300 days, respectively.	186
Figure 3. Effluent sulfide concentration profile from phase III of LS column (a), and MS column (b). After ~ 200 days of operation, with effluent sulfide concentration of < 2 □M in both columns, out flowing sulfide from MS column increases to concentration 6x higher than the value measured in LS column effluent.	191
Figure 4. Evolution of incongruent Fe/As release is evident through three arsenic leaching regimes. As non-stoichiometric release from Fe starts in the transition from phase II to phase III.....	192
Figure 5. Evolution of incongruent Fe/As release is evident through three arsenic leaching regimes. Non-stoichiometric As release from Fe starts in the transition from phase II to phase III.....	193

LIST OF TABLES

Table 2.1. Iron/Arsenic sludge characteristics	44
Table 2.2. Composition of synthetic landfill leachate solution used as column feed (adopted from Field et al., 2003)	45
Table 2.3. Specific surface area and As adsorption capacity of iron minerals.	59
Table 2.4. XRD analysis shows iron transformation into biominerals along the column. The XRD patterns compared to the database show vivianite and siderite as the main species.	59
Table 2.5. Siderite and vivianite capacity for arsenic adsorption obtained from literatures and our experimental results.	66
Table 2.6. Freundlich isotherm parameters describing the arsenic sorption capacity of siderite based on the data obtained in this study, where k_F represents the adsorption capacity of the adsorbent, and n_F represents the adsorption intensity parameter.	66
Table 2.7. Langmuir parameters describing the arsenic sorption capacity of vivianite, where α represents the sorption maxima, and β represents the sorption intensity.	70
Table 3.1. Designations, distinctive feed characteristics and durations of operation of simulated mature landfill columns used in study.	84
Table 3.2. Biominerals generated under LS and HS sulfate influent conditions.	92
Table 3.3. Specific surface areas and sorption capacities of iron minerals observed after trial termination.	95
Table 4.1. Arsenic and Iron K-edge XANES fit results.	113
Table 5.1. Thermodynamic favorability of methanogenesis and sulfate reduction from different substrates. Adopted from Alday, 2010.	127
Table 5.2. Iron/Arsenic sludge characteristics.	131
Table 5.3. Summary of column characteristics.	132
Table 5.4. Biomineral transformation under the influence of different sulfate concentration.	144
Table 1. Column Synthetic Landfill Leachate.	171
Table 2. Column Design Specifications.	172
Table 3. Matrix for Fe XRF from mapped energy (eV) and the measured fluorescence for each reference mineral. The matrix is used at each pixel to assign a mineral phase.	172
Table 4. Arsenic and Iron K-edge EXAFS fit results ^a	173
Table 1. Iron/Arsenic sludge characteristics.	182
Table 2. Total fraction of iron and arsenic leached out of LS and MS columns for all the 3 phases over time.	187
Table 3. Biomineral transformation over time under the influence of different sulfate concentration, detected by powder-XRD.	194

ABSTRACT

Lowering the Maximum Contaminant Level (MCL) for arsenic in drinking water in the U.S., has caused a significant increase in the volume of Arsenic Bearing Solid Residuals (ABSRs) generated by drinking water utilities. Most of the affected utilities are smaller water treatment facilities, especially in the arid Southwest, and are expected to use adsorption onto solid sorbents for arsenic removal. Because of their high adsorption capacity and low cost, iron sorbents are used treatment technology and, when the sorbent's capacity is spent, these ABSRs are disposed in municipal solid waste (MSW) landfills and as a consequence arsenic is likely being released into leachate. However, a mature landfill is a biotic, reducing environment, which causes arsenic reduction and mobilization from the ABSRs. It is well documented that iron and sulfur redox cycles largely control arsenic cycling and, because iron and sulfur are ubiquitous in MSW, it is suspected that they play key roles in arsenic disposition in the landfill microcosm. The purpose of this study is to investigate the degree to which sulfate can prevent arsenic from leaching into landfill through biomineralization and to study ABSRs biogeochemical weathering effect on arsenic sequestration. The primary routes of iron and sulfate reduction in landfills are microbially mediated and biomineralization is a common by-product. In this case, biomineralization is the transformation of ferric (hydr) oxides into ferrous iron phase and sulfate into sulfide minerals such as: siderite (FeCO_3), vivianite ($\text{Fe}_3(\text{PO}_4)_2$), iron sulfide (FeS), goethite ($\alpha\text{-FeOOH}$), and realgar (AsS). In this work, long-term microbial reduction and biomineralization of iron, sulfur, and arsenic species are evaluated as processes that both cause arsenic release from landfilled ABSRs and may possibly provide a means to re-sequester As in a recalcitrant solid state. The work uses long-term, continuous flow-through laboratory-scale columns in which controlled conditions similar to those found in a mature landfill prevail. In these simulated landfill column experiments, formation of biominerals, same as those that would naturally occur in typical non-hazardous MSW landfills, will be investigated. The feed contains lactate as the carbon source and primary electron donor, and ferric iron, arsenate, and a range of sulfate concentrations as primary electron acceptors. Our results suggest that biomineralization changes the stability of arsenic through a number of different processes including (i) release of arsenic through reductive dissolution of iron-based ABSRs; and (ii) readsorption/incorporation of released arsenic to secondary biominerals. The influence of biominerals,

which have less surface area and adsorption capacity than original AFH, on the retention of arsenic is also investigated in this study. Our results show that the concentration of sulfate fed to the system affects the biomineral formation, and that the relative amounts and sequence of precipitation of biominerals affect the free arsenic concentration that can seemingly be engineered by the concentration of sulfate fed to the system. Comparison between the columns with different sulfate concentrations indicate that inflow sulfate concentration higher than 2.08 mM decreases As mobilization to <50%.

Key words: Arsenic, Sulfate, Biomineralization, Arsenic-Bearing Solid Residuals (ABSRs), Amorphous Ferric Hydroxide, Vivianite, Siderite, Fe sulfide, and As sulfide.

CHAPTER 1

INTRODUCTION AND OVERVIEW

1. Background

Arsenic is a naturally occurring element widely found in the earth crust that is spontaneously released into drinking water sources, such as groundwater from natural sources, through the dissolution of minerals, and from anthropogenic sources, like pesticides, herbicides, and wood preservatives.

Several health effects are also related to arsenic exposure. Long term exposure to contaminated drinking water has been cited as the most widespread threat to human health posed by arsenic (Nordstrom 2002; Smedley and Kinniburgh 2002). Because of the awareness of the presence of arsenic in drinking water and its associated risks to people, the U.S. Environmental Protection Agency (US EPA) lowered the Maximum Contaminants Level (MCL) of arsenic in drinking water from 50 ppb to 10 ppb. As a consequence, the amount of arsenic waste generated from the treatment plants would widely increase (as projected by Meng et al., 2001). This would cause generation of more than 6 million pounds of ABSRs every year, which would be then disposed of in mixed-solid waste landfills (USEPA, 2003).

As a requirement of the Safe Drinking Water Act (SDWA), the United States Environmental Protection Agency (USEPA) recommended different best available technologies (BATs) to comply with the new arsenic maximum contaminant regulation (USEPA, 2001). These technologies include precipitation/coagulation, adsorption and ion exchange. The technologies available and under development for arsenic removal by small utilities depend primarily on adsorption of arsenic onto a throwaway or regenerable solid media. One option is to use iron oxide/hydroxide media to remove arsenic, either as adsorbent in drinking water treatment plants (USEPA, 2000), or as a precipitate to treat arsenic wastes produced from ion exchange and membrane filtration processes (USEPA, 2003). Based on Toxicity Characteristic Leaching Procedure (TCLP) results, these wastes may be disposed of in municipal solid waste (MSW) landfills where reducing conditions predominate because of the high natural organic matter (NOM) content and microbial activity. Under such conditions iron and arsenic will be reduced and, as a consequence, arsenic will be released to the leachate (Ghosh et al., 2004). It is known that reducing conditions increase aqueous arsenic concentration as a result of reductive dissolution of iron (hydr)oxides (Tufano et al., 2008).

A mature landfill leachate has a pH of 6.5-9 and high concentrations of anions, mainly carbonate, phosphate, and sulfate. It also supports a diverse population of microorganisms, including methanogens, arsenic, iron, and sulfate reducers (Christensen et al., 2001; Van Geen et al., 2004; Ludvigsen et al., 1999).

The primary routes of iron and sulfate reduction in landfills is microbially mediated and biomineralization is a common by-product. Biomineralization leads to formation of ferrous iron crystalline phases such as siderite, vivianite, and into mixed-valence mineral forms, such as magnetite and green rust in the presence of sulfide, sulfide minerals such as ferrous sulfide (FeS) and realgar (AsS). Therefore, in sulfidic environment, sulfate reducing bacteria (SRB) also has a significant impact on arsenic mobilization.

Under anaerobic conditions Fe (hydr)oxides can be used as terminal electron acceptors in a process termed Dissimilatory Iron Reduction (DIR) (Lovley 1991). DIR causes the reduction of structurally bound Fe in (hydr)oxide particles thereby inducing reductive dissolution and subsequently biomineralization (Sturm et al., 2008). In the proposed study, biomineralization, as a function of sulfate concentration, will be studied as a key component in controlling iron and arsenic leaching from ABSRs in landfills. More importantly, biomineralization is potentially an engineered process by which leach resistant arsenic/iron/sulfur minerals could be generated with an overall goal of stabilizing arsenic in recalcitrant crystalline mineral phases. A wide range of sulfate concentrations, from 1 to 52 mM, occur in municipal solid waste (MSW) landfills (Ghosh et al., 2006). At these concentrations a broad community of SRB is expected to be present in MSW landfills, which in addition to reducing sulfate may be able to reduce arsenate by using it as a terminal electron acceptor (Hoeft et al., 2001; Harrington et al., 1998; Newman et al., 1997).

Besides microorganisms, which are capable of direct As(III) oxidation and direct As(V) reduction, the iron reducing and the sulfate-reducing bacteria can have an important effect on the arsenic solubility.

Microbial transformations are likely major contributors to arsenic dissolution that would occur in the long residence times of landfills (Alday 2010; Kocar et al., 2010; Fendorf et al., 2010; Johnston et al., 2010; Burton et al., 2011b).

This work investigates role of sulfate on arsenic reduction and mobilization by applying a range of sulfates concentration in anaerobic column packed with Fe/As sludge. In previous work of Alday (2010), SRB reduced the available sulfate from the influent concentration of 0.064 mM and 2.08 mM to below detection levels in the effluent, under landfill simulated conditions. SRB, as arsenic reducer, could play an important role in reducing and mobilizing arsenic and in addition at high sulfate concentrations by reduction to sulfide and possibly subsequent formation of arsenic-sulfide minerals. Biomineralization could be employed either as a pretreatment prior to arsenic disposal or as a process to stabilize previously landfilled arsenic bearing solid residuals.

The goal of this research is to investigate biomineralization as a possible process to control iron and arsenic release from ABSR in landfills. The microbially generated sulfide can interact with environmentally important elements such as Fe and As and affect geochemical transformation of ABSRs via redox couple formation with As(V) and Fe(III) or sulfide biomineral formation.

If arsenic treated wastes, in mineral forms, could be safely disposed of in municipal landfills, while maintaining their integrity and stability under such conditions, then the potential expense associated with either hazardous waste disposal or cleaning up groundwater contacted by arsenic-laden leachate from non-hazardous landfills could be avoided.

1.1. Iron/Arsenic Fate in Anaerobic Environment

Natural aqueous systems contain not only dissolved organic matter but also dispersed mineral (e.g., clay and metal oxides) particles. Iron is the most abundant element in the lithosphere so the iron oxides are widespread in environmental systems (Illes et al., 2005). Iron (hydr) oxides are found in most soils at varied concentration and several forms (e.g., hematite, goethite, magnetite, etc.). Temperature, pH, and redox conditions influence the iron-mineral formation in soils and aqueous systems (Zachara et al., 2002; Dixit et al., 2003, Roh et al., 2003). Freshly precipitated iron (hydr) oxide minerals, such as amorphous ferric (hydr) oxides (AFH) and ferrihydrite ($\text{Fe}_5\text{HO}_8 \cdot 4\text{H}_2\text{O}$), have no or very low crystallinity with high specific surface area. Ferrihydrite is a poorly crystalline, metastable mineral, and a common secondary weathering product found in soils, unsaturated and saturated subsurface materials, and aquatic sediments. Transformations of these (hydr) oxides generate iron minerals with higher crystallinity, such as hematite, goethite and magnetite (Dixit and Hering 2003). The high degree of structural disorder and high specific surface area of ferrihydrite make it one of the most reactive of the iron oxide minerals and an important sink for inorganic and organic compounds in the environment. Ferrihydrite is especially important as an electron acceptor in soils, sediments, and aquifers because it is more bioavailable to dissimilatory

metal reducing bacteria (DMRB) than crystalline ones (Lovley et al., 1991). Iron-surface charge is variable and highly dependent on pH and ionic strength. Either cations or anions can be sorbed onto distinct iron-surface sites because the surface charge of these (hydr) oxides can be either positive or negative. Silicate, phosphate, and molybdate (inorganic anions); citrate, fulvic and humic acids, and biocides (organic anions); and aluminum, copper, lead, vanadium, zirconium, cobalt, chromium, and nickel (cations) are some of the particular compounds that sorb onto the iron surface (Dixon and Weed 1989). Iron sorption capacity also plays an important role in attenuating the concentration of several contaminants in the environment, such as arsenic, through adsorption and co-precipitation.

Iron is commonly found in two different oxidation states: ferric iron (Fe^{3+}) and ferrous iron (Fe^{2+}). The abundance of ferric minerals in the subsurface and their affinity for contaminants through adsorption has made solid-phase iron reduction a subject of importance with respect to understanding the biogeochemical dynamics of groundwater contaminants (Royer et al., 2002). Iron oxide may be reduced through biotic or abiotic electron transfer reactions with organic compounds (Scott et al., 1998). Iron speciation in soils and groundwater is mostly mediated by bioprocesses, as specific microorganisms reduce metals to obtain energy for growth under anaerobic conditions. The fate of both organic and inorganic contaminants has been found to be influenced by microbial iron reduction. Secondary reactions of Fe(II) may include aqueous Fe(II) complexation, adsorption to the oxide, and precipitation of ferrous minerals; FeCO_3 in HCO_3^- buffered

systems, $\text{Fe}_3(\text{PO}_4)_2 \cdot 8\text{H}_2\text{O}$ in systems with phosphate, Fe_3O_4 , and FeS in sulfidogenic environments.

Several studies have demonstrated that the microbial reduction of As-bearing Fe(III)(hydro)oxides result in a dissolution of the solid phase, and this could potentially mobilize sorbed arsenic on the surface of the iron oxides (Xinjun et al., 2009). The Fe(III) reduction could also form secondary iron crystalline phases with less surface area for arsenic adsorption, such as siderite (FeCO_3), vivianite ($\text{Fe}_3(\text{PO}_4)_2 \cdot n\text{H}_2\text{O}$) and iron sulfide (FeS_x) and mixed valent mineral forms, such as magnetite ($\text{Fe}^{\text{II}}\text{Fe}^{\text{III}}_2\text{O}_4$) and green rust ($[\text{Fe}^{\text{II}}_6 - x\text{Fe}^{\text{III}}_x(\text{OH})_{12}]^{x+}(\text{A}^{2-}_{x/2} \cdot y\text{H}_2\text{O})^{x-}$ (Benner et al., 2002). The rate of iron reduction correlates linearly with the iron surface area. AFH, with the highest surface area, is rapidly reduced compared to crystalline ferric (hydr) oxides such as goethite and hematite (Fredrickson et al., 1998). More in depth study on the characteristics of reduced iron phases and incorporation of arsenic into mineral structure is needed to better understand mechanisms of arsenic release within aquifer systems under reducing condition in presence of biological iron minerals.

In a study with Zachara et al. (2002) key factors controlling the identity of the secondary mineral were determined to be electron donor and acceptor concentrations, ferrihydrite aging/recrystallization status, sorbed ions, and co-associated crystalline Fe(III) oxides. Three different combinations of electron donor/acceptor, lactate/ferrihydrite, from deficient to excess (0.5 mmolL^{-1} lactate and 47, 50, and 150 mmolL^{-1} ferrihydrite), were used in this study. Transmission Mossbauer spectra of 2-line ferrihydrite indicates that the

electron donor to acceptor ratio can affect the biomineralization products resulting from the action of DMRB on iron (hydr) oxides. When ferrihydrite was at great excess, it was transformed to a complex mixture of Fe(III) oxides including hematite, goethite, lepidocrocite, and more crystalline ferrihydrite. In the case with the electron donor in excess, the 2-line ferrihydrite was almost fully transformed to fine-grained magnetite, with a small residual concentration of 6-line ferrihydrite.

Arsenic is a naturally occurring element widely found in the earth crust that is spontaneously released into drinking water sources, such as groundwater. Certain regions have higher incidences of arsenic in groundwater. Arsenic is also a component of man-made products, such as pesticides, pyrotechnics and wood preservatives. Arsenic can appear in a number of different methylated organic forms, and at least two inorganic forms: arsenate (H_2AsO_4^-) or arsenite (H_3AsO_3). Arsenate or As(V) is the oxidized state of arsenic and is typically found under aerobic conditions. Arsenite or As(III) is the reduced state of arsenic and is found under anaerobic conditions (Dixit and Hering 2003). As(V) exists under the conditions of natural waters as a negatively-charged monovalent (H_2AsO_4^-) or divalent (HAsO_4^{2-}) ion that readily sorbs onto metal hydroxide or ion-exchange resin surfaces, while As(III) is a zero-valent molecule (H_3AsO_3) that is not readily sorbed. Arsenic(V) binds strongly to most mineral components of soil, inclusive of clay minerals, iron, manganese, and aluminum oxides. In contrast, As(III) adsorption is more specific, binding exclusively to iron (hydr)oxides (Tufano et al., 2008).

In the environment arsenic desorption from solids can occur as a result of ligand displacement, dramatic shifts in pH, reduction of As(V), and reductive dissolution of iron

or manganese (hydr)oxides (Smedley and Kinniburgh 2002; Smith et al., 1998). However, a transition from aerobic to anaerobic conditions is thought to be the most common pathway by which As is released to the aqueous phase (Tufano et al., 2008). Inorganic As can also be transformed to biomethylated species such as monomethylarsonic acid (MMAA), dimethylarsinic acid (DMAA), and trimethylarsine oxide (TMAO) as a result of microbial activity (Wilkin et al., 2003; Rochette et al., 2000).

Research by Tuffano et al. (2008) address abiotic and biotic arsenic adsorption and desorption experiments using ferrihydrite, goethite and hematite coated sands loaded with either As(V) or As(III) in the abiotic experiments and ferrihydrite and goethite coated sands loaded with only As(V) in biotic experiment. Both set of experiments were run under continuous flow columns at the same rate for 55 days. Feed for abiotic columns set contained only basal salts buffer, whereas the feed to the biotic columns set also included trace minerals, vitamins and lactate, as electron donor. The abiotic results of ferrihydrite loaded column show that the effluent for both arsenic species reached the highest peak at initial stages of the experiment. The final amount desorbed varies at different arsenic loadings to the ferrihydrite coated sands, increasing initial loading were correlated with higher As released. The experiment was done comparing Fe/As leaching by using a wild-type (WT) and mutants of Fe/As reducing bacteria (*Shewanella sp. ANA 3*). The results of the ferrihydrite coated sands column inoculated with the wild-type bacteria, which is closer to natural environments, show an initial high As desorption followed by a steady state, low level of As release until the finalization of the experiment. On the other hand

the column with the mutant bacteria, without the ability to reduce As, the amount desorbed was only 1.4% and in the column with mutant bacteria, unable of reducing Fe, the As desorbed almost double the amount released in the WT column experiment. Comparing the abiotic to the biotic columns experiments loaded with almost the same quantity of As(III), abiotic desorption of As(III) was almost twice as much as the biotic experiment.

A study with Horneman et al. (2004), on the sediment profiles in the groundwater of Bangladesh revealed a particular point where As release is independent of the Fe activity outcompeting its desorption rate by several folds where dissolved As and Fe are generally greater at deeper depths under reducing environment.

In another research by Ghosh et al. (2006), incongruent Fe/As release was reported from a long-term, flow-through column study on the behavior of a common iron-based ABSRs when subjected to simulated landfill conditions. It was observed that during the early stages of operation, most arsenic and iron leaching was associated with suspended particulate matter generated by microbial erosion of ferrihydrite (Tadanier et al., 2005), and iron was lost proportionately faster than arsenic and in later stages, the arsenic leaching rate increased by more than 7-fold while the rate of iron leaching declined due to formation of secondary minerals leading to decreased sorption capacity and slower dissolution rates (Benner et al., 2002; Hansel et al., 2004 and 2005). Motivated by these research works, a set of column experiments were conducted by Alday (2010). These experiments were running under anaerobic condition, to mimic microbially mediated

processes that influence arsenic leaching from arsenic bearing solid residuals (ABSR) in mature municipal solid waste (MSW) landfills. The total arsenic leaching from these columns were usually higher than 80%, with As(III) nearly always higher than As(V), whereas Fe leached out less than 7% of the initial solid's content. Effluent As concentration starts releasing in a non-stoichiometric ratio from Fe at about 30 pore volumes (60 days) and increased constantly until it reached plateau for approximately 100 pore volume (200 days), and then decreased continuously. These results strongly suggest incongruent Fe/As release in which reduced iron re-precipitate in form of secondary mineral whereas released arsenic mobilizes out of the system.

One other important factor in such systems is presence of sulfate and sulfate reducing bacteria (SRB), and their role in arsenic reduction and mobilization. There are varieties of microbial communities capable of arsenic reduction; among those SRB has a considerable contribution to arsenic reduction under landfill condition (Hoeft et al., 2002; Harrington et al., 1998; Newman et al., 1997). Sulfate is present in landfill at relatively high concentration, from 105 to 4900 mgL⁻¹ (Ghosh et al., 2006). Within this concentration range, a broad community of SRB is present in MSW landfills, which are capable of reducing arsenate by using it as terminal electron acceptor. In addition, at high sulfate concentrations SRB reduce sulfate to sulfide which play an important role in mobility and availability of arsenic through formation of arsenic thioanions complex, arsenic-sulfide minerals and chemical reduction of Fe(III) (O'Day et al., 2004; Kocar et al., 2010; Couture et al., 2011; Burton et al., 2011). A geochemical model from study on a former pesticide-manufacturing facility in East Palo Alto, CA was proposed by O'Day

et al. (2004), applying spectroscopic observations that show the ratio of reactive iron to sulfur in the system controls the distribution of solid phases capable of removing arsenic from solution under reducing conditions. Under this condition with sulfate presents, the concentration of dissolved arsenic and its incorporation with minerals depends on the rate of microbially mediated sulfate reduction to sulfide phases and the formation of stable sulfide mineral. The XANES/EXAFS spectra of sediment shows formation of arsenic sulfide phases at the molecular scale and that the co-precipitation of arsenic with sedimentary iron sulfide minerals is not the dominant mechanism of arsenic uptake.

1.2. Biomineralization in Landfill

Microbial reductive dissolution and therefore transformation of iron oxides, can cause the release of adsorbed or incorporated species (Pederson et al., 2006). The biomineralization products are important in that they influence the overall thermodynamics of the bioreduction reaction, and consequently its extent. Biomineralization products may retard bioreduction by coating or passivating the residual Fe (III) oxide. Biomineralization products may also sequester trace elements associated with the original oxide by co-precipitation or surface complexation. The primary factor controlling the nature of the secondary iron mineral suite appears to be the Fe(II) supply rate, magnitude, and its surface reaction with the residual oxide and other sorbed ions (Zachara et al., 2002). Phosphate, carbonate, sulfate, and organic ligands are expected to be important factors influencing microbial reduction of iron oxides. A considerable amount of organic matters in landfill promotes high level of microbial activity under anaerobic conditions which

may lead to transformation of ferric iron (Fe^{3+}) to ferrous iron (Fe^{2+}) and/or sulfate to sulfide secondary formation of crystalline iron and sulfur phases. As (V) introduced to this system from ABSR may release in anoxic conditions, first as As(V) and then as As(III), during the reductive dissolution of arsenic bearing amorphous iron phase. Recent investigations suggest that certain iron-reducing bacteria capable of respiring anaerobically on arsenate may reduce iron oxide carrying arsenate efficiently, with arsenite incorporated in the crystal lattice during the formation of secondary minerals (Kocar et al., 2006).

Initial As(V) concentration is also an important factor impacting iron reduction rate, its mineralogy, and final arsenic speciation. Chow et al. (2009) finding from amendment of Chattahoochee River sediment with two different arsenic concentrations, $\leq 1 \mu\text{M}$ and $\leq 10 \mu\text{M}$ As(V), indicates that the activity of iron-reducing bacteria was spurred by the addition of even small concentrations of arsenate, but that As(V) probably inhibited iron reduction in the highest amendments. Results from lower arsenic amended experiment suggest that arsenate was removed during the recrystallization of iron, partly by adsorption and incorporation into the crystal lattice of iron oxides. The secondary mineralization of poorly crystalline iron oxides to more crystalline Fe/S phases reduces specific surface area, and thus site densities, which decreases arsenic sorption. Ona-Nguema et al. (2008) has studied arsenic and iron speciation in the products of anaerobic reduction of pure and As(V) or As(III)-adsorbed lepidocrocite by *Shewanella putrefaciens* ATCC 12099. The XRD patterns of samples from bioreduction of pure lepidocrocite after 9 months exhibit characteristic of hydroxycarbonate green rust GR1

(CO₃) and ferrous-carbonate hydroxide FCH whereas samples from bioreduction of As(III)-adsorbed lepidocrocite reveal FCH to be the dominant reaction product mixed with a minor amount of GR1(CO₃) after 22 months. These results indicate that the presence of As(III) slows down the reduction of Fe(III)-bearing GR1(CO₃) into FCH by *S. putrefaciens*. The complete reduction of Fe(III) to FCH was observed in samples from bioreduction of As(V)-adsorbed lepidocrocite after only 5 months. The poor crystallinity of FCH suggests that a fraction of arsenic adsorbed on the surfaces of FCH particles during the nucleation process, thus limiting their size. As K-edge XAFS results of product samples showed that As(V)/As(III)-lepidocrocite does not reduce or oxidize, respectively, under anoxic, abiotic condition and confirmed reduction of As(V)-lepidocrocite in the presence of *S. putrefaciens*, whereas no As(III) oxidation was observed in As(III)-lepidocrocite samples, in which *S. putrefaciens* reduced lepidocrocite and GR1(CO₃) to FCH. This study provides the first evidence for the formation of multinuclear arsenite surface complexes at the edges of nano-sized Fe(II)-bearing layered minerals. XEDS analysis also suggests sorption of arsenite on the surface of the FCH particles. Although biomineralization of Fe(III)-bearing minerals can lead to release of associated arsenic to aqueous solution, Fe(II) biominerals products are capable of sequestering back a fraction of the mobilized arsenic species. The Mossbauer results suggest that Fe(II)-containing biomineral co-precipitate with As(III) to form a minor As(III)-Fe(II)-containing solid phase. Under reducing conditions ~97% of As(III) was retained within biogenic Fe(II)-containing reaction products. These results indicate that, at least under some circumstances, bacterial reduction can promote As(III) sequestration in the form of As-Fe-containing biomineral.

For both thermodynamic and kinetics reasons, Fe(III) should serve as excellent electron acceptors for anaerobic respiration, with redox potential well above that of sulfate (Nealson et al., 1992). With decreasing oxidation potential in sulfidizing environments, ferrihydrites become thermodynamically unstable with respect to various ferrous/sulfide containing solid phases.

The number and complexity of factors influencing arsenic mobilization as redox conditions transition from oxidizing to reducing makes prediction of arsenic leaching from ABSR under mature landfill conditions a challenging task.

2. Objectives

The important role of specific microbial activity (Fe/As reducers) in arsenic reduction and mobilization under reducing condition has been fully studied, but the long-term nature and mineralogical properties of the newly formed phases in the presence of broad suite of microbial communities that are present and evolve in mature landfill, as well as significant role of sulfate concentration controlling arsenic fate under reducing condition are poorly understood. SRB in the environment with wide range of sulfate concentration, such as in landfill, could play an important role in arsenate reduction and mobility, and at high sulfate concentrations by reducing sulfate to sulfide and subsequent formation of arsenic-sulfide mineral which could contribute to arsenic sequestration. The goal of this project is to study two new innovative processes for the sequestration of arsenic released

in landfills: iron biomineralization and arsenic re-precipitation. A series of flow-through bench-scale columns has been set up under anoxic conditions to simulate conditions similar to those found in a mature landfill to investigate relevant processes, biomineralization and arsenic sorption/co-precipitation, controlling the release of arsenic from ABSR and its sequestration under landfill reducing conditions. These columns are packed with a sludge of As co-precipitated with AFH (as a representative ABSR), with Fe/As ratio of 20:1, and with mixed consortium of bacteria such as iron reducing bacteria, and sulfate reducing bacteria obtained from anaerobic digester sludge produced in a wastewater treatment plant. All columns are continuously fed with a solution of micro and macro nutrients required by the bacteria for growth, different sulfate concentration including one containing SRB inhibitor, and the addition of lactate as the only organic electron donor and carbon source for the microorganisms. Results of these manipulations will be evaluated based on reduction of arsenic and iron leaching from the columns. Also characterization of the mineral phases formed and arsenic, iron, and sulfate speciation of these heterogeneous mineral mixtures will be carry out by the end of each column run, using X-ray diffraction (XRD) spectroscopy, micro-focused X-ray fluorescence (XRF) mapping, and X-ray absorption spectroscopy (XAS) including extended X-ray absorption fine structure (EXAFS) and X-ray absorption near edge structure (XANES). There are no previous long-term studies reported on the use of biomineralization as remediation technique to stabilize the residuals that are disposed of in landfills. This research will focus on how arsenic-bearing wastes will be influenced by iron and sulfur biominerals formation in presence of sulfate under simulated landfill conditions and how different

concentration of sulfate contributes to the order and extent of biomineralization and potentially to the long-term stabilization of arsenic under such conditions.

3. Dissertation Overview

This dissertation is divided into 7 core chapters. A brief description of each of the chapters is described below.

Chapter 1: of the dissertation is intended to be introductory in nature; providing a general summary of the project, a brief literature review, and research objectives; including ABSRs disposal issues, iron and arsenic fate after disposal, biomineralization process and its impact on ABSRs.

Chapter 2: "Ferrous Biomineral Formation and Its Affinity for Arsenic Sequestration under Simulated Landfill Conditions". This chapter describes a complete long-term column study under simulated landfills conditions that shows the main processes occurring in landfills; including As-bearing Fe(hydr) Oxide biotransformation to show how high affinity iron phase transforms to low affinity minerals through biomineralization, arsenic and iron leaching and non-stoichiometric release, and looks at siderite and vivianite adsorption/co-precipitation isotherms. Freundlich and Langmuir isotherm equations are used to describe the partitioning behavior of the system.

Chapter 3: is submitted to *The Journal of Environmental Science and Technology* with the title of "**Bio mineralization controls arsenic mobility in landfill conditions**". This chapter evaluates the effect of sulfate on biomineral diversity and arsenic retention by comparing low sulfate column (0.064 mM) with medium sulfate (2.08 mM), using a broad set of analytical techniques to analyze aqueous chemistry and speciation. Incongruent Fe/As release effect is also evaluated in this chapter.

Chapter 4: is published under the title "**Microscale speciation of arsenic and iron in ferric-based sorbents subjected to simulated landfill conditions**" in *Environmental Science and Technology* with Robert Root (first author), Sahar Fathordoobadi, Fernando Alday, Wendell Ela, and Jon Chorover as coauthors. This paper describes the effect of sulfate concentration on solid phase sorbent and sorbate speciation. By combining X-ray absorption spectroscopy (XAS) and multiple energy micro X-ray fluorescence (ME- μ XRF) mapping (elemental and chemical).

Chapter 5: "**How sulfur redox cycle and concentration impacts ABSRs fate under simulated landfill conditions.**" This chapter evaluates the effect of sulfate concentration on column's mineralogy and the final species redox state by comparing medium (2.08 mM) and high sulfate (20.8 mM) columns, looks at possible mechanisms and pathways (biotic, abiotic), explains electron consumption model, and thermodynamic favorability of relevant redox couples using Lactate as electron donor.

Chapter 6: This section provides a summary of the conclusions of the study undertaken in the 6 core chapters of this research and recommendation on future work in this research field.

Appendix A: "Time dependent arsenic release into landfill leachate from Arsenic Bearing Solid Residuals (ABSRs) under different sulfate concentrations." This section discuss biomineral transformation over time under the influence of two different sulfate concentration by looking at replicate columns of moderate and high sulfate at 3 different arsenic leaching regimes within a column's life; by the end of lag phase, when arsenic effluent concentration reaches its maximum, and after its concentration declined back, at the end of run.

CHAPTER 2

FERROUS BIOMINERAL FORMATION AND ITS AFFINITY FOR ARSENIC SEQUESTRATION UNDER SIMULATED LANDFILL CONDITIONS

1. Introduction

The U.S. Environmental Protection Agency revised Maximum Contaminant Level(MCL) of arsenic in drinking water from 50 to 10 ppb, became enforceable on January 23, 2006 (US EPA, 2001), and has caused a significant increase in the volume of arsenic-bearing solid residuals (ABSRs) generated by drinking water utilities (as projected by Meng et al., 2001). Because of their high adsorption capacity and low cost, iron sorbents are widely utilized for treatment and, when spent, comprise the bulk of the waste generated. For their performance the iron-based sorbents depend on oxidized iron (Fe^{3+}) surfaces, typically forms of ferrihydrite ($\text{Fe}(\text{OH})_3 \cdot n\text{H}_2\text{O}$ or goethite ($\alpha\text{-FeOOH}$) (Amy et al., 2000; Impellitteri and Sheckel 2006; Mohan and Pittman 2007). Based on Toxicity Characteristic Leaching Procedure (TCLP) results, these ABSR may be disposed in municipal solid waste landfills(US EPA, 2003). Even though ABSR are required to pass the standard TCLP before being disposed of in nonhazardous landfills, there is evidence that the TCLP does not accurately reflect long-term leaching that would occur under landfill conditions (Meng et al., 2001; Ghosh et al., 2004).

Mature solid waste landfills are complex systems characterized by mildly alkaline, reducing conditions, with diverse microbial communities and high organic matter content. As a result, landfill environments display a variety of physical, chemical, and microbial processes affecting the transfer of contaminants from the disposed waste into the leachate (Christensen et al., 2001; Ghosh et al., 2006; Kjeldsen et al., 2002). Iron reduction in landfills is microbially mediated and biomineralization leads to common by-products of ferrous iron crystalline forms, such as siderite, vivianite, and mixed-valence mineral forms, such as magnetite and green rust (Kocar et al., 2006; Burnol et al., 2007; Kirk et al., 2010; Root et al., 2013). Iron reducing bacteria produce these biominerals as a by-product of their microbial respiration. Studies have shown that when ABSR is subjected to simulated landfill conditions, the mobility and speciation of iron and arsenic change through time, with extensive arsenic leaching taking place (Ghosh et al., 2004 and 2006; Jing et al., 2008; Alday 2010; Clancy et al., 2013). This shows that ABSR are not stable under the conditions found in mature landfills. It has also been observed (Burnol et al., 2007) that the As/Fe ratio in the leachate varies through time, indicating that there is not a direct correlation between the mobility of arsenic and iron. This means that the transport of arsenic cannot be accounted for only by the dissolution of ABSR. In this work, biomineralization is evaluated as a possible process to control iron and arsenic release from ABSR in landfills.

The sorbents employed for drinking water arsenic treatment are mineralogically the same as those implicated in arsenic immobilization in natural oxidized systems, primarily ferric (hydr)oxides (Amy et al., 2000; Benner et al., 2002; Smedley and Kinniburgh 2002;

Mohan and Pittman 2007; Cances et al., 2008). In turn, iron reduction in municipal solid waste (MSW) landfills, just as in natural environmental systems, is microbially mediated and leads to formation of secondary minerals such as siderite, vivianite, and magnetite (Hansel et al., 2003; Ghosh et al., 2006; Ona-Nguema et al., 2009). These minerals have been suggested as potential As sinks (Charlet and Polya 2006; and references therein). However, most of the secondary iron biominerals are crystalline with relatively low specific surface area and sorption sites. As a consequence, biominerals may not be as effective in As removal as amorphous iron phases. Despite many studies on adsorption and/or incorporation of As into Fe-sulfides (Farquhar et al., 2002; Wolthers et al., 2005; Cances et al., 2008; Kirk et al., 2010) and magnetite (Dixit and Hering 2003) there is a lack of such data for siderite and vivianite. Specifically, data concerning vivianite reactivity in any context are sparse. Few studies on As sorption by siderite have been reported (Guo et al., 2007 and 2009). Therefore, there is also a need to study the kinetics and As sorption capacity of siderite and vivianite, and to evaluate the effectiveness of these two common iron biominerals in arsenic sequestration.

The redox cycle of iron in landfills is controlled by interactions between porewater (leachate) constituents and the solid phase, and is often driven by microbial processes. The reductive dissolution of iron (hydr)oxides can release ferrous iron to the pore water and/or promote the precipitation of secondary mineral phases (Benner et al., 2002; Hansel et al., 2003; Tufano et al., 2008; Ona-Nguema et al., 2009). The sorption/desorption of arsenic initially loaded on Fe(III) (hydr)oxides is then strongly influenced by iron reducing bacteria (Burnol et al., 2007; Tufano et al., 2008). Fe(II)-

induced transformation of iron(hydr)oxides may lead to incongruent partitioning of arsenic between the aqueous and solid phases. Upon reduction, Fe(II) is released to the leachate, and ferrous biomineral phases may precipitate. The specific mineral products of microbial Fe(III) reduction depend on the crystalline state of the initial (hydr)oxide phase, the presence and concentration of co-precipitated or sorbed constituents, and the solution chemistry, especially iron and sulfate concentrations (Benner et al., 2002; and references therein). Secondary phases include mixed valent minerals such as magnetite ($\text{Fe}^{\text{III}}_2\text{Fe}^{\text{II}}\text{O}_4$), ferrous-bearing solids such as siderite (FeCO_3) and vivianite ($\text{Fe}_3(\text{PO}_4)_2 \cdot n\text{H}_2\text{O}$), and in the presence of sulfide, biominerals such as ferrous sulfide (FeS) and realgar (AsS). Therefore, in sulfidic environments, sulfate reducing bacteria (SRB) have a significant impact on arsenic mobilization (O'Day et al., 2004; Burton et al. 2011).

The fate of As is tied to S and Fe reduction. Secondary mineralization of ferrihydrite occurs via a coupled, biotic-abiotic pathway (Hansel et al., 2003). Ferrous sulfide minerals are also commonly formed under sulfidic environments, usually contributing to As mobilization due to their limited surface area (Burton et al., 2011 and 2013). Iron sulfides could form through both biological (in presence of iron reducing bacteria) and chemical (in presence of aqueous sulfide) routes (Millero et al., 1995; Poulton et al., 2003 and 2004). In some instances, kinetic limitations may produce solid phases that are not in thermodynamic equilibrium with the contacting solution; alternatively, micro-environmental variations at a scale not measured by the experimental or sampling design may account for solids in apparent disequilibrium (Benner et al. 2002).

Factors controlling the specific biomineralization pathway include pH, redox potential, microbial activity, carbonate, phosphate, and sulfate concentration (Zachara et al., 2002; Dixit et al., 2003). Final solid phases have more structured crystal geometry and lower reactive site density. However, some of these minerals can effectively incorporate As. Therefore, there is a need for more detailed and in depth evaluation of all the contributing factors and reactions in biomineral formation which are influencing arsenic fate under landfill conditions. Figure 2.1 illustrates the mechanisms affecting the fate of ABSR after landfill disposal.

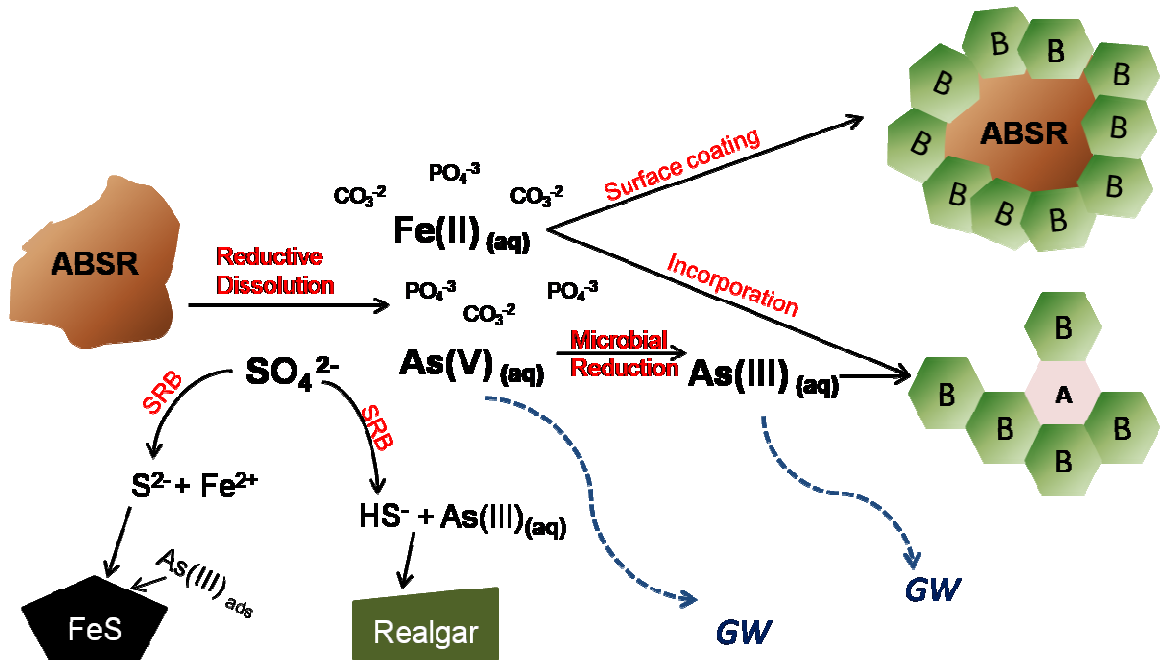


Figure 2.1. The primary routes of iron and sulfate reduction in landfills are microbially mediated and secondary mineral formation is a common by-product. Biomineralization plays a key role in determining whether or not desorbed As will be sequestered under landfill conditions. SRB: Sulfate reducing bacteria; B: Biomineral; A: Arsenic.

The goal of this project is to understand how biomineralization affects arsenic mobility under simulated landfill conditions and to evaluate the feasibility of applying biomineralization as a process to stabilize arsenic in landfills. Specifically, this work focuses on studying two common iron phases that form as a result of reductive dissolution under anaerobic conditions. According to previous experiments (Alday 2010; Root et al., 2013), the main two iron crystalline biominerals formed under landfill conditions are siderite and vivianite. We also evaluate the affinity of these minerals for arsenic re-adsorption through batch isotherm tests carried out under anaerobic conditions. A set of column experiments were conducted under anaerobic conditions to mimic key microbially mediated processes that occur in mature MSW landfills. The columns were loaded with sludge of As co-precipitated with ferric hydroxide (as a representative ABSR) and inoculated with a mixed microbial consortium, including iron reducing bacteria, from the anaerobic digester sludge from a municipal wastewater treatment plant. The research highlights the importance of iron on the fate of arsenic after iron mineralization and how these minerals influence its mobility.

2. Materials and Methods

2.1. Column Experiments

2.1.1. Sludge Preparation

An arsenic-bearing iron sludge was prepared to simulate the waste generated from arsenic removal processes. Sodium arsenate heptahydrate ($\text{Na}_2\text{HAsO}_4 \cdot 7\text{H}_2\text{O}$, KR Grade, Sigma-

Aldrich) was dissolved in purified water (Milli-Q Water System by Millipore) to prepare a 1 L solution with a concentration of about 70 ppb as As. Ferric chloride hexahydrate($\text{FeCl}_3 \cdot 6\text{H}_2\text{O}$, ACS reagent, Sigma-Aldrich) was added to the As solution to produce a supersaturated Fe, resulting in Fe:As molar ratio of 22:1. This mixture was stirred on a reciprocating shaker table (Orbit, reciprocating speed 100 rpm) and the pH of the solution was adjusted to 7.0 ± 0.2 adding 10.0 M sodium hydroxide (NaOH, flakes, EMD Chemicals). The produced AFH sludge was equilibrated for 2 days while the pH was maintained at 7 ± 0.2 . After equilibration and settling, a supernatant sample was filtered through a $0.45 \mu\text{m}$ cellulose acetate syringe filter (Whatman) for determination of concentrations of dissolved As and Fe (Table 2.1). Iron concentration was below detection. Subsequently, the residual sodium chloride content of the AFH was reduced by decanting off the supernatant and filling a 4 L flask to the top with Milli-Q water, mixing gently, and allowing the solid to settle for 3-4 hours and decanting off the water. This procedure was repeated until the conductivity of the supernatant was below 1.0 mS cm^{-1} . During the process the pH remained constant (7.0 ± 0.2) without needing further adjustment. The remaining slurry was vacuum-filtered through a $0.45 \mu\text{m}$ filter (cellulose nitrate, Whatman). The final AFH water content was calculated by weight loss of a sample dried at 70°C for 2 days. Characteristics of the sludge are presented in Table 2.1. The sludge was stored in a capped-glass container for no more than three weeks at 4°C .

Table 2.1. Iron/Arsenic sludge characteristics

pH	Supernatant As Concentration (ppb)	SupernatantFe Concentration (ppb)	[mg As / g dry sludge]	[mg Fe / g dry sludge]	Fe:As Ratio	% Water Content
7.00	69.6	BDL	31.2	521	22.4	83.4

BDL: below detection limit

Total Fe and As in the AFH were determined by digestion of 1 g (dry wt.) sample, using 15 mL of 70% by volume HNO₃(J.T. Baker) in a CEM microwave digester (method SW 821-8051). Iron was determined by the 1,10-phenanthroline method (APHA 1998) using a spectrophotometer at 510 nm wavelength (Spectronic Genesys 5). Total and speciated arsenic were measured by Ion Coupled Plasma Mass Spectrometer (ICP-MS, Agilent 7500a).

2.1.2. Column Characteristics

Chromatography-type Columns (Spectrum Chromatography; 2.5 cm ID × 30 cm length) were packed with about 80 g (wet wt.) of the prepared iron/arsenic sludge, mixed with 120 g of glass beads (0.8 mm diameter) used as inert support. Anaerobic digester sludge (25 mL of slurry) obtained from Ina Road Wastewater Treatment Plant, Tucson, Arizona was added as the microbial source for the experiment (Figure 2.2). The column was fed

with a synthetic landfill leachate adapted from Field et al. (2003)(Table 2.2) by replacing all chloride with sulfate salts to avoid chloride peaks overlapping other anion peaks in ion chromatography (IC). Effluent samples, filtered through 0.45 μm cellulose acetate syringe filters (Whatman), were analyzed to quantify arsenic, iron, and lactate. ICP-MS (Ion Coupled Plasma Mass Spectrometer, Agilent 7500a) was used to evaluate total and speciated arsenic. 1,10 phenanthroline method (APHA, 1998) using a spectrophotometer (Spectronic Genesys 5) was used to determine iron speciation. The influent feed was purged with nitrogen gas and fed continuously into the columns using a multi-syringe pump (BS-9000-6 programmable multi-syringe pump, Braintree Scientific) at an average rate of 2 pore volumes day^{-1} .

Table 2.2. Composition of synthetic landfill leachate solution used as column feed (adopted from Field et al., 2003)

Inorganic compounds		Organic compounds	
	mg/L		mM
KH_2PO_4	37	Lactate	5.5
$\text{Ca}(\text{OH})_2$	5		
$\text{MgSO}_4 \cdot 7\text{H}_2\text{O}$	10		
Mg	9		
NH_4HCO_3	987		
NaHCO_3	951		
Trace Nutrient Element Solution Compounds $\mu\text{g/L}$			
H_3BO_3	50		
$\text{FeSO}_4 \cdot 7\text{H}_2\text{O}$	2800		
$\text{ZnSO}_4 \cdot 7\text{H}_2\text{O}$	106		
$\text{MnSO}_4 \cdot \text{H}_2\text{O}$	415		
$(\text{NH}_4)_6\text{Mo}_7\text{O}_{24} \cdot 4\text{H}_2\text{O}$	50		
$\text{AlK}(\text{SO}_4)_2 \cdot 12\text{H}_2\text{O}$	175		
$\text{NiSO}_4 \cdot 6\text{H}_2\text{O}$	113		
$\text{CoSO}_4 \cdot 7\text{H}_2\text{O}$	2360		
$\text{Na}_2\text{SeO}_3 \cdot 5\text{H}_2\text{O}$	100		
$\text{CuSO}_4 \cdot 5\text{H}_2\text{O}$	157		
EDTA	1000		
Resazurin	200		

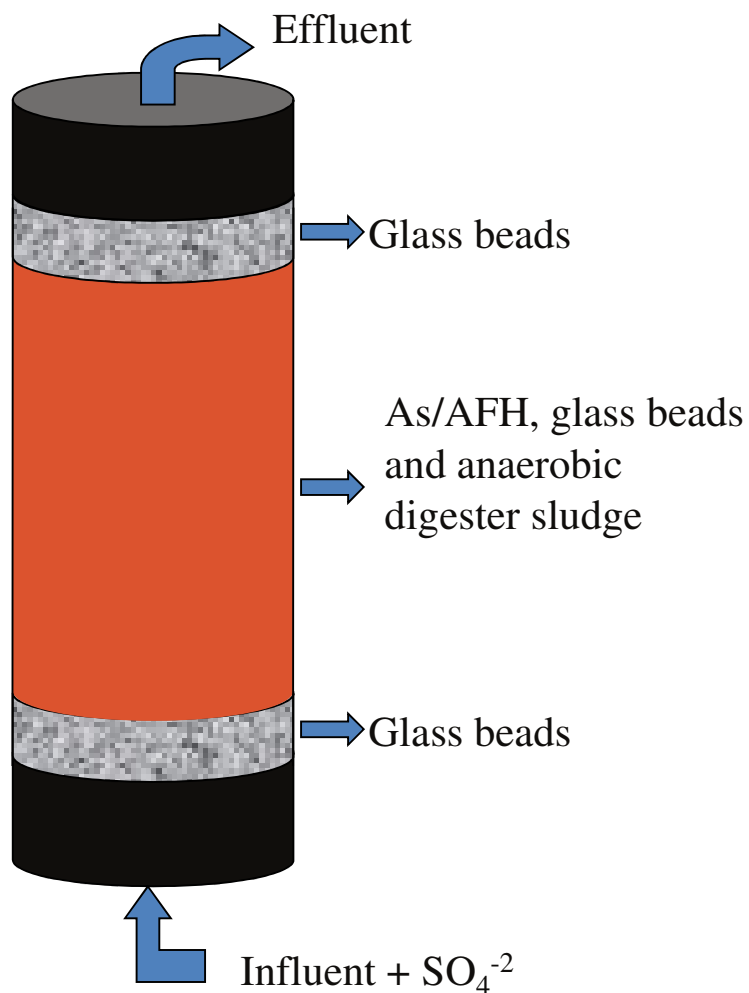


Figure 2.2. Experimental Set-up; Up-flow bench-scale column, packed with laboratory synthesized Fe/As sludge of 20:1 molar ratio mixed with glass beads and inoculated with anaerobic digester sludge obtained from Ina Road wastewater treatment plant. The feed contains lactate as the carbon source and primary electron donor (5.5 mM), and ferric iron and arsenate as primary electron acceptors.

2.1.3. Solid Phase Characterization

The column was run for 665 days (332 PV). Effluent pH was measured every other week and it fluctuated between 7.5 and 8. After termination, column was opened in an oxygen free glove box (Terra Universal 100). The contents of the column (initially containing a mix of AFH, glass beads and anaerobic digester sludge) were divided into four approximately equal volume sections. Each layer was dried in the glove box at room temperature for 7 days after which a 0.5 mm mesh was used to separate the glass beads from the solids. Solid phases were analyzed by Powder X-ray Diffraction (XRD), by a Scintag XDS 2000 PTS Diffractometer with Cu-K α radiation ($\lambda = 1.54060 \text{ \AA}$) operated at a voltage of 40 kV and a current of 40 mA. Diffraction patterns were recorded by continuous scans from 10° to 70° at 2 degrees/minute. The mineral phases were identified using the instrument software and the International Centre for Diffraction Data (ICDD) database.

2.2. Batch Adsorption/Co-precipitation Experiments

Batch tests were performed utilizing synthesized siderite and vivianite to remove arsenic from aqueous solution through adsorption and co-precipitation. All experiments were performed inside an anaerobic glovebox, kept under a constant flow of nitrogen gas to maintain anoxic conditions. Deoxygenated water (DO) was also used for solution preparation. DO water was prepared by bringing Milli-Q water to a boil while bubbling nitrogen gas for 60 minutes.

Experimental conditions were kept constant for all adsorption/co-precipitation experiments, except for initial arsenic concentration. Reagent grade chemicals were used. All vials, tubes, and glassware were cleaned in an acid bath and rinsed with Milli-Q water before use.

2.2.1. Arsenic Stock Solutions

Arsenic salts (NaAsO_4 for As(III) and $\text{HNa}_2\text{AsO}_4 \cdot 7\text{H}_2\text{O}$ for As(V)) were used for the preparation of stock solutions. The dry mass of the corresponding salt was dissolved in 100mL of DO water to obtain different As(III) and As(V) stock concentrations in the range of $0.2\text{-}3500 \text{ mgL}^{-1}$ in siderite experiments and $150\text{-}1200 \text{ mgL}^{-1}$ in vivianite experiments.

2.2.2. Vivianite Synthesis

This synthesis method was adopted from Rosado et al. (2001). Each sample was prepared inside the glove box in a 50mL glass bottle by dissolving the dry mass of phosphate (0.2706g of NaH_2PO_4) in DO water and adjusting to pH7 before adding the dry mass of iron (0.8577g of $\text{FeCl} \cdot 7\text{H}_2\text{O}$) at room temperature. Precipitation started immediately after the addition of iron. The final volume was adjusted to 50mL for all samples. The pH was readjusted using 10 M NaOH as needed throughout the experiment to maintain pH 7 ± 0.2 .

A circumneutral pH was maintained in order to replicate mature landfill environments (Christensen et al., 2001), as well as to maintain consistency between experiments.

2.2.3. Siderite Synthesis

This synthesis method was developed based on modification of synthesis procedures by Singer et al. (1970), Bruno et al. (1992), and Wiesli et al. (2004). Artificial siderite was synthesized inside the glove box with ferrous chloride ($\text{FeCl}_2 \cdot 4\text{H}_2\text{O}$) and sodium bicarbonate (NaHCO_3). Ferrous carbonate was precipitated by drop-wise addition of 0.05M Fe^{2+} solution into 0.15M HCO_3^- solution on a magnetic stirrer at room temperature. Carbonate salt was used in excess ($\text{CO}_3^{2-}/\text{Fe}^{2+}$: 3:1) to consume all the iron in solution. The suspension was stirred for 1 h inside the glove box before it was set aside for 24 h for the pale precipitate to settle to the bottom of the container.

2.2.4. Batch Vivianite Adsorption

Adsorption experiments were performed by the addition of either an As(III) or an As(V) solution to pre-synthesized vivianite. The vivianite suspension was left to stabilize for at least 2h before adding arsenic from a previously made stock solution. The volume of arsenic solution added varied among samples based on the target initial arsenic

concentration, but the final volume was kept constant at 50 mL. The final suspension was allowed to equilibrate for 72h, stirring and checking the pH twice a day.

2.2.5. Batch Siderite Adsorption

The batch experiments to study the removal of As from solution were carried out by mixing 50mL of As solution in 100mL polyethylene bottles with 0.5 g of the sorbent. Isotherm studies were conducted with initial As(V) or As(III) concentrations between 0.2 and 100 mgL⁻¹, and a contact time of 2 weeks. After a predetermined contact time, the aqueous samples in each bottle were filtered through a 0.45µm cellulose acetate filter (Whatman). The supernatant was analyzed for dissolved Fe and As. The effect of contact time (1day–6weeks) was examined at room temperature with initial arsenic concentrations of 100 mgL⁻¹.

2.2.6. Vivianite Co-precipitation

Co-precipitation experiments were performed by synthesizing vivianite in the presence of either As(III) or As(V) solutions. The arsenic solution was mixed with the phosphate before adding the dry mass of iron to the arsenic/phosphate solution. Different volumes of arsenic solution were added initially to each sample in order to obtain a range of arsenic concentrations. As with adsorption experiments, the suspension was allowed to equilibrate for 72h, maintaining a circumneutral pH.

After 72 h, the samples were presumed to have reached equilibrium, at which point the amount of arsenic bound to the solid, and that remaining in the aqueous phase, was no longer changing. The equilibrium point was determined based on results of preliminary studies in our lab. The samples were taken out of the glove box and allowed to settle. The solids were separated from the aqueous phase using a vacuum filter with 1 μ m cellulose acetate filter (Whatman). While filtering, the solids were rinsed with Milli-Q water to dispose of salts that may have accumulated on the vivianite surface. The filtration process lasted 5 minutes to limit oxygen exposure. The wet solid weight was recorded and then the solid was divided in two portions for different analyses. One portion was sampled in a small plastic vial and transferred inside the glove box to air dry for 7 days before being sent for X-ray diffraction (XRD) analysis to confirm the identity of the solid. The remaining wet solid was dried in an oven for 24h at ~90°C. The wet and dry weights measured were used to calculate the water content of the solid after filtration and to determine the dry weight of the initial solid before it was divided.

Samples (~0.1g) of dry solid were mixed with 10mL of 65% HNO₃ for extraction on a shaker table continually mixed for 48h. This digestion process ensured that all contents of the solid were dissolved for quantitative measurement of arsenic content. The solutions were then diluted and stored with EDTA (as chelating agent to sequester iron from solution) and acetic acid (as a buffer) until they could be analyzed by ICP-MS.

Solid samples dried inside the glove box were analyzed by XRD. Digested samples, as well as arsenic stock solutions, were analyzed by ICP-MS to obtain initial and solid arsenic concentrations. The arsenic concentration remaining in the aqueous was calculated by difference.

2.2.7. Siderite Co-precipitation

Co-precipitation experiments were performed by synthesizing siderite in the presence of either an As(III) or an As(V) solution. The arsenic solution was mixed in the ferrous chloride solution before addition to the bicarbonate mixture. Different volumes of arsenic solution were added initially to each sample in order to obtain desired range of arsenic concentrations ($0.2\text{--}3500\text{ mgL}^{-1}$). The suspension was allowed to equilibrate for 24 h inside the glove box. After 24 h, the solids were separated from the aqueous phase using $0.45\mu\text{m}$ cellulose nitrate filters (Whatman). The filtered aqueous phase was sampled for arsenic measurement. The wet solid weight was recorded and then the solid was transferred in a weighing boat outside the glove box to air dry on the bench for 7 days. The wet and dry weights measured were used to calculate the water content of the solid after filtration and to determine the dry weight of the initial solid.

Aqueous samples were diluted and stored with EDTA (as chelating agent to sequester iron from solution) and acetic acid (as a buffer) until they could be analyzed for dissolved arsenic concentration by ICP-MS. The arsenic content of the solid phase was then calculated by difference in mass balance.

The effect of contact time (1–4 days) was examined at room temperature with initial arsenic concentrations of 100 mgL⁻¹.

3. Results and Discussions

3.1. Column Study

More than 10 column experiments were conducted over the course of 5 years of this study. All ABSR-loaded columns exhibited a qualitatively similar trend in effluent arsenic concentration as a function of time. An asymmetric bell-shaped curve characterizes these trials as well as the arsenic-leaching from advective-flow, long-duration studies previously reported (Ghosh et al., 2006; Kirk et al., 2010; Meng et al., 2001). Column experiment conducted to evaluate the role of ferrous biomineral in arsenic sequestration in this work run for about 2 years (665 days) with an average effluent arsenic concentration of about 0.3 mM. Initially, low arsenic concentrations were detected in the effluent (Figure 2.3). This early retention stage (termed here lag phase) may be due to microbial acclimatization, or the re-adsorption of released arsenic onto newly exposed AFH and re-precipitated iron surfaces (Kocar et al., 2006; Pederson et al., 2006; Tufano et al., 2008) as Fe³⁺ undergoes reductive dissolution. The lag phase is followed by a continuous increase of effluent concentration to a maximum. This increase in the effluent arsenic concentration occurs as a result of Fe³⁺ transformation and precipitation of secondary iron minerals with limited sorption capacity (Table 2.3). Following the arsenic peak, the effluent concentration dissipates to below 0.1mM to the

end of column's operation. This arsenic leaching behavior is qualitatively consistent with that observed in the other few long-term column studies (Ghosh et al., 2006; Kirk et al., 2010). The reactor was kept running for 665 days, and by the time it was stopped there was almost no arsenic retained in the solid phase inside the column.

During the course of the experimentation, two arsenic leaching regimes were observed in the column (Figure 2.3); For the first 300 days of operation, As(V) is the dominant aqueous species, after which arsenic in the effluent is mostly As(III) until the termination of experiment.

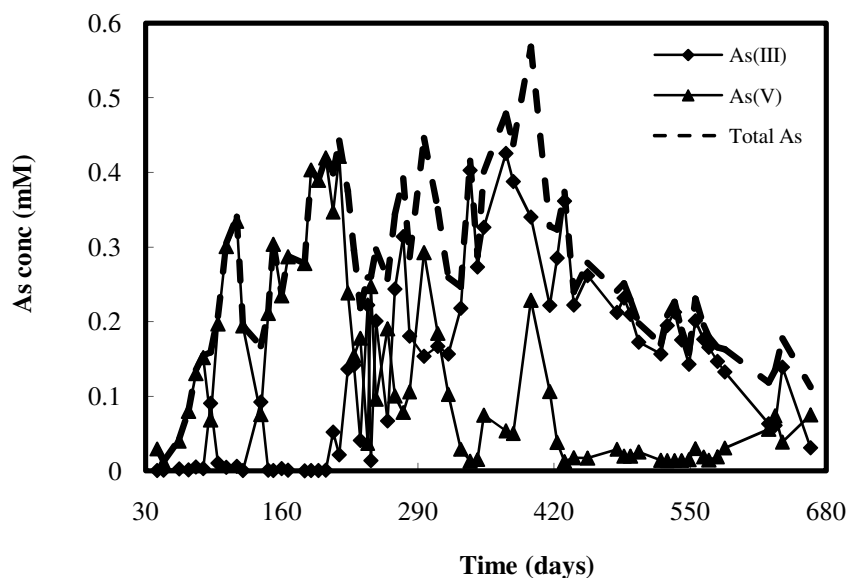


Figure 2.3. Column effluent total arsenic and speciation shows As(V) being dominant during the first half of column life and As(III) being major species from 319 days to the end of column's life. Almost all of the initial arsenic mass (~100%) leached out of the column after 665 days.

The iron leaching trend does not follow that of arsenic. Throughout the course of experiment, less than 1% of the total iron leached out, with average concentration ca. 0.05mM. The effluent Fe^{2+} concentration was much higher than Fe^{3+} throughout the column's life. The Fe^{3+} concentration during almost all the experiment was low with only a few increases probably due to oxidation during sample handling and processing and/or due to detachment and release of colloidal particles from the solid phase. Overall, iron concentration did not follow a clear trend and fluctuated throughout the run (Figure 2.4).

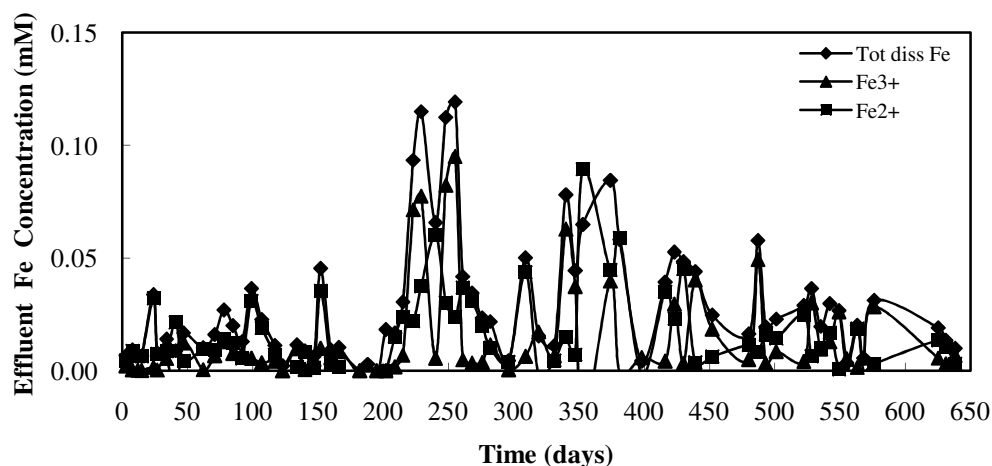


Figure 2.4. Column effluent total iron concentrations. <1% of the iron initially loaded into both columns leached over the duration of the experiment.

During the experiments, leaching of As and Fe did not correspond to the initial molar proportions in the ABSR. This incongruent Fe/As release was evident in all of our experiments, as well as in previous works (Alday 2010; Ghosh et al., 2006; Burnol et al., 2007). The Fe/As molar ratio in the effluent (ca. 0.25) was always appreciably lower than

the initial Fe/As loading ratio of 22 (Figure 2.5). Early ferrihydrite reductive transformation initially enhances arsenic retention due to re-adsorption of released arsenic onto newly exposed AFH and re-precipitated iron surfaces (Kocar et al., 2006; Pederson et al., 2006; Tufano et al., 2008), while prolonged reduction enhances arsenic desorption due to the depletion of sorption sites resulting from continued iron reductive dissolution and biomineral formation (Tufano et al., 2008). Also, arsenate may remain adsorbed onto the ferrihydrite surface until the surface area and the number of surface sites become too small to contain all the arsenate (Pedersen et al., 2006). Batch incubation experiment with As(V) sorbed on, or co-precipitated with, 2-line ferrihydrite, in a work by (Burnol et al., 2007) revealed that arsenic and iron leaching are in a non-stoichiometric ratio: most of the leachable arsenic but only a small fraction of the leachable iron, was released over a 2-month period and arsenic release can appear after Fe(III) reduction, rather than simultaneously.

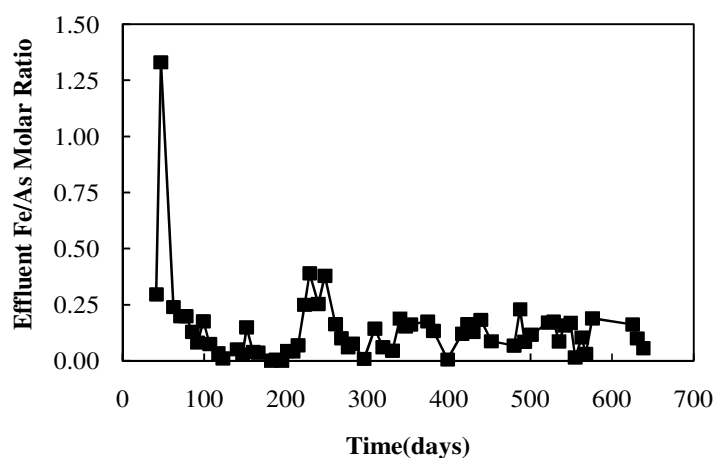


Figure 2.5. Fe/As molar ratio in the effluent: As/Fe non-stoichiometric release was evident since the initial loading Fe/As molar ratio was 22:1.

Under landfill conditions, iron (hydr)oxides undergo reductive dissolution, releasing aqueous Fe(II) to leachate and promoting long-term arsenic release/desorption. Dissolved iron in the presence of phosphate and carbonate, two of the constituents commonly found in landfills, forms thermodynamically more stable crystalline minerals such as vivianite and siderite with lower capacity to retain arsenic due to their lower specific surface area (Alday 2010; McCormick et al., 2002; Thinnappan et al., 2008). Dissolved iron migrates downstream in the column, creating a pore-water Fe^{2+} front which led to formation and precipitation of Fe(II)-bearing minerals. Therefore, the decrease in number of sorption sites from the initial AFH to the final ferrous minerals significantly decreases arsenic sorption capacity (Table 2.3). Iron phase transformation within columns is also evident from change of color in solid phase from orange-brown (iron hydroxide) to darker shades of brown and grey, suggestive of Fe^{2+} -minerals formation, siderite and vivianite, that were detected in the solid samples using XRD (Table 2.4). Although XRD was employed as a qualitative technique, the intensity of the peaks of the solid samples became larger along the direction of the flow, suggesting an increase in the crystalline mineral content from bottom to top of the column as a result of dissolved iron relocation. Thus, the capacity of iron biominerals to sequester arsenic through adsorption or incorporation into secondary solid phases must be evaluated in order to fully understand the partitioning behavior of As between the aqueous and solid phase.

In contrast to our findings, other column studies on As elution from iron(hydr)oxide-coated sand, in presence of Fe(III) and As(V) reducing bacteria, have shown that reductive transformation of ferrihydrite promotes As retention rather than release (Tufano

et al., 2008; and Kocar et al., 2006). Enhanced retention of arsenic maybe due to incorporation/adsorption to secondary minerals or formation of an Fe(II)-As(III) precipitate (Kocar et al. 2006; Thoraj et al., 2005). However, their finding is relevant to the specific conditions at which their experiments were run. Columns in their study were selectively inoculated with only Fe(III) and/or As(V) reducing bacteria as compare to our reactors where anaerobic digester sludge (mixture of microbial consortium) was added as microbial source, containing variety of microbial groups capable of Fe/As reduction. Moreover, certain microbial groups such as sulfate reducing bacteria (SRB), which is also commonly found in anaerobic digester sludge, have the capability to reduce arsenate by using it as terminal electron acceptor (Hoeft et al., 2001; Harrington et al., 1998; Newman et al., 1997). When arsenate and sulfate ions are present together, the rate of arsenate reduction could be faster than the rate of sulfate reduction. This results in higher rate of arsenic reduction which subsequently promotes arsenic release. Also, most of column experiments studying arsenic behavior in iron rich, anaerobic soil/sediments, have run for relatively short periods of time, usually less than a month, which is comparable in duration to the arsenic lag phase (ca. 30 d) in our reactors. With increased reaction time, cessation of the phase transitions and ensuing reductive dissolution result in prolonged release of As(III) to the aqueous phase (Tufano et al., 2008). Their results suggest that arsenic retention during iron reduction is temporally dependent on secondary precipitation of iron phases. Nevertheless, as it is shown in Table 2.3, the association of arsenic with iron varies with the mineralogy.

Table 2.3. Specific surface area and As adsorption capacity of iron minerals.

Compound	Specific Surface Area (m ² g ⁻¹)
Amorphous ferric hydroxide (Fe(OH) ₃)	600 ^a
Goethite (α -FeO(OH))	54 ^b
Siderite (FeCO ₃)	1.58 ^c
Vivianite (Fe ₃ (PO ₄) ₂ .nH ₂ O)	4.8 ^d

^a Roden and Zachara, 1996

^b Dixit and Hering, 2003

^c McCormick et al., 2002

^d Thinnappan et al., 2008

Table 2.4. XRD analysis shows iron transformation into biominerals along the column. The XRD patterns compared to the database show vivianite and siderite as the main species.

Column's Section (numbers increase in the flow direction)	Column's Mineralogy
IV	Siderite and Vivianite
III	Siderite and Vivianite
II	Siderite and Vivianite
I	Siderite and Vivianite

3.2. Batch Adsorption/Co-precipitation Study

The solids synthesized in our experiments were identified by XRD as crystalline siderite. Figure 2.6 shows an identification match between a sample and the corresponding siderite pattern. All the solids displayed a characteristic pale green color.

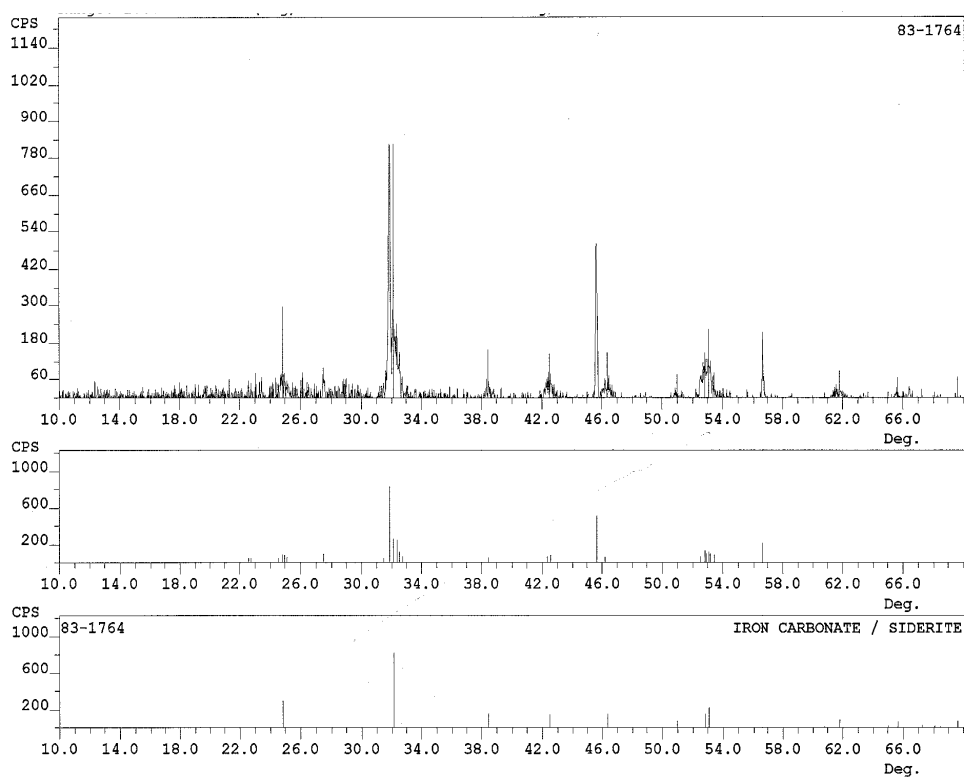


Figure 2.6. Powder-XRD pattern of synthesized mineral and match to siderite pattern.

3.2.1. Effect of Contact Time on Siderite Adsorption

We performed batch experiments utilizing synthesized siderite to study removal of arsenic from solution. The arsenic adsorption kinetic study was carried out with adsorbent dosage of 10 gL⁻¹ and initial As concentration of 100 mgL⁻¹. Results shown in Figure 2.7 demonstrate that adsorbed As, and therefore removal efficiency, increased with an increase in contact time for the first 2 weeks of the experiment with As(III) adsorption significantly higher than As(V). The adsorption rate slowed down afterwards and stayed relatively constant to the termination of the experiment after 6 weeks. This decrease in adsorption is likely due to the saturation of surface sorption sites indicating that system has reached equilibrium. About 35% of As(V) and 54% of As(III) were removed by the time that adsorption equilibrium was almost achieved after two weeks. The kinetic data show that As removal mainly occurred within the first 15 days and there was < 10% removal after this time up to 6 weeks. It means that an equilibrium of As adsorption on siderite was roughly attained after 2 weeks.

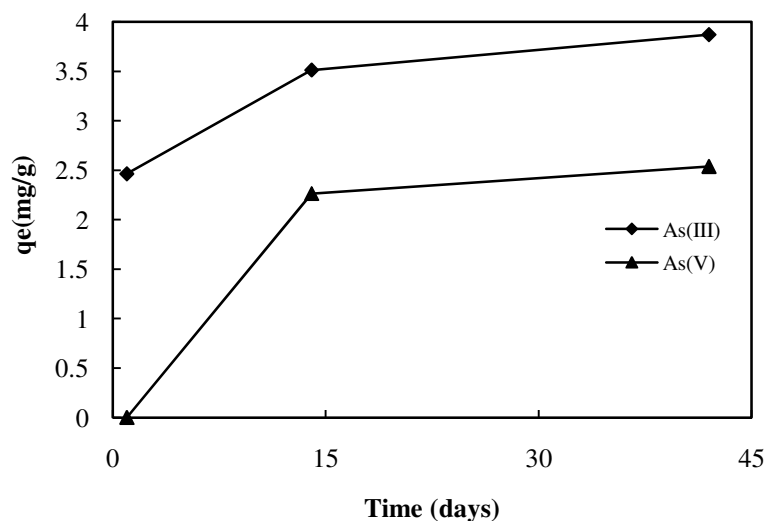


Figure 2.7. Effect of contact time on As concentration in the sorbent (q_e) from As(V) and As(III) solutions by siderite. Conditions: Adsorbent dosage =10 gL⁻¹, initial As concentration = 100 mgL⁻¹. For both As(V) and As(III), adsorption capacity increase over time for the first 2 weeks of the experiment after which it reached equilibrium to the termination of the experiment.

3.2.2. Effect of Contact Time on Siderite Co-precipitation

The arsenic co-precipitation study was carried out with initial As concentration of 100 mgL⁻¹ and final solid production of 80 gL⁻¹. Results presented in figure 2.8 show that after 24 h, the amount of As(V) precipitated with siderite slowly decreases, reaching < 65% of its first 24 h. Interestingly, As(III) co-precipitation and therefore its removal, follows a relatively constant, flat trend with only a minor drop after 72 h. In contrast with adsorption experiment, As(III) has lower tendency of co-precipitation with siderite compare to As(V). Therefore, it could be concluded that adsorption is the favorable mechanism of As(III) removal by siderite

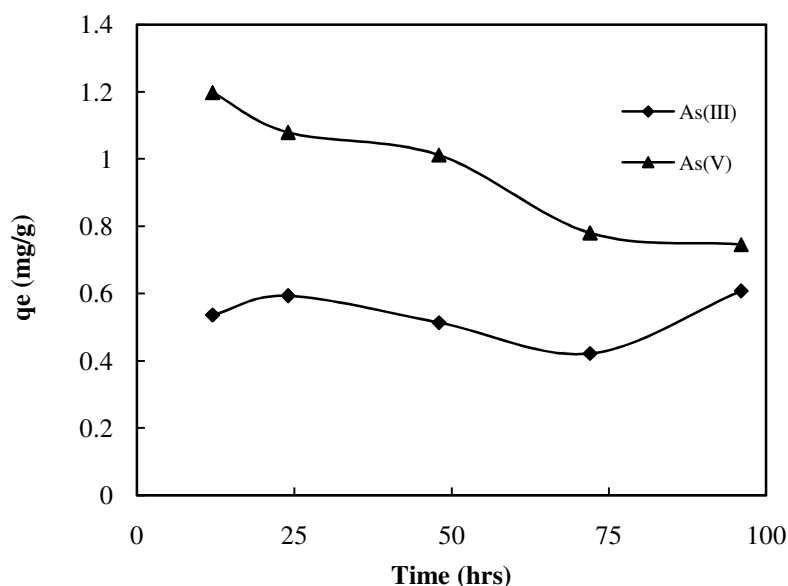


Figure 2.8. Effect of contact time on As co-precipitation from As(V) and As(III) solutions by siderite, with reaction conditions: solid produced = 80 gL^{-1} , initial As concentration = 100 mgL^{-1} . There was not a considerable removal difference in As(III) within duration of experiment, however, 30% removal decrease was observed in As (V) at the end which was still 20% higher than that of As(III).

3.2.3. Siderite Adsorption Isotherm

The adsorption isotherms were measured at room temperature for a range of arsenite and arsenate initial concentrations of 0.2-100 ppm and pH of ~ 7.5 with adsorption maxima being highest for As(III) at 100 ppm with adsorption capacity of 3.52 mgg^{-1} (Table 2.5).

The choice of an isotherm model was based on its ability to fit the sorption equilibrium data for at least one of the arsenic redox species studied. In this study, the Freundlich isotherm satisfied this condition by yielding a better fit to the experimental data with

regard to As adsorption on the synthetic siderite and therefore was adopted (Figure 2.9). Arsenic adsorption data fit to Langmuir isotherm is presented in supplementary information. The Freundlich isotherm is given by:

$$q_e = k_F \cdot C_e^{1/n_F} \quad (1)$$

where q_e (mg g⁻¹) is the amount adsorbed per unit mass of the adsorbent, C_e is the solution concentration at equilibrium (mg L⁻¹), and k_F and n_F are Freundlich constants denoting the adsorption capacity and intensity respectively. Because Freundlich isotherm model can be applied to multilayer sorption as well as non-ideal sorption on heterogeneous surfaces (Gue et al., 2009), it could be speculated from our data that the multilayer adsorption would be involved in the process of As removal by the synthetic siderite. The values of k_F and n_F were obtained from the slope and intercept of the linear Freundlich plots and listed in Table 2.6. The calculated n_F lies in the range between 0.2 and 0.7, denoting favorable adsorption of As(V) onto the synthetic siderite.

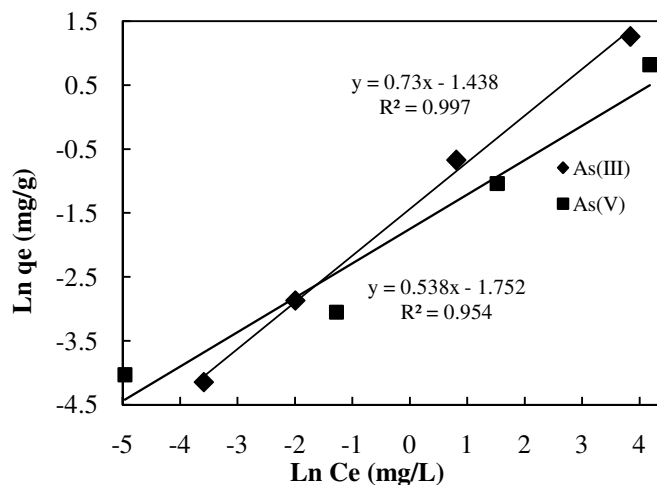


Figure 2.9. Freundlich plots for As adsorption from As(V) and As(III) solutions on siderite, with reaction conditions: adsorbent dosage = 10 gL⁻¹; initial concentrations = 0.2–100 mgL⁻¹; contact time = 2 weeks.

3.2.4. Siderite Co-precipitation Isotherm

The co-precipitation isotherms were measured at room temperature for a range of arsenite and arsenate initial concentrations of 0.2–3500 ppm and pH of ~7.5 with removal maxima being highest for As(III) at 3500 ppm with adsorption capacity of 440.60 mgg⁻¹ (Figure 2.10). Removal capacity for initial As(III) solution of 100 ppm in co-precipitation experiment is 0.59 mgg⁻¹, which is about 43% of its value from adsorption experiment. It could be concluded that at a given initial arsenite concentration, arsenic removal through adsorption is more efficient than co-precipitation. However, both As(III) and As(V) are following a very similar removal trend, with As(V) following slightly behind.

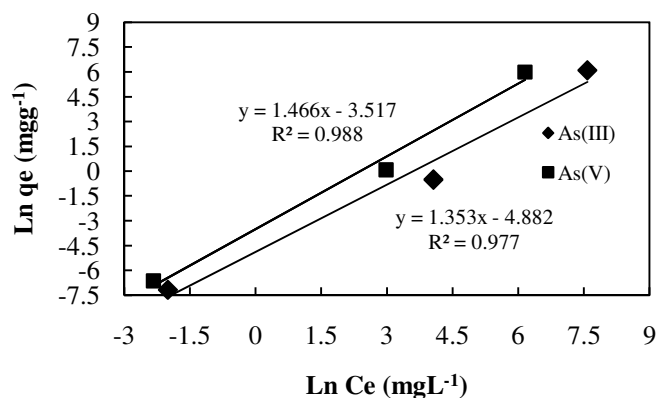


Figure 2.10. Freundlich plots for As co-precipitation from As(V) and As(III) solutions on siderite, with reaction conditions: Solid mass produced = 80gL^{-1} ; initial concentrations $=0.2\text{--}3500\text{ mgL}^{-1}$; contact time = 24 h.

Table 2.5. Siderite and vivianite capacity for arsenic adsorption obtained from literatures and our experimental results.

Mineral	Literature Values		Lab Results	
	Adsorption Capacity for Arsenate	Adsorption Capacity for Arsenite	Adsorption Capacity for Arsenate	Adsorption Capacity for Arsenite
	($\mu\text{mol g}^{-1}$)	($\mu\text{mol g}^{-1}$)	($\mu\text{mol g}^{-1}$)	($\mu\text{mol g}^{-1}$)
Siderite (FeCO_3)	6.94^a	13.9^a	30.3^*	46.9^*
Vivianite ($\text{Fe}_3(\text{PO}_4)_2 \cdot n\text{H}_2\text{O}$)	N/A	N/A	421	496

^a Gue et al, 2007 (Natural Siderite)

*Values reported based on highest q_e obtained in the experiment.

Table 2.6. Freundlich isotherm parameters describing the arsenic sorption capacity of siderite based on the data obtained in this study, where k_F represents the adsorption capacity of the adsorbent, and n_F represents the adsorption intensity parameter.

	$k_F[(\text{mg/g})(\text{L/mg})^n]$	n_F
As(V) Co-precipitation	-3.517	1.466
As(III) Co-precipitation	-4.882	1.353
As(V) Adsorption	-1.752	0.538
As(III) Adsorption	-1.438	0.730

3.2.5. Synthesized Vivianite Characterization

The solids synthesized in these experiments were identified by XRD as crystalline vivianite with no major impurities. Figure 2.11 shows an identification match between a sample and the corresponding vivianite pattern.

All the solids displayed a characteristic green color, although different shades were observed. We may attribute this to different degrees of structural oxidation of iron in the mineral, as has been previously documented to occur in vivianite at circumneutral pH (Thinnappan et al., 2008 and references therein). This oxidation was enough to cause changes at a macroscopic level, but no structural changes were detected by XRD. Generally, experiments with As(III) resulted in lighter green solids than experiments with As(V).

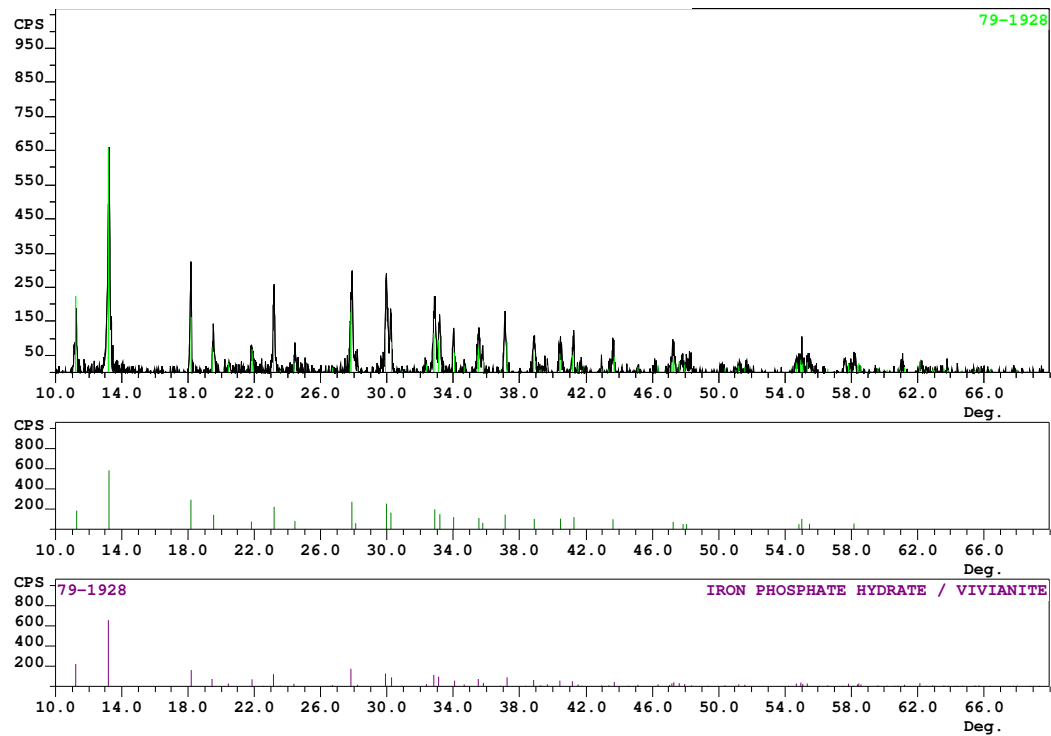


Figure 2.11. Powder-XRD pattern of synthesized mineral and match to vivianite pattern.

3.2.6. Vivianite Sorption/Co-precipitation Isotherms

Arsenic concentrations in the aqueous phase and in the solid were used to construct sorption isotherms. Data points for each of the synthesized samples were plotted with aqueous arsenic concentrations (in mgL^{-1}) in the x-axis, and solid arsenic concentrations (in mg of As/g of dry solid) in the y-axis. Langmuir isotherm models of the form:

$$qe = \frac{\alpha\beta Ce}{1+\beta Ce} \quad (2)$$

were used to describe the data, where q_e is the solid arsenic concentration, C_e is the aqueous arsenic concentration, and α and β are parameters that can be fitted to data (Table 2.7). Data were available for co-precipitation experiments in the range of 1200 mgL^{-1} aqueous concentration. Data for the adsorption experiments were only available in the range of 150 mgL^{-1} aqueous concentration. Co-precipitation (Figure 2.12, plots a and b), as well as adsorption (Figure 2.12, plots c and d) isotherms show a curve flattening out, indicating a decreasing sorption capacity as aqueous arsenic concentrations increase in the experimental range used, as is characteristic of a Langmuir-type process.

The average dissolved arsenic concentrations are below 80 mgL^{-1} for both natural environments (Smedley and Kinniburgh 2002) and the expected leachate from ABSR under landfill conditions (studies from our lab). The present study shows that within this relevant range, vivianite has a very similar sorption capacity for As(III) and As(V). More strikingly, both adsorption and co-precipitation experiments display very close trends in sorption isotherms. These similarities hint to a single common binding mechanism defining the sorption of arsenic onto vivianite. Table 2.4 presents arsenic adsorption capacity obtained from our lab work in comparison with literature values.

Comparing the results from co-precipitation with adsorption for both siderite and vivianite experiments, it could be concluded that co-precipitation is a much more efficient mechanism of removing arsenic from aqueous phase than adsorption.

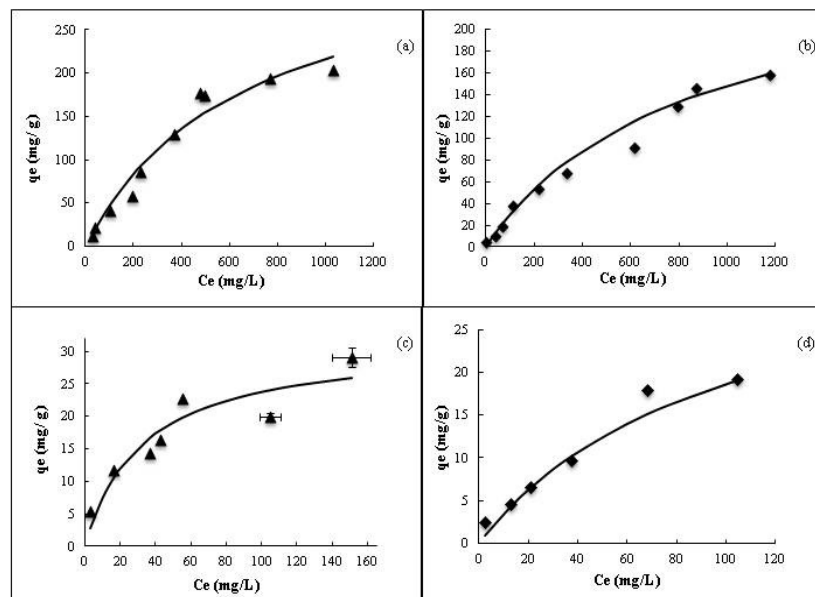


Figure 2.12. As(V) and As(III) co-precipitation (plots a and b) as well as adsorption (plots c and d) isotherms. Adsorption experiments were run at arsenic concentration: 150 mgL⁻¹ and co-precipitation experiments were run at arsenic concentration: 1200 mgL⁻¹.

Table 2.7. Langmuir parameters describing the arsenic sorption capacity of vivianite, where α represents the sorption maxima, and β represents the sorption intensity.

	α (mgg ⁻¹)	β
As(V) Co-precipitation	357.08	0.00154
As(III) Co-precipitation	274.33	0.00119
As(V) Adsorption	31.55	0.03054
As(III) Adsorption	37.14	0.01006

The mobilization of arsenic from arsenic-bearing solid residuals (ABSR) in non-hazardous landfills is known to be a consequence of ABSR reductive dissolution and subsequent formation of secondary minerals. Vivianite and siderite have been identified as two of secondary Fe(II) phase commonly formed in landfill environment, creating questions about its specific role in the mobilization of arsenic. Different nature of experimental conditions does not allows direct comparison between batch and column arsenic removal performances; Static vs. dynamic, abiotic vs. biotic, and short-term vs. long-term studies. However, it help us to better evaluate behavior of arsenic towards siderite and vivianite under reducing conditions.

The adsorption and co-precipitation results of this study indicate that synthesized vivianite and siderite may be good candidates as an arsenic sink in anoxic environments for a short period of time. They both show high removal capacity for arsenic in short-term batch experiments under static flow conditions. Arsenic is removed via both adsorption and co-precipitation, but overall uptake is greater in the vivianite/siderite co-precipitation experiment. It could be due to the fact that in the presence of arsenic species, precipitation of ferrous biominerals would incorporate As(III)/As(V) mainly into the crystalline matrix instead of sorption on the mineral surface which is the main removal mechanism for adsorption experiments, thereby removing more arsenic from solution than adsorption alone. Freshly synthesized ferrous minerals have much more active sites on the surface. However, as the mineral ages over time, its sorption capacity reduces resulting in release of more labile sorbed arsenic species.

Under dynamic column conditions, reductive dissolution of AFH drives formation of siderite and vivianite, resulting in removal of mobilized arsenic back to the freshly formed biominerals in early stage of column operation via both incorporation in and sorption on to the minerals. However, naturally formed biominerals have less affinity for arsenic removal than synthetic minerals (Guo et al., 2007 and 2009; Thinnappan et al., 2008) as naturally occurring, well-crystallized biominerals have limited surface area (Table 2.3). Moreover, naturally precipitated siderite/vivianite have been aged for a long-term period inside the simulated landfill column and therefore have lost their active sites over time. Also, different mechanisms control arsenic removal with natural and synthetic siderite; adsorption on the synthetic siderite is a relatively quick process predominated by chemical reactions, whereas the adsorption on the natural siderite is a more complex process controlled by diffusion, exhibiting the slowest step in the primary and secondary porosity (Guo et al., 2009).

The results of this study suggest that vivianite and siderite could be two potential sinks for As removal under landfill conditions with more stable, efficient removal through co-precipitation. However, the Fe(II) minerals are not nearly as effective at sorbing arsenic as iron (hydr)oxides.

4. Conclusions

Understanding the effect of biomineralization on arsenic mobility is crucial to predict the fate of arsenic in landfills, and ultimately, to make the most informed decisions about

ABSR disposal. The adsorption and co-precipitation results of this study indicate that synthesized vivianite and siderite may be good candidates as an arsenic sink in anoxic environments for a short period of time. However, short term batch experiments underestimate the long-term sorption/retention behavior of ferrous minerals towards arsenic. The simplified experimental conditions used in this study inevitably will lead to overestimation of the sorption capacity of siderite/vivianite in landfills and natural environments, as they fail to account for competition with other organic and inorganic ligands that would be present.

Comparing the results from co-precipitation with adsorption for both siderite and vivianite experiments, it could be concluded that co-precipitation is a more efficient mechanism of removing arsenic from aqueous phase than adsorption as arsenic gets incorporated into the crystalline matrix through co-precipitation instead of sorption on the mineral surface that is a weaker association and may release the sorbate back into the solution because of surface aging and reduction of sorption sites.

Moreover, minerals like siderite/vivianite that are formed from iron reduction of solid residuals have a greater capacity to sorb arsenic than naturally occurring minerals. This is due to the fact that different mechanisms control arsenic removal with natural and synthetic mineral; adsorption on the synthetic mineral is a relatively quick process predominated by chemical reactions, whereas adsorption on the natural mineral is a more complex process controlled by diffusion.

Further work on the sorption/co-precipitation of arsenic and determination of efficiencies and uptake mechanisms under conditions relevant to those govern in landfills as well as XAS investigation of arsenic species association with iron, in presence of siderite and vivianite is warranted.

CHAPTER 3

BIOMINERALIZATION CONTROLS ARSENIC MOBILITY IN MATURE LANDFILL CONDITIONS

1. Introduction

The U.S. Environmental Protection Agency revised the Maximum Contaminant Level (MCL) of arsenic in drinking water to $10 \mu\text{g L}^{-1}$, enforceable January 23, 2006, and this has caused a significant increase in the volume of arsenic-bearing solid residuals (ABSR) generated by drinking water utilities (as projected by Meng et al., 2001). Because of their high adsorption capacity and relatively low cost, iron-based sorbents are widely utilized and, when spent, comprise the bulk of the ABSR waste stream generated by water utilities in the U.S. The iron-based sorbents depend on ferric (Fe^{3+}) surface sites for adsorption; typical sorbents are some form of ferrihydrite ($\text{Fe}(\text{OH})_3 \cdot n\text{H}_2\text{O}$) or goethite ($\alpha\text{-FeOOH}$) (Amy et al., 2000; US EPA., 2002; Impellitteri and Scheckel, 2006; Mohan and Pittman, 2007). Commonly, the ABSR pass the Toxicity Characteristic Leaching Procedure (TCLP), which enables them to be disposed to nonhazardous, municipal solid waste (MSW) US landfills (US EPA, 2003). However, mature MSW landfills are complex systems characterized by mildly alkaline, reducing conditions, with diverse microbial communities and high organic matter content (Christensen et al., 2001; Ghosh et al., 2006; Kjeldsen et al., 2002). Thus, when ABSR are subjected to landfill conditions, the mobility and speciation of both iron and arsenic can be affected, often leading to

enhanced leaching (Ghosh et al., 2004; Ghosh et al., 2006; Jing, 2005; Jing et al., 2008; Clancy et al., 2013).

The iron based drinking water arsenic sorbents are similar mineralogically to those implicated in arsenic immobilization in natural oxidized systems, primarily ferric (hydr)oxides (Amy et al., 2000; Benner et al., 2002; Smedley and Kinniburgh, 2002; Nordstrom and Archer, 2003; Mohan and Pittman, 2007; Cances et al., 2008). As in natural suboxic environments, Fe(III) reduction in MSW landfills is mediated microbially, and subsequent Fe(II/III) biomineralization in supersaturated solutions generates common secondary minerals, such as siderite, vivianite, and mixed-valent iron minerals such as magnetite and green rust (Meng et al., 2001; O'Day et al., 2004; Ghosh et al., 2006; Burnol et al., 2007; Root et al., 2009; Kirk et al., 2010; Kocar et al., 2010; Root et al., 2013). When sufficient sulfide is present, immobilized arsenic is generally found in (or associated with) sulfidic minerals (Cullen and Reimer, 1989; O'Day et al., 2004; Blanchard et al., 2007; Cances et al., 2008; Nordstrom et al., 2003; Smedley and Kinniburgh, 2002; Root et al., 2009; Kirk et al., 2010). However, when a transition from oxidizing to reducing conditions occurs with sulfate present, the degree to which iron-associated arsenic remains sequestered, is re-sequestered by formation of new mineral phases containing either or both iron and sulfur, or is released to aqueous solution is complicated and has been the subject of considerable research (Root et al., 2009). Potentially important factors include the initial solid-phase arsenic bonding environment (Burnol et al., 2007; Dixit and Hering, 2003; Ford et al., 2006; Burton et al., 2012; Jeong et al., 2010); the concentrations of aqueous species, including but not limited to Fe, As,

and S (Ghosh et al., 2006; Ford et al., 2006; Mukiibi et al., 2008; Charlet and Polya, 2006); the hydrodynamic conditions (Benner et al., 2002; Hansel et al., 2005; Herbel et al., 2006); kinetics and local microenvironments creating disequilibrium conditions (Benner et al., 2002; Hansel et al., 2003; O'Day et al., 2004; Postma and Jakobsen, 1996); and the time frame of interest (Majzlan et al., 2007; O'Day et al., 2004; Ghosh et al., 2006; Pigno et al., 2006). In landfill conditions, the fate of As is tied to the microbially-mediated reduction of S and Fe coupled to the oxidation of organic carbon. The mass fraction of arsenic sorbed to iron(oxyhydr)oxides decreases upon reductive dissolution and transformation of these ABSRs to more crystalline phases because of an attenuation of surface site reactivity (Bose et al., 2002; Pedersen et al., 2006; Tufano and Fendorf, 2008). However, in the presence of excess $S^{2-}_{(aq)}$, mobilized As(III) could be re-sequestered via precipitation of amorphous As_2S_3 or other crystalline As-S phases, and/or via sorption to newly formed Fe-S phases (O'Day et al., 2004; Gallegos et al., 2009; Kirk et al., 2010; Upadhyaya et al., 2010; Root et al., 2013). These secondary Fe and As sulfides can form through both biotic and abiotic routes (Canfield et al., 1992; Hansel et al., 2003; Poulton et al., 2003 and 2004; Saalfield et al., 2009; Kirk et al., 2010).

Diverse SRB species also have the capability to reduce arsenate as a terminal electron acceptor and, therefore, molybdate, a well-known SRB inhibitor, also inhibits arsenate reduction by SRB (Hoeft et al., 2002; Harrington et al., 1998; Newman et al., 1997). Newman et al. (1997) suggests that dissimilatory arsenate reduction might occur in the sulfidogenic zone at arsenate concentrations of environmental interest. They showed nearly complete inhibition of arsenate reduction when molybdate was added in a

monocultural set of experiments, where the particular microbial community (*Desulfotomaculum auripigmentum* sp. nov.) chosen was able to reduce both arsenate and sulfate. Figure 3.1 illustrates the possible fates of ABSR arsenic after landfill disposal. The number and complexity of factors influencing arsenic mobilization, as redox conditions transition from oxic to suboxic and anoxic, makes prediction of arsenic leaching from ABSR under mature landfill conditions very difficult. Improved understanding can be obtained through mechanistic studies on simplified systems that nonetheless represent the complexity of process couplings and feedbacks discussed above. However, mature MSW landfill, complex-system, ground-truthing studies are largely lacking to date.

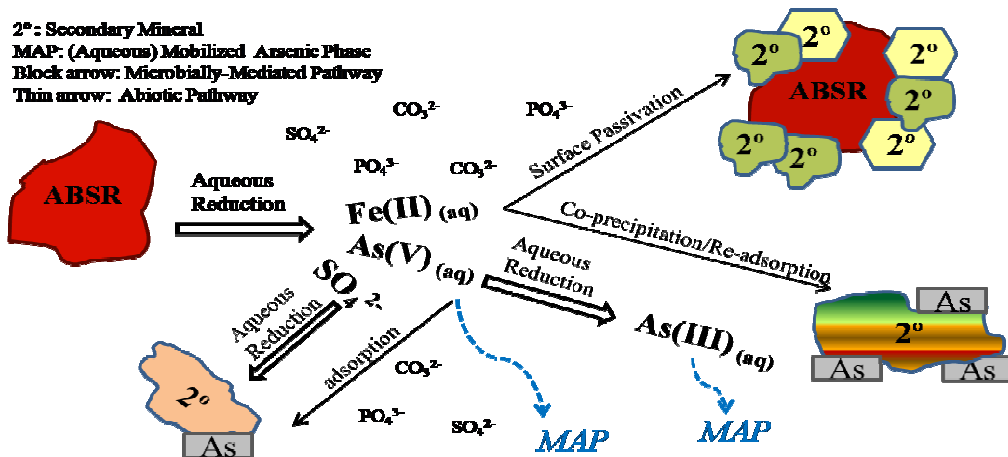


Figure 3.1. The primary routes of iron and sulfate reduction in landfills are microbially mediated and secondary mineral formation is a common by-product. Biomineralization plays a key role in determining whether or not desorbed As will be sequestered under landfill conditions.

In the present work, we conducted a series of advective-flow, column experiments to simulate the biochemical and hydraulic conditions of a mature MSW landfill. The aim was elucidation of mechanisms controlling arsenic leaching from an amorphous ferric hydroxide sorbent ABSR, such as those generated in removal of arsenic from drinking water directly or in removal of arsenic from the aqueous residual streams of ion exchange and membrane processes used for removal of arsenic from drinking water. A primary focus was on the generation and effects of secondary minerals derived from transformations of the amorphous ferric hydroxide (AFH). Most prior column studies have been short-term experiments of less than 3 months, which fail to demonstrate long-term Fe/As transformations and the mobilization of end-products, that would likely occur under long-term mature landfill disposal of ABSR. Additionally, many reported column experiments employ a single microbial strain rather than the broader microbial consortium that is present in a mature landfill. The current work differs from related, arsenic-bearing ferric sorbent studies focused on transition to a reductive environment in the extended duration of the trials (up to 400 d) (Kocar et al., 2010; Pederson et al., 2006; Tufano et al., 2008a; Tufano et al., 2008b; Benner et al., 2002; Burnol et al., 2007; Fredrickson et al., 1998; Herbel and Fendorf, 2006; Hansel et al., 2003; Impellitteri et al., 2006; Kocar et al., 2006; Jing et al., 2008;), the mixed bacterial consortia used (Kocar et al., 2010; Burton et al., 2013; Tufano et al., 2008a; Tufano et al., 2008b; Benner et al., 2002; Burnol et al., 2007; Fredrickson et al., 1998; Herbel and Fendorf, 2006; Hansel et al., 2003; Impellitteri et al., 2006; Kocar et al., 2006), the varied sulfate influent concentration as an independent variable (Pederson et al., 2006; Tufano et al., 2008a; Tufano et al., 2008b; Burnol et al., 2007; Fredrickson et al., 1998; Herbel and Fendorf, 2006;

Impellitteri et al., 2006; Kocar et al., 2006; Jing et al., 2008;), and hydraulic flow through the reactor (Saalfeld et al., 2009; Pederson et al., 2006; Fredrickson et al., 1998; Jing et al., 2008;);all of which are necessary to simulate ABSR response to disposal in mature landfills. The results demonstrate that As release from ABSRs may readily exceed the arsenic toxicity characteristic for extended durations, bringing into question the wisdom of the current practice of disposal in non-hazardous landfills.

2. Materials and Methods

2.1. Sludge Preparation

Arsenic-bearing iron sludge was prepared to simulate the waste generated by treatment of brines from arsenic removal ion exchange/membrane processes generally employed in drinking water treatment. Sodium arsenate heptahydrate ($\text{Na}_2\text{HAsO}_4 \cdot 7\text{H}_2\text{O}$, KR Grade, Sigma-Aldrich) was dissolved in purified water (Milli-Q Water System by Millipore) to prepare a 1 L solution with a concentration of 0.047 M As. Ferric chloride hexahydrate ($\text{FeCl}_3 \cdot 6\text{H}_2\text{O}$, ACS reagent, Sigma-Aldrich) was added to the As solution to produce supersaturated, 0.935 M Fe solutions with final Fe:As molar ratios of 27, 21, 21, and 24 for the low sulfate (LS; 0.064 mM), LS-BES, (LS with 1 mM 2-bromoethanesulfonic acid added) LS-Mo (LS with molybdate added), and HS (high sulfate; 2.08 mM) columns, respectively. Mixtures were stirred on a reciprocating shaker table (Orbit, reciprocating speed 100 rpm) for 1 h before adjusting the pH to 7.0 ± 0.2 with 10.0 M sodium hydroxide (NaOH, flakes, EMD Chemicals). The ferric hydroxide solid

product was identified by X-ray diffraction as two-line ferrihydrite ($\text{Fe}(\text{OH})_3 \cdot n\text{H}_2\text{O}$) and is hereafter referred to as amorphous ferric hydroxide (AFH). The AFH was equilibrated for 2 d while the pH was maintained at 7.0 ± 0.2 . After equilibration (48 h) and settling, a supernatant sample was syringe filtered through a $0.45 \mu\text{m}$ cellulose acetate filter for determination of concentrations of dissolved As and Fe in equilibrium with the solid. Subsequently, the residual salt content (sodium chloride) of the AFH was reduced by decanting the supernatant solution and washing the solid residual in a 4 L flask with deionized (DI) water, mixing gently, and allowing to resettle for 3-4 hours. This procedure was repeated until the conductivity of the supernatant solution was below 1.0 mS cm^{-1} . During this process, the pH remained constant (7.0 ± 0.2) without further adjustment. The final slurry was vacuum filtered through a $0.45 \mu\text{m}$ filter (cellulose nitrate, Whatman). The AFH water content was calculated by mass loss at 70°C for 2 d. The AFH was stored in a capped-glass container at 4°C and used within 3 weeks.

2.2. AFH Characteristics

Total Fe and As in the AFH were determined by digestion of 1 g (dry wt.) sample, using 15 mL concentrated (70%) HNO_3 (J.T. Baker) in a CEM microwave digester following method SW 821-8051. Ferrous and total iron were determined by the 1,10-phenanthroline method (APHA, 1998) at 510 nm wavelength (Spectronic Genesys 5). Total and speciated arsenic were measured by inductively coupled plasma mass spectrometer (ICP-MS, Agilent 7500a) and HPLC-ICP-MS, respectively. The solid-phase As and Fe concentrations were, respectively, $340.6 \text{ mmol kg}^{-1}$ (25.52 mg g^{-1}) and $9172 \text{ mmol kg}^{-1}$.

(513.06 mgg⁻¹) for the LS column and 417.0 mmol kg⁻¹ (31.24 mgg⁻¹) and 9169 mmol kg⁻¹ (521.03 mgg⁻¹) for the HS column. Chromatography-type columns (Spectrum Chromatography; 2.5 cm ID × 30 cm length) were packed with 80 g (wet wt.) of the arsenic-laden AFH, mixed with 120 g of glass beads (0.8 mm diameter), to give packed material hydraulic permeability and a homogenous distribution. Anaerobic digester sludge obtained from Ina Road Wastewater Treatment Plant, Tucson, Arizona (25 ml of slurry) was added as the mixed, anaerobic microbial community source. Column feed was a synthetic landfill leachate (Field et al., 2003) adapted by replacing all chloride with sulfate salts to avoid chloride peak interference in ion chromatographic (IC) analysis. The influent sulfate concentrations were 0.064 mM for the LS columns and 2.08 mM for the HS columns. The influent feed was made with de-gassed water and purged with nitrogen gas after mixing. Synthetic landfill leachate influent was fed continuously into the columns using a multi-syringe pump (BS-9000-6, Braintree Scientific) at an average rate of 2.0 pore volumes d⁻¹ for columns LS-1, LS-BES, and LS-Mo and 0.6 pore volumes d⁻¹ for HS column. Effluent samples, filtered through 0.45 µm syringe filters (cellulose nitrate, Whatman), were analyzed to quantify arsenic and iron. Ion chromatography (IC, Dionex, DX-500) was used to quantify sulfate, lactate and acetate.

For all columns, the organic carbon source was 5.5 mM lactate fed continuously. The HS column feed included 2.08 mM sulfate, while LS columns received 0.064 mM sulfate. Two of the LS columns were run under the influence of microbial inhibitors. In one (LS-BES), acetoclastic methanogenic bacteria were inhibited by the addition of 1 mM 2-bromoethanesulfonic acid (BES) sodium salt (BrCH₂CH₂SO₃Na, Sigma-Aldrich) (Perkins et al., 1994; Oremland and Capone, 1988). BES addition started on day 139 (of 327 d) to

investigate how inhibition of methanogens as a substrate (acetate) competitor might influence As reduction. Methanogenic bacteria utilize acetate and hydrogen as their electron donors and, consequently, may compete with iron, sulfur, and arsenate reducing bacteria for a portion of the e^- donor pool, thus potentially decreasing the activity of the processes of primary interest. The second inhibited column (LS-Mo) received addition of 2-sodium molybdate(VI) dehydrate ($\text{Na}_2\text{MoO}_4 \cdot 2\text{H}_2\text{O}$, Acros Organics) to inhibit sulfate reducers. Molybdate was added at a concentration of 0.5 mM at day 99, increased to 1 mM at day 121, and to 10 mM at day 124. The molybdate concentration was decreased to 5 mM after 175 days, 2.5 mM at day 191, and finally stopped at day 208. Although the sulfate concentration in the influent was only 0.064 mM, extra molybdate was added to block the activity of the SRB that would be reducing sulfate and potentially arsenate.

2.3. Solid Phase Characterization

The landfill simulation columns were run for durations from 327 to 432 days (Table 3.1). After termination, the columns were opened in an oxygen free glove box (Terra Universal 100). The contents were divided into four, approximately equal volume sections, numbered sequentially in the upward direction of flow. Each section was dried in the glove box at room temperature for 7 days after which a 0.5 mm sieve was used to separate glass beads from other solids. Solid phases were analyzed by powder X-ray Diffraction (XRD), scanning electron microscopy (SEM), X-ray absorption spectroscopy (XAS), X-ray fluorescence (XRF), and sequential extraction. XAS and XRF were conducted at the Stanford Synchrotron Radiation Lightsource (SSRL) with details and results described

elsewhere (Root et al., 2013). Powder XRD was conducted using a Scintag XDS 2000 PTS Diffractometer with Cu-K α radiation ($\lambda = 1.54060 \text{ \AA}$) operated at 40 kV and 40 mA. Diffraction patterns were recorded by continuous scans from 10° to $70^\circ 2\theta$ at a scan rate of $2^\circ 2\theta \text{ min}^{-1}$. Mineral phases were identified using the International Centre for Diffraction Data (ICDD) database. Solid phase extractions were performed for Fe and As quantification. The extraction was by 6M HCl followed by aqua regia (3:1 HCl/HNO₃), although in no case the aqua regia extract more than 10% additional Fe or As. The dried solid had about 1% moisture (w/v). For extraction step 1 and 2 the samples were stirred on a reciprocating shaker table (Orbit, 100 rpm) for 48 h and the supernatant sample was filtered through 0.45 μm filter (cellulose nitrate, Whatman), before analysis. For step 3 the samples were stored at 4°C for 12 h before analysis of filtered supernatant solution.

Table 3.1. Designations, distinctive feed characteristics and durations of operation of simulated mature landfill columns used in study.

Column ID	[SO ₄ ⁻²] (mM)	Feed Additives (microbial activity inhibitors)	Retention Time (hrs)	Duration of Operation	
				Time (Days)	PV
LS	0.064	-	12	432	864
LS-Mo	0.064	Molybdate	12	327	654
LS-BES	0.064	2-Bromoethanesulfonic acid (BES)	12	327	654
HS	2.08	-	36	331	198

3. Results and Discussion

3.1. Arsenic and Iron Leaching Trends

Effluent pH was measured bi-weekly and fluctuated between 7.5-8.0 for all LS (0.064 mM) columns and between 7.5-8.3 for the HS column. Despite differences in influent sulfate concentration and the presence or absence of microbial inhibitors, all ABSR-loaded columns exhibited a qualitatively similar trend in effluent arsenic concentration as a function of time (Fig. 2). An asymmetric bell-shaped curve characterized these trials, similar to arsenic-leaching from prior advective-flow, long-duration studies (Ghosh et al., 2006; Kirk et al., 2010; Menget et al., 2001). Leaching from the columns' ABSR starts with a phase of relative arsenic retention, despite immediate AFH reduction as indicated by the presence of Fe^{2+} in the effluent (not shown). This period of AFH reductive dissolution without substantial arsenic mobilization from the column varied from 58 to 65 d (37 to 130 PV). The early retention stage may be due to microbial acclimatization, or the re-adsorption of released arsenic onto newly exposed AFH and re-precipitated iron (predominantly magnetite, $\text{Fe}^{3+}_2\text{Fe}^{2+}\text{O}_4$) as AFH undergoes reductive dissolution (Kocarek et al., 2006; Pederson et al., 2006; Tufano et al., 2008), or a combination of these factors. In column trials lasting 90 d, Tufano et al. (2008) observed that AFH reductive transformation initially enhanced arsenic retention (relative to release from an abiotic column), depending on the influent lactate concentration (0.08 to 7.7 mM). In the simulated landfill columns here receiving 5.5 mM lactate, the lag phase was followed by a continuous increase of effluent concentration to a maximum occurring after 3-4 months. The onset of this period of increasing arsenic release was also observed by Tufano et al. (2008) (but not subsequently monitored or quantified) and it was attributed therein to

the depletion of Adsorption sites resulting from continued iron reductive dissolution. In all LS and HS columns, this phase was characterized by effluent arsenic concentrations in excess of 200 μM (15 mgL^{-1}As). After peak As leaching, effluent concentrations dissipated rapidly to below 50 μM by about 200 d before tailing off more slowly through the balance of the trial. This arsenic leaching behavior is qualitatively consistent with that observed from the commercial, ferric iron-based sorbent, GFH, during a 900 d leaching trial (Ghosh et al., 2006) and with an As-S-Fe system 300 d trial using arsenic-feed and a goethite ($\alpha\text{-FeOOH}$) sorbent (Kirk et al., 2010). A number of flow-through leaching studies of As-Fe and As-S-Fe systems have not reported this four stage release (lag, rapid increase, peak-tapering, and finally decrease) behavior in As leaching (Kocar et al., 2006 and 2010; Tufano et al., 2008; Impellitteri and Scheckel, 2006; Burton et al., 2011 and 2013; Herbel et al., 2006). Evidently, study durations of less than 3 months typically miss the leaching trends described here.

3.2. Mobilized As Concentration

The arsenic-laden AFH mimics the spent residual generated in a coagulation/filtration process using addition of iron salts for removal of arsenic from drinking water or the brine stream from a membrane or ion exchange arsenic removal process (Scott et al., 1995; US EPA, 2002; Amy et al., 2000; Hering et al., 1996). Currently the ABSR from water treatment processes generally pass the TCLP used to determine if an ABSR may be disposed in a non-hazardous landfill, (Ghosh et al., 2006; Meng et al., 2001). TCLP passage requires arsenic release below the “Toxicity Characteristic” (TC) limit of 5 mgL^{-1}

(60 μM) from ABSRs. Based on the concept that a leaching test, such as the TCLP, must challenge the residuals with an environment that is at least as aggressive as the final disposal environment, passing the TCLP implies that ABSRs will leach less than the TC after landfill disposal. However, results of the simulated landfill column trials indicate arsenic concentrations higher than 5 mgL^{-1} for extended time periods (Figure 3.2). The maximum leaching concentration in the four columns ranged from 15 to $35.7 \text{ mgL}^{-1} \text{As}$ (200 to $476 \mu\text{M}$), with durations of arsenic leaching in excess of the TC ranging from 166 to 498 pore volumes. The likelihood that arsenic release by ABSRs under mature landfill conditions is not well predicted by use of the TCLP has been suggested for over a decade (Hooper et al., 1998; Ghosh et al., 2004; Meng et al., 2001). However, most studies of ABSRs or similar sorbents' behavior under landfill conditions were short term experiments (Kocar et al., 2006 and 2010, Tufano et al., 2008, Burton et al., 2011 and 2013), did not employ ABSRs or surrogates (deLemos et al., 2006; Veselska et al., 2013), or used a single microbial species to induce greater experimental control, and consequently did not fully demonstrate the mature MSW landfill environmental impact on ABSR-bound arsenic fate. Long-term exposure of ABSR to simulated mature landfill conditions in the presence of realistic microbial consortia indicates that the TCLP significantly underestimates arsenic leaching from water treatment residuals and that the leaching may readily exceed the arsenic TC (Figure 3.2).

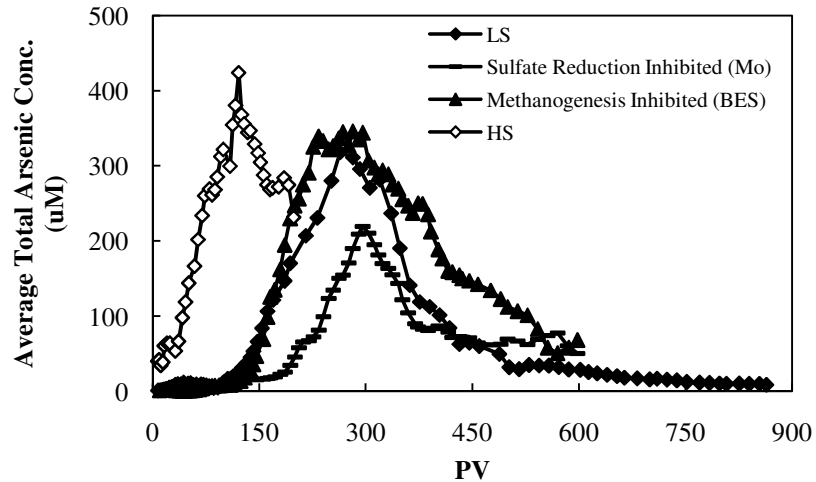


Figure 3.2. Arsenic leaching from all columns followed the same asymmetric bell curve, including an approximately 60 day lag phase, a rapid increase to an effluent concentration greater than 200 mM, and a slow tapering decline.

3.3. Fe/As Leaching Stoichiometry

The issue of arsenic release (or lack thereof) from iron (oxyhydr)oxide sorbents (both natural and engineered sorbents and under both natural and engineered conditions) has been of intense interest for well over a decade (Cummings et al., 1999; Ghosh et al., 2006; Tufano et al., 2008; Muramatsu et al., 2012; Burton et al., 2013a; Langner and Inskeep, 2000; Burton et al., 2013b; Appelo et al., 2002; Zobrist et al., 2000). The corollary issue of the relative release of iron and arsenic has been discussed often (Cummings et al., 1999; Zobrist et al., 2000; Horneman et al., 2004; van Geen et al., 2004; Burnol et al., 2007; Cortinas et al., 2008; Silva et al., 2012). Despite other differences in arsenic leaching behavior and variation in the fraction of arsenic leached over the duration of the runs as discussed later, the iron to arsenic leaching ratio was in all cases proportionately much less than the initially loaded ratio. This has been sometimes referred to as decoupling of iron and arsenic where decoupling is defined operationally

(Horneman et al., 2004; van Geen et al., 2004; Burnol et al., 2007) as disproportionate leaching of iron to arsenic compared to that initially present in the system. In all columns the initial Fe:As molar ratio of the ABSR was $25 \pm 3:1$, whereas the effluent ratios were never greater than 1:100 and the average cumulative ratio of leached masses was between 1.4×10^{-4} - 8.2×10^{-3} (Figure 3.3). A significant decrease in the Fe:As molar ratio signaled the end of the lag phase, which in all cases lasted from 58-65 d. Lag phase Fe/As ratios were 6.8, 12.5, 6.4, and 11.1 times greater than the post-lag phase ratio for LS, LS-Mo, LS-BES, and HS columns, respectively (Figure 3.3). An earlier ABSR-landfill study showed similar disproportionate arsenic to iron leaching, although there iron was released more readily from the commercial, iron-based sorbent during the initial retention stage, whereas in all later phases, as here, arsenic release was proportionately much greater than that of iron (Ghosh et al., 2006). Similarly, others investigating the relationship of arsenic to iron release in natural systems observed a particular point where As release became independent of the Fe activity and exceeded its desorption rate by several fold (Horneman et al., 2004; van Geen et al., 2004; Burnol et al., 2007). Horneman et al. (2004) showed Fe/As non-stoichiometric release from sediment profiles into the groundwater of Bangladesh, where although dissolved As and Fe generally increased with depth, there was no correlation between their aqueous concentrations. The van Geen et al. (2004) study using sediment incubations from Bangladesh is particularly relevant to this work as a primary independent variable determining the Fe:As release ratio was the presence or absence of acetate amendment to the incubations. In mature (methanogenic) landfill conditions, volatile fatty acids, including acetate, are a dominant electron donor and, as in the Bangladesh study, may determine the proportionality of iron to arsenic aqueous

mobilization. In the sediments amended with acetate, van Geen et al. (2004) found the total As released was between 60 to 80% of the initial solid content, while the Fe was between 0.5 to 2%. Non-stoichiometric release of Fe and As is consistent with either preferential As release from the intact AFH adsorbent or incongruent sorbent-sorbate transformation, where solubilized Fe was preferentially reprecipitated into a neo-formed solid phase. Results discussed below indicate predominance of the latter in the present set of experiments, but with precise mineral transformation paths being sensitive to influent sulfate concentration.

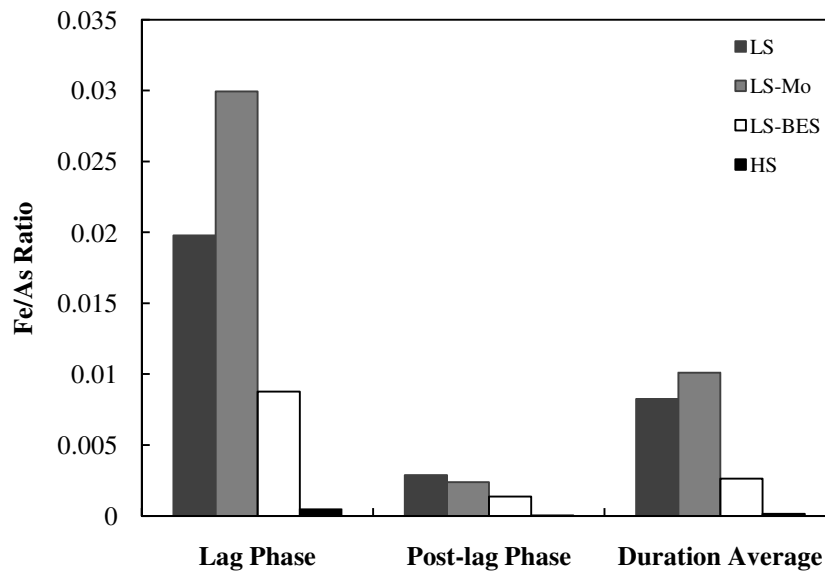


Figure 3.3. The lower Fe:As molar ratio in the effluent than the initial ABSR Fe:As molar ratio of greater than 22:1 demonstrates decoupling of iron from arsenic leaching in all trials. In addition, the lag phase ratio was greater than 6 times more than the post-lag phase ratio for any given column.

3.4. Secondary Mineral AsSorption

After termination, each column was divided into four zones of ca. equal bulk volume for solids characterization. During the first three weeks of operation all columns changed from orange to black in color, suggesting a solid phase iron redox transformation likely to magnetite (Zachara et al., 2002; Pederson et al., 2006; Tufano et al., 2008; Burton et al., 2011). Most work on microbial iron/arsenic transformation under reducing conditions, where formation of magnetite was confirmed, have been short term studies of 1 to 2 months (Zachara et al., 2002; Kocar et al., 2006 and 2010; Pederson et al., 2006; Tufano et al., 2008; Burton et al., 2011). Although magnetite peaks were not detected in our XRD scans of the final solids, an X-ray amorphous species cannot be ruled out and/or magnetite may have been a temporally transient phase (Table 2). Poorly-crystalline green rust and magnetite are potential mixed Fe(II)/Fe(III) intermediate phases preceding the formation of final Fe^(II) and other iron species detected by XRD and XAS (Table 3.2). Although early phase magnetite presence was not confirmed, its poorly-crystalline occurrence is consistent with Fe²⁺ pore water concentrations that were sufficiently high to poise the system for ferrous and green rust mineral precipitation, rather than Fe²⁺ sorption to ferrihydrite catalyzing enhanced goethite (α -FeOOH) formation (Zachara et al., 2002; Tufano et al., 2009; Yang et al., 2010; Raghav et al., 2014).

Table 3.2. Biominerals generated under LS and HS sulfate influent conditions.

Column's Section (In the Direction of Flow)	LS (Sulfate Conc. 0.064 mM)	LS-BES (Sulfate Conc. 0.064 mM)	LS-Mo (Sulfate Conc. 0.064 mM)	HS (Sulfate Conc. 2.08 mM)
I	Vivianite and Siderite	Vivianite, Siderite and Goethite	Vivianite and Siderite	FeS, AsS and Siderite
II	Vivianite and Siderite	Vivianite, Siderite and Goethite	Vivianite and Siderite	FeS, AsS, Siderite and Vivianite
III	Vivianite, Siderite and Goethite	Vivianite, Siderite and Goethite	Vivianite, Siderite and Goethite	FeS, AsS, Siderite and Vivianite
IV	Vivianite, Siderite and Goethite	Vivianite, Siderite and Goethite	Vivianite, Siderite and Goethite	Siderite, Vivianite, Green rust and Goethite

Selective chemical extractions of the column solids showed the mass of extractable iron species increased progressively in the direction of flow with the influent quadrant retaining less than 10% of its initial iron, while the mass increased progressively in the flow direction with the outlet quadrant (Q4) containing greater than 100% of the original mass present for the LS case (Figure 3.4a). In the HS case, more than 50% of the initial mass of iron relocated to the top two quadrants. Slower mass movement in HS case may be partially due to the lower flow rate of HS, at about 1/3 of the LS column, with the total of 198 and 864 PV passing through HS and LS columns, respectively. Since the sole reactive solid introduced into the columns was the simulated ABSR, the down-gradient relocation of iron mass indicates the reductive dissolution of AFH and transport of Fe^{2+} with subsequent secondary mineral formation along the flow path. Introduction of the primary electron donor generated the greatest reducing potential at the inlet, and consequently the most AFH reductive dissolution occurred there. A redox gradient in iron species was evident with ferrous species dominating the inlet, with an increasing

proportion of Fe^{3+} species with distance toward the outlet. As discussed in a companion paper that details the solid phase Fe and As speciation dynamics (Root et al., 2013), ferrous minerals, vivianite ($\text{Fe}_3(\text{PO}_4)_2 \cdot n\text{H}_2\text{O}$) and siderite (FeCO_3), were detected in all columns in all quadrants analyzed by XRD with the exception of the inlet quadrant of the high sulfate column, where vivianite was absent. Iron X-ray adsorption spectroscopy (XAS) data of the terminal solids showed mackinawite (FeS) and green rust ($[\text{Fe}^{2+}_6\text{Fe}^{3+}_x(\text{OH})_{12}]^{x+}[\text{A}^{2-}_{x/2} \cdot n\text{H}_2\text{O}]^{x-}$ where A^{2-} typically is CO_3^{2-} or SO_4^{2-}), in addition to vivianite and siderite in the HS quadrants interrogated (Root et al., 2013). As the reductive activity decreased in the flow direction, Fe^{3+} minerals became proportionately more evident; secondary goethite was detected by powder XRD (Table 3.3) and ferric (oxy)hydroxide was evident in XAS (Alday, 2010). The observed translocation of Fe^{2+} from AFH reductive dissolution was concurrent with precipitation of siderite, vivianite, and mackinawite for the HS case. We hypothesize that an under-saturated condition (with respect to ferrous minerals) resulted in the appearance of goethite in down-gradient column quadrants, since kinetics of its formation are favored during reactive transport of soluble Fe^{2+} that adsorbs to AFH surface hydroxyls, promoting the rate of AFH transformation to goethite (Zachara et al., 2002; Tufano et al., 2009; Yang et al., 2010; Raghava et al., 2014). Reactive transport of Fe in these columns resulted in the inlet quadrants being almost completely devoid of Fe^{3+} species (Table 3.2) and depleted in total Fe (Figure 3.4). This observation reflects the coupled influence of reduction and advection. Fluid flow not only causes the redistribution of solids along the flow path, but also the nature of solid species formed, since batch studies have shown ferric species

surfaces being surface passivated and their presence preserved(Roden and Zachara, 1996; Roden et al., 2000; Hansel et al., 2003).

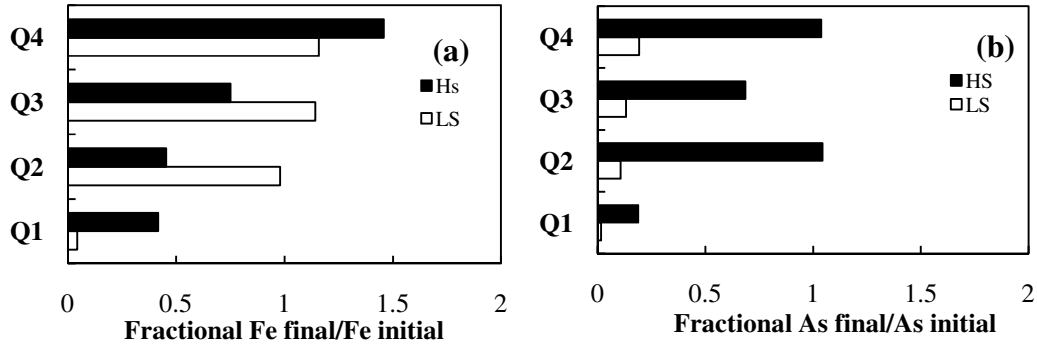


Figure 3.4. Final Fe (a) and As (b) mass distribution in LS and HS columns. More than 100% of the initial Fe mass present for the LS and HS cases relocated to the top two quadrants. Arsenic was retained mainly in the Q4 and Q3 of both LS and HS cases.

Table 3.3. Specific surface areas and sorption capacities of iron minerals observed after trial termination.

Solid	Specific Surface Area (m ² g ⁻¹)	Adsorption Capacity for Arsenate (μmol g ⁻¹)	Adsorption Capacity for Arsenite (μmol g ⁻¹)
Amorphous ferric hydroxide	600 ^a	2675 ^b	3514 ^b
Goethite (α-FeOOH)	54 ^b	173 ^b	173 ^b
Ferrous Sulfide (FeS)	3.2 ^c	N/A	14 ^c
Siderite (FeCO ₃)	1.58 ^d	6.94 ^e	13.88 ^e
Vivianite (Fe ₃ (PO ₄) ₂ ·nH ₂ O)	4.8 ^{f*}	13	

^aRoden and Zachara, 1996

^bDixit and Hering, 2003

^cBostick et al., 2003

^dMcCormick et al., 2002

^eGuo et al., 2007

^fThinnappan et al., 2008

^{f*} Particle size of 30 μm

Sulfate reduction can contribute significantly to secondarybiomineral formation under landfill and natural environment conditions throughprecipitation of sulfide minerals such as iron mono- and di-sulfides (FeS_{x,1≤x≤2}). Where arsenic is present at sufficient activity, arsenic sulfides (e.g., realgar[AsS], orpiment [As₂S₃], or arsenopyrite[FeAsS]) are expected to form (Bosticket al., 2003; O'Dayet al., 2004; Kirk et al., 2010; Burton et al., 2013). TheLS and HS effluent sulfate concentrations decreased from nearly 100% of the influent initially to below detection and <10%, respectively, after 60 d, which we postulate may be the time needed for sulfate reducing bacterial (SRB) acclimatization. No reduced sulfur solid species were detected in the low sulfate columns, whereas FeS

(mackinawite) and a realgar-like species (AsS) were the dominant solid phases detected in the HS column (Table 3.3). The higher sulfur activity in the HS column provides conditions of supersaturation of these sulfide phases. Based on Fe/As EXAFS analysis, realgar and ferrous sulfide comprise 100% of the solid phase (within the detection limit) close to the inlet, the active zone of sulfidogenesis. Formation of biominerals sequesters sulfide in the near-inlet sections. Hence, as the concentration of aqueous sulfide decreases in the direction of flow, so also does the percentage of sulfide minerals in the solid phase. Although the analytic techniques utilized did not allow differentiation between carbonate and sulfate green rust, the only zone where a possible sulfate mineral was detected was the outlet quadrant of the HS column, where green rust was detected. In accord, sulfide secondary mineral precipitation decreased with distance in the direction of flow (and reductive activity) and matched the trend of ferrous mineral presence.

The iron mineral transformation from ferric to either mixed-valent or ferrous phases causes a significant decrease in the specific surface area and reactive surface site density contributing to As adsorption capacity of the Fe minerals (Table 3.2). Considering the minerals that were formed in both LS and HS columns, the decrease in sorption sites from the initial AFH to the final ferrous minerals, siderite and vivianite, in the LS column and additionally mackinawite in the HS column is considerable. Likewise the goethite detected in the down-gradient column sections also has a lower specific surface area than the AFH initially present (Table 3.3). Based on the greater sorption capacity of the detected Fe^{3+} to Fe^{2+} species, the increase in proportion of Fe^{3+} species with downgradient distance (Table 3.2), and the increase in total iron mass downgradient (Figure 3.4a), it is

reasonable that the retained arsenic mass also increased progressively in the flow direction (Figure 3.4b), although the mass was much lower than that originally present.

Total arsenic mass percentage leached from the columns was: HS = 35%, LS-Mo = 37%, LS = 81% and LS-BES = 81%. The marked increase in arsenic retention of HS versus LS (except LS-Mo) is a consequence of the arsenic sequestration in sulfide biominerals. A possible mechanism is sorption of arsenite (As^{3+}) on mackinawite and subsequent reductive arsenite transformation to a realgar-like (AsS) solid phase and transformation of iron to green rust through oxidation of the FeS (Gallegos et al., 2003; Bostick and Fendorf, 2013; Root et al., 2013). For all columns, the loss of AFH is accompanied by almost complete retention of iron through secondary iron mineral precipitation (the total Fe leached was less than 5%). However, for the LS case this transformation resulted in a loss of arsenic sorption capacity and an observed 81% mobilization of arsenic from the column. For the HS case, loss of arsenic sorption capacity also occurred, but the generation of the realgar-like phase (Root et al., 2014) greatly increased overall arsenic retention.

Competition between methanogens and iron, sulfate, and arsenic reducers for the available electron donors (primarily lactate, acetate, and H_2), did not impact arsenic retention under the simulated mature MSW conditions. The arsenic release from the column with methanogenic inhibition (LS-BES) showed the same high loss of arsenic as the LS column without such inhibition, suggesting the competition of methanogens for electron donors did not significantly decrease Fe, S or As reductive activity.

The arsenic leached from the LS-Mo column was 38%, which is noticeably lower than the approximately 80% leached from LS and LS-BES column experiments. This result is surprising in the face of suggestions that stimulation of bio-sulfidogenesis may lead to greater arsenic retention (Kirk et al., 2004; Keimowitz et al., 2007). This decrease in arsenic release suggests a significant contribution of SRB in arsenic reduction and mobilization from the host solid phase, even in a condition with a relatively low concentration of sulfate available. Since some SRB can reduce arsenate (Hoeft et al., 2002; Harrington et al., 1998; Newman et al., 1997) and subsequently decrease its adsorption affinity and stability (Herbeland-Fendorf, 2006; Tufano et al., 2008), and since sulfide derived from bio-sulfidogenesis can readily reduce Fe^{3+} causing reductive dissolution of AFH (Poulton, 2004; Kocar, 2010), hindrance of these mechanisms could explain the increase in LS-Mo arsenic retention.

CHAPTER 4

MICROSCALE SPECIATION OF ARSENIC AND IRON IN FERRIC-BASED SORBENTS SUBJECTED TO SIMULATED LANDFILL CONDITIONS

This chapter was published in the journal of *Environmental Science and Technology* with Robert Root (first author), Sahar Fathordoobadi, Fernando Alday, Wendell Ela, and Jon Chorover as co-authors with collaboration between the Department of Chemical and Environmental Engineering, and the Department of Soil, Water and Environmental Science, University of Arizona, Tucson, AZ, 85721.

In the recent years there has been a good number of studies in which effect of short-term microbial reductive dissolution of Arsenic Bearing Solid Residuals (ABSRs), under the influence of an isolated microbial strain, has been investigated. Such short-term experiments are failing to demonstrate long-term Fe/As mobilization and transformation into the end-products and therefore unable to simulate mature landfill conditions. In addition, most of column studies employ only one isolated microbial community which again does not offer a valid representation of actual landfill condition.

In this research, we set up series of continuous flow-through columns to study long-term effect of sulfate on ABSRs under simulated landfill condition, using anaerobic digester sludge (mixture of microbial consortium) as microbial source that contains variety of microbial groups capable of Fe/As reduction. As and Fe concentration and speciation

were measured weekly in the effluent. At the termination of each column experiment, the solid content was characterized, using X-ray absorption spectroscopy (XAS) and X-ray fluorescence (XRF) imaging to examine the effect of influent sulfate concentration on ABSR under microbially-induced reducing conditions (Current chapter).

My contribution to this paper consist of:

- i) Experimental design, execution, maintenance and termination.
- ii) Aqueous sample collection, preparation and analysis.
- iii) Solid phase sample preparation for XAS and XRF analysis.

1. Introduction

Arsenic is a known environmental toxin (O'Day., 2006; Smedley and Kinniburgh., 2002) that is affecting the health of millions of people worldwide through natural and anthropogenic contamination of drinking water sources (Smith et al., 2000). Because of its environmental abundance, toxicity, and potential for human exposure, As has been designated the number one priority toxin by the Agency for Toxic Substance and Disease Registry (e.g. 1997-2011). Since 2006, when the USEPA adopted a maximum contaminant level of $10 \mu\text{g L}^{-1}$ in drinking water, more than 4000 US water utilities have been required to reduce concentrations of product water As (USEPA, 2001).

The high chemical affinity of arsenic for adsorption to hydrous ferric oxide (HFO) surfaces enables economical methods for removing it from drinking water (Pierce and Moore., 1982) by exploiting inner-sphere complexation of As(V) under oxic

conditions (e.g. (Manceau., 1995;Waychunas et al., 1993). The combined low-cost and effectiveness of ferric-based sorbents have contributed to their wide use by water treatment utilities, leading to significant increases in the volume of arsenic-bearing solid residuals (ABSR) (Mohan andPittman., 2007).

Iron based As “filter” media are typically non-regenerable and, in the US, can be disposed in municipal solid-waste (MSW) landfills if shown to pass the USEPA toxicity characteristic leaching procedure (TCLP). An estimated $3\text{--}12 \times 10^3 \mu\text{g}$ of ABSR are generated annually, typically loaded to $>1\text{:}200$ As:Fe mole ratio, creating 15-60 Mg of localized point-source As (Ghosh et al., 2004). ABSR are subjected to landfill (bio)geochemical conditions, including organic-rich reducing environments, which are not simulated by the TCLP (Menget al., 2001;Hooper., 1998). Prior studies have shown that reductive dissolution of iron oxides can result in mobilization of sorbed or co-precipitated As (e.g.(Nickson et al., 2000;Kirk et al., 2010)) - a potential fate for ABSR in mature MSW landfills as well (Ghosh et al., 2006).Indeed, the coupled cycling of As and Fe in landfills is impacted by microbial Fe reduction; where spent As sorbent, labile organic matter, and a consortium of heterotrophic reducing bacteria results in release of As and Fe into mobile pore waters (Cortinas et al., 2006;Jing et al., 2008). Although it is generally recognized that biogeochemical As cycling is closely coupled to the bio-availability of redox sensitive Fe, S, and organic carbon (C_{ORG}) (e.g., O'Day et al., 2004;Polizzotto et al., 2006)), the specific reactions driving arsenic release and sequestration following ABSR disposal in landfills have not been fully characterized. In particular, the influence of sulfate activity is poorly resolved. Sulfate in landfill leachate

ranges from 1 to 51 mM, and is likely a key driver of neo-precipitate formation and potential secondary phase As sequestration (Ghosh et al., 2006). For example, in laboratory batch studies of ferric based ABSRs, it was found that reduction of influent dissolved sulfate resulted in precipitation of iron sulfide (FeS_2) coincident with 80-100% reduction of As(V) to As(III) during a 2 year incubation (Liu et al., 2008).

The current study used X-ray absorption spectroscopy (XAS) and X-ray fluorescence (XRF) imaging to examine the effect of influent sulfate concentration on ABSR under microbially-induced reducing conditions. Briefly, laboratory columns were packed with As(V)-loaded HFO, inoculated with a diverse heterotrophic microbial consortium from a wastewater treatment plant, and reacted with a synthetic landfill leachate (SLL) containing either low (LS) or high (HS) sulfate concentrations (0.064 mM and 2.1 mM, respectively). Effluent samples were collected for complete aqueous chemical analysis as presented elsewhere (Alday., 2010). The focus of the present study is on the solid phase transformation of ABSR under the two influent sulfate concentrations. By combining X-ray absorption spectroscopy (XAS) and multiple energy micro X-ray fluorescence (ME- μ XRF) mapping (elemental and chemical), we elucidate changes in sorbent and sorbate speciation, binding environments, and co-associations that enable improved prediction of As fate in mature landfills.

2. Materials and Methods

2.1. Column Design

Columns (Spectrum Chromatography, 2.5 cm dia; 30 cm long) were packed with 73.3 g (15.1 g dry mass) of As(V) loaded ferric sludge (20:1 molar Fe:As), 120 g of 0.8 mm glass beads to provide tractable porosity ($\Phi = 41.7\%$), and 25 ml of anaerobic digester sludge from a wastewater treatment plant (76% water, 18% organic matter; Ina Road Wastewater Treatment Plant, Tucson AZ USA). The anaerobic digester sludge was chosen, in lieu of a pure strain inoculum, for its miscellany of microbes consistent with the broad diversity of anaerobic organisms in a mature MSW landfill. The sludge was a poorly crystalline ferric hydroxide, similar to 2L ferrihydrite (referred to hereafter as AFH), coprecipitated with As(V) by dissolving 0.935 M ferric chloride hexahydrate (ACS reagent, Sigma-Aldrich) and 0.047 M sodium arsenate heptahydrate (KR Grade, Sigma-Aldrich) in 1 L of purified water. The AFH was washed 5x to a supernatant EC $< 1 \text{ mScm}^{-1}$ and adjusted to pH 7.0 with NaOH. The SLL contained minerals and nutrients necessary for microbial activity and lactate as the organic electron donor and carbon source (Table 1, Appendix B). The SLL was sparged with nitrogen and fed continuously with a multi-syringe pump (Braintree Scientific) in up-flow mode at 5.1 mlh^{-1} (2 pore volumes [PV] d^{-1}). The Darcy's velocity was 0.25 m d^{-1} (hydraulic conductivity $\sim 10^{-3} \text{ cm d}^{-1}$) to represent saturated, semi-pervious landfill conditions. Columns were fed SLL with either 0.064 mM (LS) or 2.1 mM (HS) sulfate for 330 days or 331 days, respectively. Sulfate influent concentrations bracketed reported groundwater (average 0.048 mM (USEPA, 1999)) and US landfill (2.78 mM (Ghosh et al., 2006)) values. The goal was to evaluate the significance of relatively small increments of sulfate in landfill systems

relative to natural groundwater environments. Column effluent samples were filtered through 0.22 μm cellulose acetate syringe filters and analyzed for As, Fe^{2+} , SO_4^{2-} , lactate, and acetate. Acetoclastic methanogenic bacteria were inhibited by the addition of 1 mM 2-bromoethanesulfonic acid (BES) sodium salt ($\text{BrCH}_2\text{CH}_2\text{SO}_3\text{Na}$, Sigma-Aldrich) in the influent of the LS column. BES was added to the LS column on day 139 (278 PV). It was observed to not change arsenic and iron leaching patterns compared to other column experiments without inhibition, and was not added to the HS (Alday, 2010). To preserve the experimental redox environment, post operation column autopsies were conducted in an anaerobic chamber, where reacted AFH was dissected and subsamples were collected before transport in crimp-sealed serum vials to a synchrotron facility for x-ray analysis.

2.2. *X-ray Spectroscopy*

Column subsections were analyzed with K-edge XAS for speciation of arsenic and iron. Spectra were collected at Stanford Synchrotron Radiation Lightsource (SSRL) on beamline 4-1. Beam energy was calibrated on an arsenic foil with the main edge inflection assigned 11,867 eV and on iron foil with the first edge inflection assigned at 7112 eV. Fluorescence was monitored with a 13-element solid-state Ge detector with a He cryostat sample holder ($\sim 8\text{--}15\text{ K}$, see SI for XAS setup and analysis details). For bulk XAS analysis, 100–200 mg of moist sludge was ground, homogenized, loaded in Teflon sample holders, and sealed with Kapton tape in an anaerobic chamber at the synchrotron facility (Coy, $\text{N}_2/\text{H}_2=95/5$).

2.3. XRF Imaging Collection and Analysis

For XRF analyses, reacted AFH was air dried in the dark in an anaerobic chamber, to minimize post-experiment photochemical/oxidative reaction, and embedded in metal free epoxy (EPO-TEK 301-2FL; Epoxy Technologies, Inc). The suspension was cured for 72 h in a vacuum desiccator, packed under N_{2(g)} and sent in a low permeability bag for thin-sectioning (30 µm, polished 2-sides) under anoxic conditions (Spectrum Petrographic, WA). Thin sections were transported to SSRL in anaerobic bags (Anaerogen™) and stored in an anoxic chamber until analyzed.

The X-ray microprobe at SSRL, beamline 2-3, was used to interrogate the local chemical environment by scanning thin-section at energies near the Fe or As absorption edge (Mayhew et al., 2011). Images collected were 400-500 µm² with a pixel step size of 2.5-3.0 µm and 50 ms dwell time. For multiple energy (ME) maps, the measured fluorescence (F_m) at a designated energy was used to compile a 2D image relating concentration (ρ) of each element (i) or species (j) to elemental fluorescence yield (ω_i), i.e. (eq.1).

$$F_m = \Sigma(\rho_{ij}\omega_i) \quad (1)$$

Species specific mapping was conducted by monitoring F_m at multiple energies across the edge jump of As and Fe. The As K-edge is diagnostic for oxidation state, with the white line peak (ca. ± 1 eV) for arsenic sulfides at 11869 eV, As(III) at 11872 eV and As(V) at

11875 eV (O'Day et al., 2004). Therefore, when the monochromator is tuned to 11869 eV, resultant fluorescence from an arsenic sulfide is measurably different from that of As(III) or As(V). The same concept of multiple energy maps was applied to the Fe edge for phase identification. However, unlike As where a clear spectral peak was associated with oxidation state, the difference in Fe fluorescence at multiple energies was compared in a fluorescence yield - energy matrix selected specifically for phase identification (see Mayhew et al. for details (Mayhew et al., 2011)). Briefly, model compound spectra were input to a matrix of normalized fluorescence and energy (eV) at the energies of the XRF maps (Figure SI1 and Table SI3). Generally, the number of energies mapped is greater by one than the number of components that can be resolved (i.e., $n+1$ energy maps for n phases). Iron and As was mapped at discrete energies (7114, 7121, 7124, 7126, and 7137 eV for Fe; and 11869, 11872, 11875, and 11880 eV for As) to assess chemical associations and speciation.

The X-ray energy was calibrated with metal foils as above for bulk XAS. Principal component analysis (PCA) was applied to the >40k pixel images to locate regions of unique components and chemical differences. The application of PCA to image data is common for processing soft X-ray transmission data (e.g. (Lerotic et al., 2004; Osanna and Jacobsen, 2000)) but has been less extensively applied to hard X-ray μ XRF data (see (Mayhew et al., 2011)). The unique components highlighted with PCA were probed with X-ray absorption near edge structure (μ XANES) and collected at the same spot-size, stage and detector position as image data, to provide additional constraint for reference models and allowed components in the linear combination fits (LCFs) of bulk XAS.

3. Results

3.1. *Column leachate aqueous chemistry*

The bioreduction of AFH released As and Fe to mobile leachate under both high and low sulfate influent conditions (Alday, 2010). After 300 d, the LS column leached 84% of the initial solid-phase arsenate and 3.3% of the iron. After 331 d, the HS column released 36% of the initially loaded arsenate and <1% of the iron. Hence, about three-times more As and Fe were retained under the higher sulfate conditions. Effluent monitoring showed that leachate pH fluctuated around circumneutral with values 7.5-8.0 for LS and 7.5-8.3 for HS. In both columns, e^- donor lactate was oxidized to acetate and carbonate. Nearly all of the lactate was converted to acetate in the effluent from the beginning through to completion of the experiment. Influent and effluent sulfate concentrations were monitored in both columns, with influent sulfate found to be constant throughout the experiment. The HS effluent sulfate decreased from nearly 100% breakthrough at 1 d to 50% at 37 d, 25% at 40 d, and <10% at 60 d, and for the duration of the experiment. The LS influent sulfate dropped from 100% breakthrough at 5 d to <10% after 15 d and remained low for the experimental duration. This indicates that sulfate reduction or sorption occurred in both columns.

3.2. *As Speciation by Bulk XAS*

Normalized As k-edge XANES spectra of LS column solids showed that initial solid phase As(V) had been mostly reduced to As(III) after 300 d. In sections LS-II, LS-III, and LS-IV, XANES showed two distinct peaks at 11872.1 and 11875.3 eV, consistent with As(III) and As(V), respectively (Figure 4.1a, fits shown in Table 4.1). Fitting of As XANES to reference spectra of As(III) and As(V) sorbed to ferrihydrite shows that 75-81% of the As(V) in the AFH was reduced to As(III). Arsenic K-edge extended x-ray absorption fine structure (EXAFS) of the LS samples showed the bulk solid to be mixed As(III) and As(V), with spectra fit to first-shell As-O scattering paths, second-shell contributions from As-Fe scattering, and a multiple scattering (MS) contribution corresponding to the As-O-O MS within the arsenate tetrahedra (Figure 4.1b-c, fits shown in Table 4, Appendix B). Including the MS paths improved the fit, whereas degeneracy, distance, and the Debye-Waller factor were linked to the determined $\text{As}^{\text{V}}\text{O}_4$ parameters (see e.g., (Ona-Nguema et al., 2005; Beaulieu and Savage, 2005)). Multiple scattering was not significant for As(III), likely because of static disorder in the ligating oxygen shell. At 10 cm into the LS column (LS-II), bulk As EXAFS were fit with As-O distances at 1.77 Å and 1.69 Å, corresponding to arsenite pyramidal coordination, and arsenate tetrahedral coordination, respectively. The second shell EXAFS contributions from As-Fe interatomic distances were fit to $3.31 \text{ Å} \pm 0.01 \text{ Å}$ and $3.46 \text{ Å} \pm 0.01 \text{ Å}$, similar to coordination environments observed in a laboratory experiment of arsenite sorption to 2-line ferrihydrite and a field site where arsenate was sorbed to amorphous hydrous ferric oxide (Root et al., 2007; Gao et al., 2013). The EXAFS determined mixed As species was consistent with XANES. Scattering at the As-Fe interatomic distance of 3.31 Å was

attributed to a ${}^2\text{C}$ coordination, bidentate-binuclear corner-sharing between $\text{As}^{\text{III}}\text{O}_3$ pyramids and FeO_6 octahedra, whereas the 3.46\AA As-Fe scattering distance was attributed to ${}^2\text{C}$ coordination of $\text{As}^{\text{V}}\text{O}_4$ tetrahedra with ferric octahedra (Figure 4.1c) (Ona-Nguema et al., 2005).

Linear combination fits to the As XANES from the HS experiment, using realgar (AsS) as model reference sulfide spectra, showed a gradient from 100% AsS to 100% As(III) from the column influx to the efflux (Figure 4.1d, Table 4, Appendix B). Differentiating among As sulfides (e.g. As_4S_4 , As_2S_3 , etc.) with XANES alone is not possible because the associated edge shifts are within energy resolution of the beamline ($\sim 1\text{ eV}$ at the As edge). Therefore, while the peak match to realgar is not mineral specific, it is diagnostic of a solid-phase As-sulfide complex. Arsenic XANES of HS-I showed a distinct peak at 11869 eV , fit to a single sulfide component. The intermediate section HS-III had an absorption maximum at 11872 with an asymmetric broadening below the main edge. The lower energy broadening feature was fit with 31% AsS ; the main peak was fit with 69% As(III) . The As XANES for the sample near the outlet of the column, HS-IV, was fit with a single component of As(III) . Arsenic EXAFS of the bulk solid in HS-I showed an As-S distance of 2.25 \AA and contributions beyond the first shell of As-As at 2.58\AA , 3.49\AA , and 3.62\AA (Figure 4.1e). The As-As backscattering features beyond the first shell observed in HS-I are unique to realgar (and associated polymorphs) and are not observed in orpiment (As_2S_3), arsenopyrite (FeAsS), As-thio complexes, or organic As-S ligands (Figure 4.1f) (Suess et al., 2009). Complete reduction of As(V) was observed in the HS column. First shell As-O distance in HS-III and HS-IV were $1.76\text{-}1.78\text{\AA}$, consistent with

As(III) in pyramidal coordination. The second shell contributions from Fe backscatters were fit at 3.49 Å, a distance longer than the As(III) ²C coordination observed in the LS column, consistent with either a monodentate ¹V coordination or ²C coordination of non-edge sharing iron octahedra.

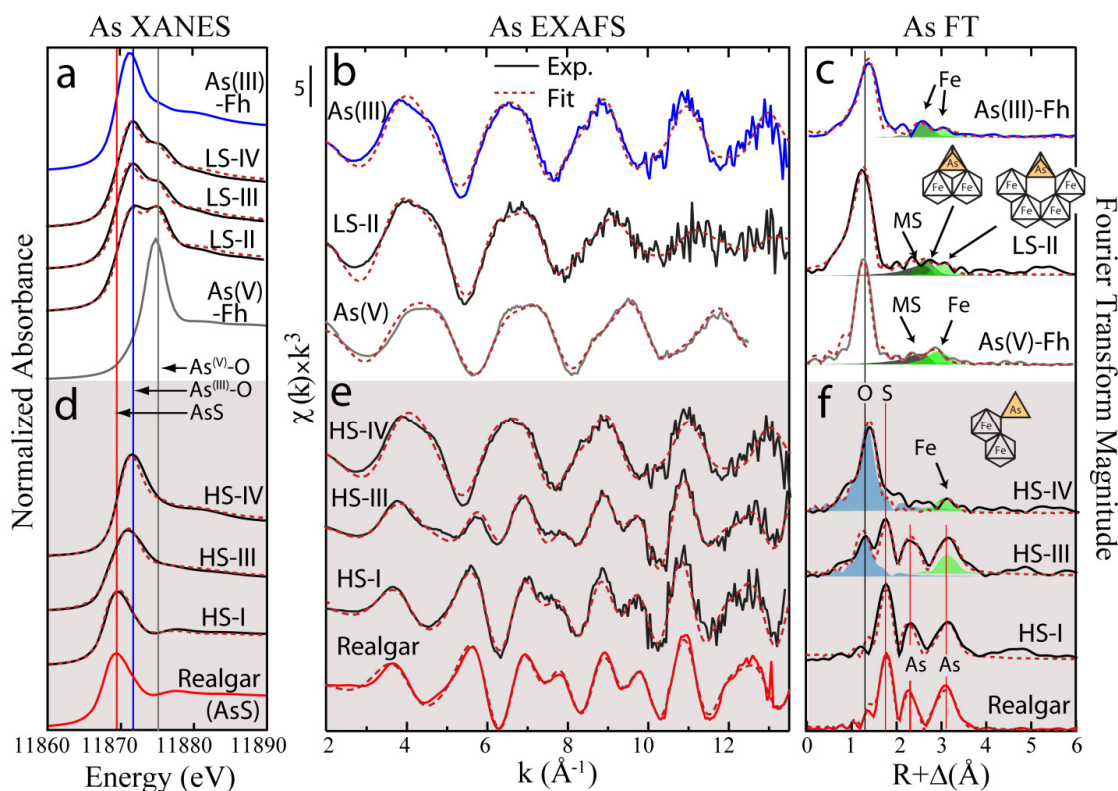


Figure 4.1. As K-edge XAS of AFH from the synthetic landfill column experiments; LS column (a) XANES (b) unfiltered k^3 weighted EXAFS, and (c) uncorrected for phase shift Fourier transformed EXAFS (FT); HS column in shaded panels (d) XANES (e) EXAFS, and (f) FT. Collected experimental spectra (black) and model reference spectra (gray = As(V)=Fh, blue = As(III)-Fh, red = realgar) together with calculated best fits to the data (stippled red). The vertical lines in (a) show reference AsS (red), As(III) (blue), and As(V) (gray); vertical lines and arrows in (c) and (f) highlight the structural features corresponding to the calculated coordination and distance, shown with inset schematic, and explained in the text; numerical fit parameters are given in Table SI4.

3.3. *Fe Speciation by bulk XAS*

Iron XAS data show the reduction of AFH-derived Fe(III) to Fe(II) and secondary Fe (bio)mineralization. Normalized first-derivative Fe K-edge XANES spectra were used for LCFs because they reveal subtle distinctions (O'Day et al., 2004). Column spectra were well described with LCF of fractional components of standard ferrous, ferric, and mixed-valent iron reference spectra, incl. ferrihydrite, siderite, carbonate green rust, vivianite, and mackinawite (Table 4.1). LCFs of the Fe XANES indicated development of a redox gradient in both columns, with the most reducing conditions near the inlet. In the LS column, 68 to 53 % of the AFH was transformed along the redox gradient. The LS spectra showed siderite and ferrihydrite as major components, and carbonate green rust and vivianite as minor components, with components constrained by μ XANES and XRD from LS-II (Figure 4.2a). In contrast, the HS column showed 100% of the AFH was transformed to ferrous iron sulfide (mackinawite) at the inlet, while ferrihydrite was co-associated with siderite and green rust at the outlet. Mackinawite and ferrihydrite did not co-occur in the HS column and ferric phosphates such as strengite could not be fit to the spectra (Figure 4.2b). Assignment of the Fe K-edge XANES to a ferrihydrite component is supported by the lack of detectable goethite peaks by XRD. Non-linear least squares fitting of the Fe EXAFS from the bulk solid in HS is consistent with the Fe solids being dominantly a mackinawite-like FeS along with a smaller green rust component (Figure 4.2c-d, Table 4, Appendix B). The Fe-S bond distances of 2.27 Å, and contributions beyond the first shell from Fe-Fe backscattering at 2.71 Å and 3.62 Å, are unique to the mackinawite structure and are not observed in pyrite or arsenopyrite (Lennie et al., 1995; Jeong et al., 2010). Additional backscatterers were needed for a good

fit to the EXAFS spectra. An Fe-O distance at 2.02 Å and a Fe-Fe distance at 3.26 Å, both consistent with green rust – a phase also suggested by the Fe XANES – improved the fit significantly. The Fe-Fe distance at 3.26 Å is close to the expected distance for edge sharing iron octahedra found in natural and synthetic green rust (3.18-3.25 Å) (Root et al., 2007). Pyrite was investigated as a possible component in reduced HS sections but was not observed; the Fe XANES LCF was better for mackinawite, as was the unique structural fit from the Fe EXAFS spectra, and XRD showed a lack of diffraction peaks diagnostic of the cubic pyrite structure.

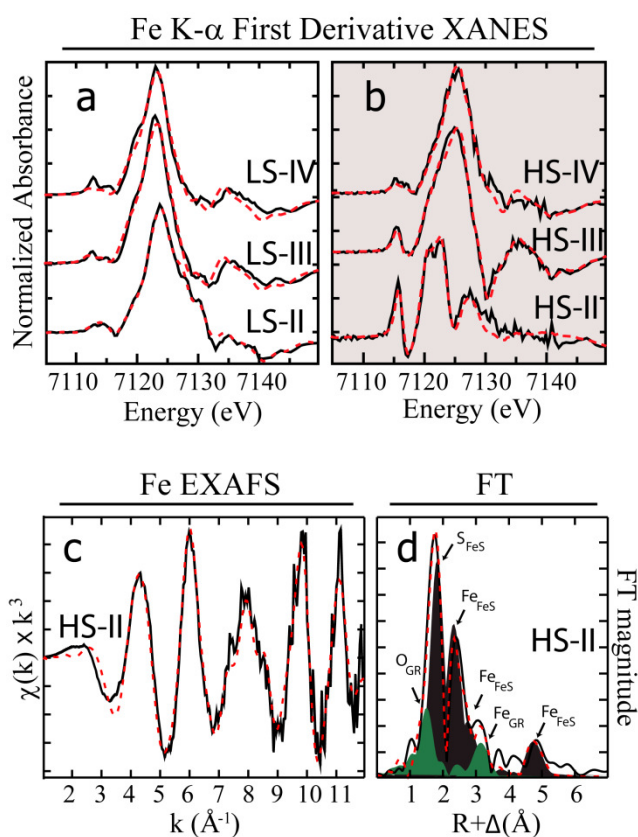


Figure 4.2. Normalized first derivative Fe K-edge XANES collected at 8-15K for a) LS and b) HS. Fe K-edge c) EXAFS and d) uncorrected for phase shift Fourier transformed EXAFS (FT). Solid lines are data, stippled lines are best fits, shaded regions in d) are mackinawite FeS (black) and green rust GR1CO3 (green) with Fe-backscatterer pair labeled; all numerical fit parameters are given Table 4.1

Table 4.1. Arsenic and IronK-edge XANES fit results.

Arsenic	fit (%) ^a				ΣAs_i ^b	
	As-S	As(III)	As(V)		Total	
LS-II	-	81	17		98	
LS-III	-	77	21		98	
LS-IV	-	75	34		109	
HS-I	97	-	-		97	
HS-III	31	69	-		100	
HS-IV	-	102	-		102	
Iron	fit (%) ^a					ΣFe_i ^b
	Mack	Sid	Viv ^c	GR ^d	Fh ^e	Total
LS-II	-	51	-	17	32	100
LS-III	-	41	5	18	36	101
LS-IV	-	34	5	12	47	98
HS-I	85	-	-	12	-	97
HS-III	30	45	19	-	-	94
HS-IV	-	33	-	17	53	103

^aResults from linear combination least-squares fits with energy varied for each component with reference mineral previously analyzed by XAS (Root et al., 2009). Dash (-) indicates a component not used in the fit. ^bFit components were not normalized to unity. ^cFit with synthetic vivianite spectrum, prepared following (Eynard et al., 1992). ^dFit with green rust 1-hydroxy-carbonate spectrum prepared following (Drissi et al., 1995). ^eFit with synthetic 2-line ferrihydrite spectrum, prepared following (Schwertmann and Cornell, 2007). Columns sections are numbered (I-IV) from the inlet to the outlet.

3.4. X-ray Fluorescence

3.4.1. Low Sulfate Column

Elemental correlations from ME μ XRF mapping images for the LS column show As primarily associated with ferrihydrite between the glass beads (Figure 4.3a-d). Fluorescence yield varies by atomic number; however, comparing per pixel fluorescence counts of Fe to As gives a correlation coefficient of 0.82 and an Fe:As count ratio of 26:1, close to the initial molar ratio of 20:1. ME μ XRF across the As edge indicates that As(III) and As(V) were distributed through the column with localized high concentrations (Figure 2, Appendix B). The Fe ME μ XRF map shows the predominance of ferrihydrite and siderite in the reacted AFH with rims of green rust (GR) forming at the solid-liquid interface. Both As(V) and As(III) are associated with the areas mapped as ferrihydrite and siderite, whereas the areas mapped as GR are associated with low As counts and As(V) only.

3.4.2. High Sulfate Column

The association of As to Fe differed in the HS column; areas of high As were observed to be mostly independent of Fe rich regions (Figure 4.3e-h). The abundance of Fe solids appeared to be lower in HS-I versus LS-II, as seen in the fluorescence map (Figure 4.3a v 4.3e) and in micrographs (Figure 3, Appendix B). Arsenic speciation maps showed As associated with sulfide widely distributed throughout the solid matrix, and As(III) located in isolated spots (Figure 4.3h). The Fe maps indicated that As(III) was generally

associated with the area mapped as siderite, and it was not found within the area mapped as FeS.

The HS ME μ XRF showed complete As(V) reduction, mostly to AsS with some As(III). Most of the arsenic in the HS-I section of the column was As-sulfide, consistent with the bulk XAS (Figures 4.2b and 4.3h). The Fe phase was mostly FeS with a GR crust co-occurring throughout, consistent with the bulk XAS. Siderite was observed - not associated with AsS phases - and generally in regions of lowest As fluorescence. The AsS and FeS phases were spatially correlated, but not uniformly; there were areas of FeS without AsS.

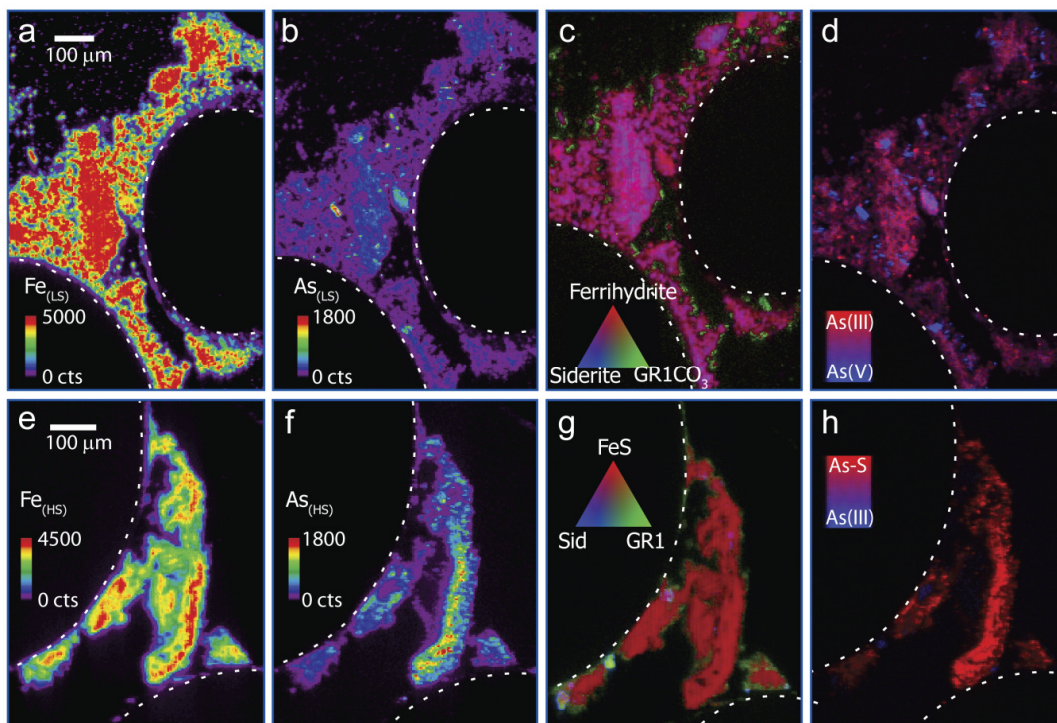


Figure 4.3. Multiple energy μ -XRF maps for the low sulfate (LS: a-d) column experiments after 300 days of bioreduction in inoculated synthetic landfill leachate, and high sulfate (HS: e-h) after 331 days of bioreduction in inoculated synthetic landfill leachate. The top panels show total Fe (a) and As (b) intensity for LS according to the color-scale shown, c.) ternary Fe speciation for LS, ferrihydrite shown in red, carbonate green rust (GR1CO_3) in green, and siderite in blue, and d.) binary distribution of As species for LS with As(III) in red and As(V) in blue, with color intensity corresponding to concentration. The bottom panels show total Fe (e) and As (f) for HS columns, g.) ternary Fe speciation for LS, with FeS shown in red, GR1CO_3 in green, and siderite in blue, and h.) binary As speciation with As sulfide and As(III) in blue. The white dashed lines delineate the edges of glass beads, and color intensity corresponds to the molar concentration of each chemical species per volume in each pixel, mapped at $3\mu\text{m}^2$ and $2.5\mu\text{m}^2$ for LS and HS respectively.

4. Discussion

In this long-term flow-through column experiment under sulfidogenic conditions, bulk XAS was used to probe the Fe and As speciation, and μ XRF imaging was employed to

determine the localization of secondary phases and As speciation. Reductive transformations of AFH are attributed microbial reduction of Fe(III) and SO_4^{2-} . Once heterotrophic microbial respiration was activated and Fe^{2+} was produced, the resulting reductive dissolution of AFH was likely by both biotic and abiotic pathways as expected in a mature landfill (Poulton., 2003). Results showed that the dissimilatory reduction of these ABSRs produced green rust, vivianite, and siderite in the LS column and mackinawite, siderite, vivianite, and greenrust in the HS column. While solid phase As(V) was reduced, the extent of arsenic mobilization and secondary iron mineral formation were dependent on the influent sulfate concentration.

4.1. As and Fe Speciation in Low Sulfate Column

Mixed valent As is distributed with iron solids in the LS column, indicating mixed coverage and no obvious preference for As(V) over As(III) at this scale at many surface sites. The LS ME μXRF maps show mixtures As(III) and As(V) in the same $3\text{ }\mu\text{m}^2$ pixel space. However, areas of highest As concentration were dominated by As(V) and ferrihydrite, identifying ferrihydrite as the energetically favorable sorbent. Our results indicate that siderite and green rust were not effective sinks for As(III), consistent with previous sorption studies (Jönsson et al., 2008). In general the areas of lowest As fluorescence were associated with regions mapped as green rust indicating that As did not partition strongly to green rust, consistent with previous findings (Kocar et al., 2010). Green rust occurred as a surface crust on ferrihydrite, whereas siderite was inter-mixed with ferrihydrite. The precipitation of green rust as rims along the ferrihydrite surface

suggests that the reducing SLL solution either induced a nucleation of GR at favorable ferrihydrite surface sites, or that it initiated a solid state transformation of ferrihydrite by reaction with free Fe^{2+} (Genin et al., 2006; Kukkadapu et al., 2004). A gradient of solid phase predominance from Fe(II) to Fe(III) was observed in both the LS and HS columns. Fe XANES show ferric, ferrous, and mixed valence phases, with greater predominance of ferrous (ferric) solids near the inlet (outlet). The siderite fraction was greatest at the inlet, owing to the oxidation of lactate to carbonate coupled to Fe(III) reduction. Our results are consistent with a laboratory study showing that the reduction of ferrihydrite by *Shewanella putrefaciens* results in the precipitation of green rust (and vivianite in the presence of phosphate) (Kukkadapu et al., 2004).

4.2. Arsenic and Iron Speciation at High Sulfate Activity

As(V) was reduced to As(III) or AsS at the HS column inlet, and for these simulated landfill solids with localized As(V)-AFH and elevated SO_4^{2-} , SLL was shown to react to precipitate realgar-like AsS and FeS as discrete phases. The precipitation of a realgar-like solid phase is consistent with the neo-formation of arsenic sulfide solids observed in microbially (Demergasso et al., 2007; Root et al., 2009) and abiotically (Sadiq., 1990) reduced sediments. An As sulfide precipitate was reported as the primary product of As(III) reaction with FeS at pH 5, and it occurred as a discrete phase, not associated with Fe, but rather an amorphous hydrous arsenic sulfide with the local structure of realgar (Renock et al., 2009). Realgar has been precipitated from the reaction of As(III) with nano-particulate iron sulfide at pH 5, while at pH 9 thio-arsenites were formed (Han et

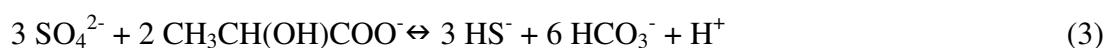
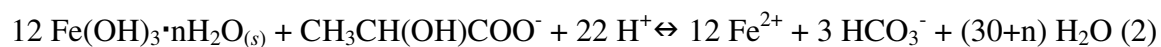
al., 2011). Upadhyaya et al. (2010) showed that under reducing conditions in a fixed-bed bioreactor, generation of iron sulfides sequestered arsenic through surface precipitation of arsenic sulfide on FeS (Upadhyaya et al., 2010). The precipitation of realgar in a high-sulfate environment subjected to reducing conditions is supported by thermodynamic modeling that predicts the formation of a realgar-like surface precipitate (Gallegos et al., 2008).

Similar to the LS experiment, a gradient from Fe(II) to Fe(III) solid phases was observed along the flow path in HS columns. The HS column XANES show FeS and green rust in the zone of greatest sulfidogenesis. It was observed that the inlet region, with the highest HS^- activity, promotes the precipitation of sulfides. The observed stability fields of ferrous sulfide and ferric (hydr)oxides do not overlap, unlike ferrous carbonate and phosphate species. Evidently, by mid-column, carbonate activity competed with HS^- activity, favoring the precipitation of siderite over FeS, and making green rust unstable. While ferrihydrite-like Fe speciation was kinetically stable near the outlet, it is expected to age to goethite over longer times (Hansel et al., 2005). The Fe-O distance of 2.02 Å, attributed to GR, is shorter than prior reports (2.06-2.12 Å), possibly indicating a higher ratio of Fe(III)/Fe(II) than ideal green rust, associated with the rapid oxidation of Fe(II), possibly by reaction with As(III) (Thoral et al., 2005). The Fe-Fe distance at 3.26 Å is close to that expected for edge sharing iron octahedra in natural and synthetic green rust (3.18-3.25 Å) (Root et al., 2007). The EXAFS is best fit to a mixture of 71% FeS and 30% green rust, a higher estimation of the green rust contribution than given by XANES, which shows 85% FeS and 12% green rust. Discrepancies between Fe EXAFS and

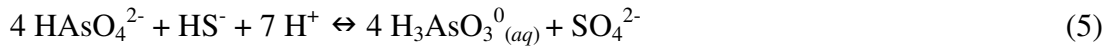
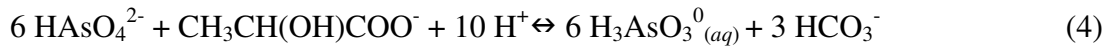
XANES fits have been shown by O'Day et al. (2004), where analysis of known pyrite:phyllosilicate mixtures showed sulfide mass contributions can be underestimated by XANES relative to EXAFS, because of stronger backscattering of sulfur relative to oxygen in the EXAFS first shell (O'Day et al., 2004). Conversely, the underestimation of FeS by EXAFS in the present study is consistent with an amplitude reduction in $\chi(k) \cdot k^3$, attributed here to low crystallinity or nano-crystalline FeS (Frenkel et al., 2001). Self-absorption was explored as a cause of dampening of the EXAFS signal because it would also manifest in an underestimation in the target phase in the EXAFS relative to XANES, but it was ruled out by concurrently collected transmission spectra that show no dampening of the EXAFS or concomitant enhancement in the XANES (esp. pre-edge region) relative to fluorescence spectra.

4.3. Fe-S-As Reactions in Sulfidic Environments

It has been shown that microbial sulfidogenesis can initiate the reductive dissolution of ferric solids including AFH (Poulton, 2003). Oxidation of lactate, and reduction of sulfate, initiated by microbial respiration will promote ferric solid phase dissolution and subsequent release of Fe^{2+} and HS^- to pore waters (eq. 2-3).



Where ferric (hydr)oxide solids are stable, oxyanion $H_xAs^V O_4^{2-x}$ has a stronger affinity for reactive surface sites than does neutral $As^{III}(OH)_3$ (Dixit and Hering, 2003). However, the reduction of As(V) to As(III) alone does not require release of As(III) to solution, the mechanism of As mobilization to porewater is via dissolution of sorbent AFH and subsequent release of sorbate As (Kneebone et al., 2002). If iron reduction is energetically favored over arsenate reduction, the dissolution of ABSR will release oxyanion $H_xAs^V O_4^{2-x}$ to solution. The reduction of arsenate to arsenite can then be coupled to microbial respiration (eq. 4) or to abiotic reaction with free HS^- (eq. 5) (Hoeft et al., 2004);

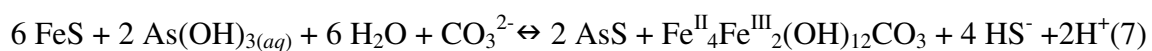


Excess Fe^{2+} and HS^- in solution at circumneutral pH can then promote the precipitation of mackinawite (eq.6) (Wolthers et al., 2003).



Bulk Fe and As XAS showed that at elevated sulfate concentrations (2.1 mM), ABSR were reduced to FeS and As(III) + AsS. We propose a possible explanation for the precipitation of realgar-like solid phases in environments similar to those found in anoxic zones in mature landfills. It has been reported that dissolved As(III) can be removed from porewater as an adsorbed species on FeS (Gallegos et al., 2008; Farquhar et al.,

2002; Wolthers et al., 2005). Additionally, it has been shown that As(III) can react with excess sulfide to form soluble thioarsenite complexes that precipitate as As–S solids, such as amorphous arsenic sulfides, orpiment (As₂S₃) at low pH, and realgar (As₄S₄) at circumneutral pH (O'Day, 2006; Wilkin and Ford, 2006; Bostick et al., 2005). It has been proposed, and supported with thermodynamic modeling, that dissolved As(III) can adsorb to reactive FeS surface sites (Bostick and Fendorf, 2003), followed by its reduction to AsS via oxidation of FeS, forming As-S polymeric (realgar-like) solid phases and precipitation of green rust (eq. 7) (Gallegos et al., 2008).



This reaction is consistent with the co-associations of FeS, green rust and polymeric AsS solids observed in the HS column of this study. The identification of intercalated anion in the green rust phase (i.e. CO₃²⁻ or SO₄²⁻) formed here was not resolved, and (eq. 7) could also be written with sulfate green rust.

In this model for mature landfill conditions it is expected that the formation of AsS is limited by the activity of dissolved As(III) and inhibited by excess HS⁻ or low pH conditions, conditions that have been reported to favor formation of thio-complexes or precipitation of orpiment (Bostick et al., 2005; Couture and Van Cappellen, 2011). The kinetics of this reaction and conditions favoring AsS precipitation require further study, as our current study examined long term reaction products after 331 d (and 661 PV). A flow-through study with As loading close to this study (and SO₄²⁻ 0.80 mM) was run for

88 d and did not show precipitation of As sulfides (Kocar et al., 2010). However, a short term (48 h) study showed XAS and XRD evidence of solid phase realgar (or polymorph) after mackinawite (5 g L^{-1}) was reacted in batch reactors with 0.5 mM As(III) (mol As:Fe =114) (Gallegos et al., 2007). Long term (400 d) dissimilatory reduction of arsenic loaded schwertmannite (ferric hydroxysulfate) produced secondary orpiment and mackinawite when excess SO_4^{2-} was absent, but no As-S formed at 100 mM SO_4^{2-} because schwertmannite transformation was inhibited and served as a sorbent for As, thus inhibiting As-sulfide precipitation (Burton et al., 2013). This indicates the importance of FeS surface site development and a concomitant lack of alternate energetically favorable sorption sites, such as those from ferrihydrite or schwertmannite, in AsS precipitation.

The present study shows that dissolved arsenic can partition into a realgar-like AsS solid that is spatially associated with $\text{FeS}_{(am)}$ under environmental conditions similar to those in a municipal landfill. The results indicate that the sulfate/sulfide redox couple is important to controlling As mobilization in high-iron environments such as those occupied by landfill-disposed AFH.

CHAPTER 5

HOW SULFUR REDOX CYCLE AND CONCENTRATION IMPACTS ABSRs FATE IN LANDFILLS

1. Introduction

Lowering the arsenic Maximum Contaminant Level (MCL) in drinking water in the U.S. has led to generation of more than 10,000 kg As_{year}⁻¹ associated with arsenic bearing solid residuals (ABSRs). Currently these ABSRs are being disposed in landfill and as a consequence arsenic is likely being released into leachate. However, a mature landfill is a biotic, reducing environment. Mature landfills also contain a significant organic matter component, which leads to a high level of microbial activity that favors anaerobic-reducing conditions. Such conditions may transform the ferric iron in ABSRs to reduced ferrous iron and, as a consequence, arsenic may be released (Ghosh et al., 2004; Meng et al., 2001).

Sulfate is one of the components commonly found in landfill leachate with concentration ranging from 1 to 51 mM. Main source of sulfate in landfill leachate comes from construction and demolition debris such as drywalls, and incinerator ash. With such a wide sulfate concentration window a broad range of sulfate reducing bacteria (SRB) community is expected to be present in MSW landfills, which in addition to reducing sulfate to sulfide may be able to reduce arsenate. Although arsenic reducing microbial communities are abundant in landfills, SRB are also expected to substantially reduce

arsenic (Hoeft et al., 2002; Harrington et al., 1998; Newman et al., 1997). In sulfidogenesis, reducing environment the couple sulfate/sulfide can inhibit some bacterial activity such as methanogenesis with hydrogen and/or low molecular weight organic compounds consumption, as sulfate reduction yields higher free energy than methanogenesis (Table 5.1). Iron and sulfur redox cycles have a considerable influence on arsenic cycling and its displacement in the landfill microcosm. The primary routes of iron and sulfate reduction in landfills are microbially mediated and biomineralization is a common by-product. Biomineralization may lead to formation of minerals such as siderite (FeCO_3), vivianite ($\text{Fe}_3(\text{PO}_4)_2$), iron sulfide (FeS), goethite (FeOOH), and realgar (AsS).

The microbially generated sulfide can interact with environmentally important elements such as Fe and As and affect geochemical transformation of ABSRs via redox couple formation with As(V) and Fe(III) or sulfide biomineral formation. Aqueous sulfide is a powerful reductant of Fe(III) that can drive the reductive dissolution of poorly crystalline ferric (hydr)oxides, such as ferrihydrite (Dos Santos and Stumm, 1992; Poulton et al., 2004). Sulfidogenesis can also drive iron sequestration through precipitation of Fe sulfide minerals, including mackinawite, greigite and pyrite (Rickard., 1974; Wilkin and Ford, 2006; Burton et al., 2007). This reaction can facilitate arsenic release under landfill conditions by triggering reductive dissolution of arsenic bearing ferric (hydr)oxides (Kocar et al., 2010). In the sulfidogenesis environment, where the sulfide concentration is high orpiment could form as the main sulfide mineral. Orpiment can then react with dissolved sulfide to form arsenic-sulfide aqueous complexes (thioarsenic) which results

in dissolution of orpiment. The formation of thioarsenic complexes could be expected at neutral to high values of pH (Wilkin et al., 2003; Helz and Tossell, 2008), as is shown in following reaction (Reaction 1):



Thiolated arsenic species are commonly known to be found under reducing Fe-rich and sulfide-rich environment and are controlling arsenic chemistry (Wilkin et al., 2003; Couture et al., 2013). However, there is not sufficient information on sorption behavior and aqueous quantification of thioarsenic species in the presence of iron sulfide and iron.

In this chapter results are presented to show that how concentration of sulfate feed into the system affects the biomineral formation, and that the relative amounts and sequence of precipitation of biominerals affect the free arsenic concentration that can seemingly be engineered by the concentration of inflow sulfate to the system.

In the advective-flow experiments performed by Burton et al. (2011), the reductive dissolution of ferrihydrite close to the in-flow end of the column with highest sulfidization activity, resulted in the formation of secondary Fe sulfide minerals such as mackinawite and was associated with substantial mobilization of arsenic. Their results indicate that the newly formed iron mineral was not effective at As sequestration. Since under advective-flow conditions as employed here and by Kocar et al. (2010), the reactants consumed through sulfate-reduction (sulfate and lactate) are continually

replenished, allowing ongoing sulfidogenesis and the accumulation of secondary iron biominerals which are very weak sorbents of As compared to ferrihydrite.

Iron (hydr)oxides are strong sorbents of arsenic that undergo reductive dissolution and transformation upon disposal in landfill where it reacts with biogenic dissolved sulfide. Arsenic originally bound to these Fe(III) (hydr)oxides will subsequently be subject to transformation upon reaction with dissolved sulfide, forming aqueous thioarsate or As sulfide phase.

Table 5.1. Thermodynamic favorability of methanogenesis and sulfate reduction from different substrates. Adopted from Alday, 2010.

Substrate	Reaction	ΔG^0 (KJmol ⁻¹ CH ₄ /SO ₄ ²⁻)
Hydrogen	$4\text{H}_2 + \text{CO}_2 \rightarrow \text{CH}_4 + 2\text{H}_2\text{O}^a$	-135.6 ^a
Acetate	$\text{CH}_3\text{COOH} \rightarrow \text{CH}_4 + \text{CO}_2^a$	-31.0 ^a
Hydrogen	$\text{SO}_4^{2-} + 4\text{H}_2 \rightarrow \text{H}_2\text{S} + 2\text{H}_2\text{O} + 2\text{OH}^-^b$	-154.0 ^b
Acetate	$\text{SO}_4^{2-} + \text{CH}_3\text{COOH} \rightarrow \text{H}_2\text{S} + 2\text{HCO}_3^-^b$	-43.0 ^b
Lactate	$\frac{1}{2}\text{SO}_4^{2-} + \text{CH}_3\text{CHOHCOO}^- \rightarrow \frac{1}{2}\text{HS}^- + \text{CH}_3\text{COO}^- + \text{HCO}_3^- + \frac{1}{2}\text{H}^{+c}$	-65.4 ^c

^a Laloui-Carpentier et al., 2006

^b Karhadkar et al., 1987

^c Kocar and Fendorf, 2009

To assess the mobility of arsenic under sulfate-reducing conditions, Couture et al. (2013) run flow-through reactors for 2 months, using lake sediment, with inflow solutions containing sulfate and soluble As(III) or As(V) and after 3 weeks they also added lactate to the reactor. Their observations suggest more efficient As retention once the dissolved sulfide and zero-valent S are buffered. Their findings raise the question on sulfide mineral ability on arsenic sequestration, knowing also that the redox transition between the zone of Fe(III) oxyhydroxides stability and As sulfides formation drives high As remobilization (Couture et al., 2013). Therefore, there is a need for more in-depth research on long term effect of sulfate on arsenic behavior and speciation under land fill conditions.

2.Objectives

In this part of the work we examine the role of sulfate concentration on ABSRs biomineralization under simulated landfill conditions and investigate biogeochemical weathering products of iron, sulfur, and arsenic by looking at possible biotic and abiotic pathways involved in the process of biomineralization. Therefore, microbial reduction and biomineralization of iron and sulfur are evaluated as processes that both promote arsenic release from landfilled ABSRs and may possibly provide a means to re-sequester it in a recalcitrant solid state.

Electron consumption order in two cases of medium and high sulfate concentration as well as the thermodynamic favorability of redox active couples relevant to landfill conditions were also evaluated using column measurements.

3. Materials and methods

3.1. Sludge preparation

An arsenic-bearing iron sludge was prepared to simulate the waste generated from the treatment of ion exchange/membrane processes brine solutions. Sodium arsenate heptahydrate ($\text{Na}_2\text{HAsO}_4 \cdot 7\text{H}_2\text{O}$, KR Grade, Sigma-Aldrich) was dissolved in purified water (Milli-Q Water System by Millipore) to prepare a 1 L solution with a concentration of 0.047 M as As. Ferric chloride hexahydrate ($\text{FeCl}_3 \cdot 6\text{H}_2\text{O}$, ACS reagent, Sigma-Aldrich) was added to the As solution to produce a supersaturated, 0.935 M as Fe solution with Fe:As molar ratio of 22:1. This mixture was stirred on a reciprocating shaker table (Orbit, reciprocating speed 100 rpm) for 1 hour before adjusting the pH to 7.0 ± 0.2 with 10.0 M sodium hydroxide (NaOH, flakes, EMD Chemicals). The ferric hydroxide solid produced was 2L ferrihydrite ($\text{Fe}(\text{OH})_3 \cdot n\text{H}_2\text{O}$) and is hereafter referred to as amorphous ferric hydroxide (AFH). The AFH was equilibrated for 2 days while the pH was maintained at 7.0 ± 0.2 . After equilibration and settling, a supernatant sample was filtered through a 0.45 μm cellulose acetate syringe filter for determination of concentrations of dissolved As and Fe with supernatant As concentration of 69.56 ppb for MS column and 77.28 ppb for HS column, respectively. Iron concentration was BDL in both batches. Subsequently, the residual salt content (Sodium chloride) of the AFH was reduced by decanting off the supernatant and filling the 4 L flask to the top with Mili-Q water, mixing gently, and allowing to resettle for about 3-4 hours and decanting off the water. This procedure was repeated until the conductivity of the supernatant was below 1.0 mScm^{-1} . During the process the pH remained constant (7.0 ± 0.2) without needing further adjustment. The remaining slurry was vacuum filtered through a 0.45 μm filter

(cellulose nitrate, Whatman). The final AFH water content was calculated by weight loss of a sample dried at 70°C for 2 days. Two batches of AFH were prepared as described above: one for use in a medium sulfate (MS: 2.08 mM) feed column and one for a high sulfate (HS: 20.8 mM) feed column. The AFH water-content was 83.4% and 83% wt/wt for the MS and HS columns, respectively. The sludge was stored in a capped-glass container at 4°C to be used as fresh sludge for a period of time no longer than 3 weeks. Previous work in our lab (Alday, 2010) using visual, SEM, and XRD analysis, has shown no evidence of phase changes under these conditions for 3 weeks, although changes are known to occur over longer time frames.

3.2. Sludge Characteristics

Total Fe and As in the AFH were determined by digestion of 1 g (dry wt.) sample, using 15 ml of 70% by volume HNO₃ (HNO₃, J.T. Baker) in a CEM microwave digester (method SW 821-8051). Iron was determined with 1,10 phenanthroline method (APHA, 1998) using a spectrophotometer at 510 nm wavelength (Spectronic Genesys 5). Total and speciated arsenic was measured by Ion Coupled Plasma Mass Spectrometer (ICP-MS, Agilent 7500a). The As and Fe per gram of dry AFH were 31.24 mg As and 521.03 mg Fe for MS column and 5.83 mg As and 94.92 mg Fe for HS column (Table 5.2).

Table 5.2. Iron/Arsenic sludge characteristics.

Column ID	pH	SupernatantAs Concentration (ppb)	SupernatantFe Concentration (ppb)	[mg As/g dry sludge]	[mg Fe/g dry sludge]	Fe:As Ratio	% Water Content
Medium Sulfate(MS)	7.00	69.56	BDL	31.24	521.03	22.38	83.43
High Sulfate(HS)	7.00	77.28	BDL	5.83	94.92	21.86	80.00

BDL: below detection limit

3.3. Columns Experiments

Chromatography-type columns (Spectrum Chromatography; 2.5 cm ID × 30 cm length) were packed with about 80 grams (wet wt.) of the prepared iron/arsenic sludge, mixed with 120 g of glass beads (0.8 mm diameter), to give packed materials porosity and homogenous distribution. Anaerobic digester sludge(25 ml of slurry) obtained from Ina Road Wastewater Treatment Plant, Tucson, Arizona, was added as the microbial source for the experiment. The column was fed with a synthetic landfill leachate adapted from Field et al. (2003) by replacing all chloride with sulfate salts to avoid chloride peaks overlapping other anion peaks in ion chromatography (IC). The inflow sulfate concentration was 2.08 mM for the MS and 20.8 mM for the HS columns, respectively. The influent feed was purged with nitrogen gas and fed continuously into the columns using a multi-syringe pump (BS-9000-6 programmable multi-syringe pump, Braintree

Scientific). Effluent samples, filtered through 0.45 μm syringe filters (cellulose nitrate, Whatman), were analyzed to quantify arsenic, iron and sulfate. Ion chromatography (IC, Dionex, DX-500) was used to quantify sulfate, lactate, and acetate.

Table 5.3.summarizes important column conditions. pH was measured with an Orion (Model 720) pH meter. ORP was measured with a Cole Palmer Platinum Single-Junction Electrode.

Table 5.3. Summary of column characteristics.

Column ID	Average [As] _(aq) (mM)	Average [Fe] _(aq) (mM)	[SO ₄ ⁻²] (mM)	Run Time (Days)
Medium Sulfate	0.22	0.27	2.08	331
High Sulfate	0.1	0.01	20.8	551

Flow rate: 0.04-0.12 L/day

Fe/As molar ratio: 22

3.4. Solid Phase Characterization

The MS and HS columns were run for 331 and 551 days, respectively. After termination of the experiment the columns were opened in an oxygen free glove box (Terra Universal 100). The contents of each column (initially containing a mix of AFH, glass beads and anaerobic digester sludge) was divided into four, approximately equal volume sections, numbered from bottom to top in the direction of flow. Each layer was dried in the glove box at room temperature for 7 days after which a 0.5 mm mesh was used to separate the beads from the solids. Solid phases were analyzed by Powder X-ray Diffraction (XRD),

X-ray absorption spectroscopy (XAS), X-ray fluorescence (XRF), and sequential extraction. XAS and XRF were conducted at the Stanford Synchrotron Radiation Light source (SSRL) and are described elsewhere (Root et al., 2013). Powder XRD was by a Scintag XDS 2000 PTS Diffractometer with Cu-K α radiation ($\lambda = 1.54060 \text{ \AA}$) operated at a voltage of 40 kV and a current of 40 mA. Diffraction patterns were recorded by continuous scans from 10° to 70° at 2 degrees/minute. The mineral phases were identified using the instrument software and the International Centre for Diffraction Data (ICDD) database.

4. Results and Discussions

4.1. Arsenic and Iron Leaching Patterns

During the time that the experiment was conducted, As(V) was always dominant species in the effluent in MS column, with As(III) concentration below 0.05 mM except for a few isolated points where the concentration was $\sim 0.1 \text{ mM}$ (Figure 5.1) and total arsenic average concentration of 0.25 mM. In contrast, As(III) was dominant in the effluent of HS column throughout the run with total arsenic average concentration of 0.15 mM (Figure 5.2). HS and MS columns are behaving very differently in terms of effluent arsenic speciation. Qualitatively the same arsenic leaching trend was observed in all the columns; a bell shaped curve. It starts with a lag phase (phase I) of microbial acclimatization, follows by continuous increase of effluent concentration to a maximum (phase II) which then follows by dissipation over time (phase III) till end of column's life.

In the medium sulfate column same arsenic release pattern is observed (Figure 5.3), except for the attenuated elongation of the maximum concentration phase and the slower, smoother drop in concentration toward the end. It could be partially a result of As(III) removal by the formation of insoluble As-S precipitates in MS system. Therefore, in the phase of high arsenic release (phase II), continuous removal of arsenite keeps the effluent concentration from reaching the maximum point.

At the end of run 35% and 46% of the initially loaded arsenic were leached out of MS and HS columns, respectively. Cumulative mass of arsenic that is leaching out follows the same trend in a comparable manner in both columns with HS reactor following a little behind due to the longer lag phase (Figure 5.5). After 331 days of operation, 35% of the total arsenic mass was released from MS column as oppose to 23% from HS column. Key factors contributing to the mass balance difference are: Initial mass of loaded sludge, run time, flow rate, and inflow sulfate concentration. Except for the lag phase in HS column, effluent arsenic concentration was always much higher than arsenic toxicity characteristic (TC) of 5 mgL^{-1} ($60 \text{ }\mu\text{M}$) that is the concentration below which arsenic waste disposal in municipal landfill is considered safe. Yet, under landfill conditions, these ABSRs are leaching arsenic at much higher concentration than arsenic TC which indicates TCLP impairment to represent landfill condition as a standard leaching test. HS column was run till concentration of arsenic in the effluent reached below TC limit, however, MS column was stopped while arsenic was still leaching out at its maximum concentration of $\sim 0.4 \text{ mM}$.

Unlike the differences in arsenic leaching trend and speciation, both columns are behaving almost identical in term of iron leaching trend, speciation, and total mass released. During the first two months of the experiments, average iron concentration was between $6\text{--}8\text{ mgL}^{-1}$ after which it stayed below 2 mgL^{-1} for the rest of the operation. From the second month to the end of the experiments, values fluctuated with only a few above or close to the initial highest peak. Although Fe reducing activity was continuous throughout the operation, the fraction of initial iron load that leached out was $<1\%$. The Fe^{3+} concentration during all the experiment was lower than that of Fe^{2+} . Iron reduction started from the very beginning of the run without any lag.

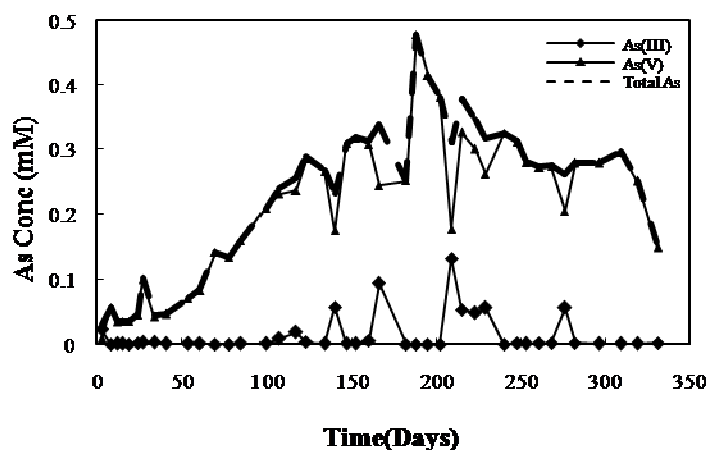


Figure 5.1. Medium sulfate column (MS) arsenic speciation with As(V) being dominant during the course of the experiment. 35% of the initial arsenic mass leached out of the reactor after 331 days.

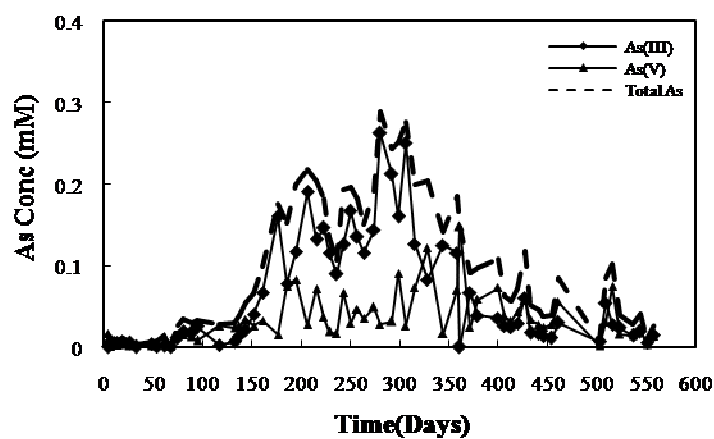


Figure 5.2.High sulfate Column (HS) arsenic speciation with As(III) being dominant during the course of the experiment. 45% of the initial arsenic mass leached out of the reactor after 551 days.

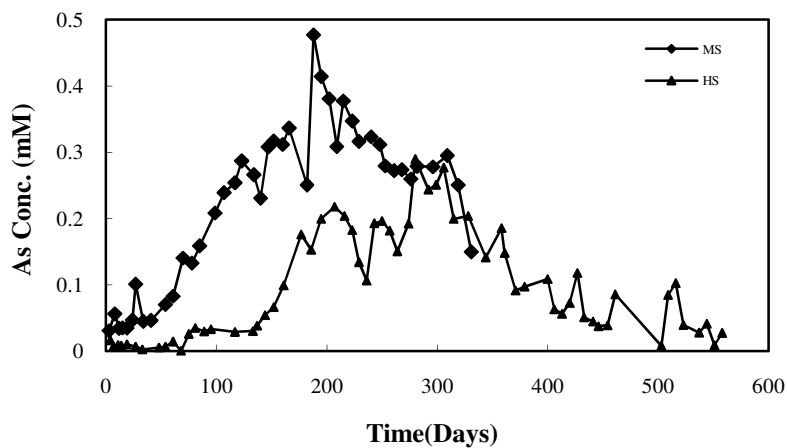


Figure 5.3.Arsenic leaching trend in both simulated landfill columns follows same pattern with different total As mass released; 35% from MS and 45% from HS column.

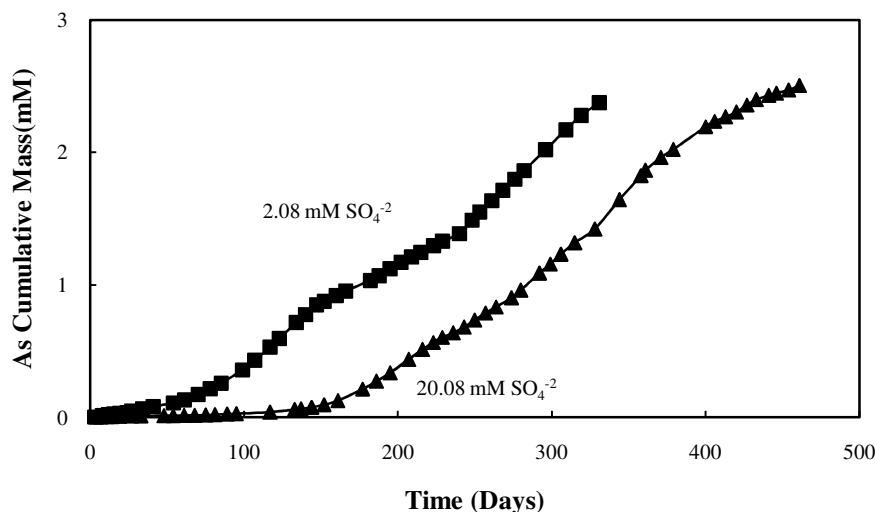


Figure 5.4. Cumulative arsenic leaching trend in medium sulfate column A and high sulfate column B. After 331 days 35% of the loaded As leached out of MS column compare to 22.85% of total As that was released from HS reactor after the same period of time.

4.2. Sulfate Consumption Rate

Influent and effluent sulfate concentration was monitored in MS column almost to the last days of its operation and half way through HS column's life. Influent sulfate concentration maintained steady into the HS and MS columns over the course of the experiment, except for a few drop points in the last few months of MS column. The effluent sulfate concentration from MS column decreased from nearly 100% breakthrough at 1 d to 50% at 37 d, 25% at 40 d, and <10% for the duration of the experiment after 60 d (Figure 5.5). The influent sulfate concentration of 20.8 mM in HS column dropped from 100% breakthrough at day 1 to 25% after 15 d, and except for an incident of 100% breakthrough at 75 d, effluent concentration kept increasing steadily to about 75% for the rest of the experimental duration (Figure 5.6). These results

indicatethat sulfate is reduced to sulfide or retained in the column as an adsorbed complex in both reactors.

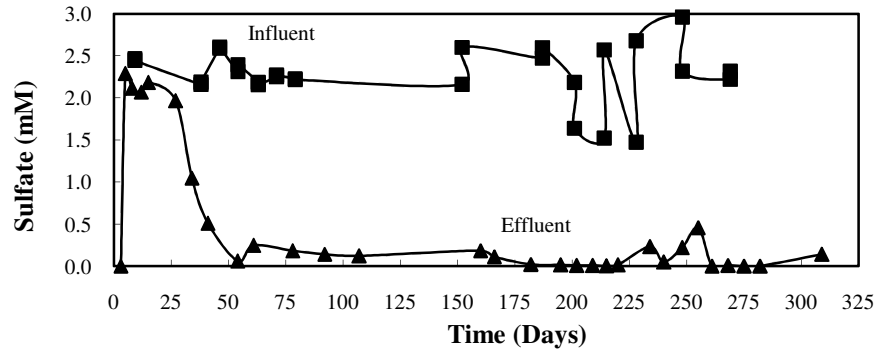


Figure 5.5. Sulfate consumption pattern in MS column. Within the first month of operation almost 50% of the input sulfate was consumed after which effluent sulfate concentration reduced to less than 10% of its influent concentration to the end of the run.

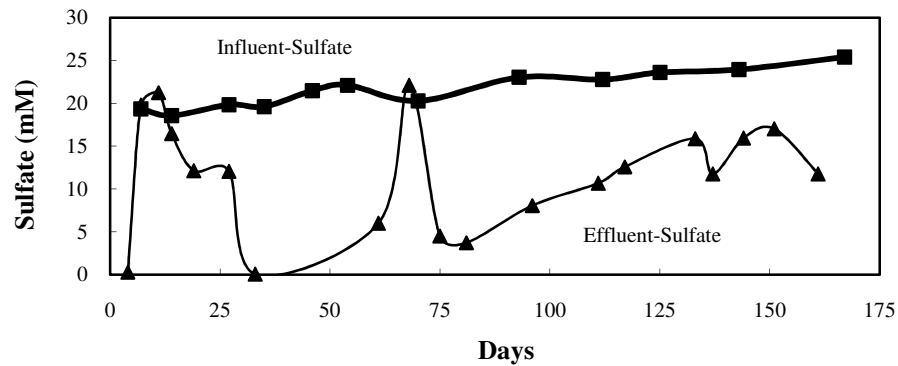


Figure 5.6. Sulfate consumption pattern in HS column. Within the first month of operation almost 25% of the input sulfate was consumed after which effluent sulfate concentration kept increasing back to about 75% of its influent concentration to the end of the run.

4.3. Solid Phase Biomineralization

MS and HS columns were stopped after 331 and 551 days of operation, respectively, and the columns were divided into four layers from bottom to top, which was the direction of the flow, to characterize the remaining solids. During the first 2-3 weeks of columns operation, changes in color, from brown to black, were noticeable in all layers of both columns, suggesting solid phase transformations of the initially loaded amorphous iron. These changes in coloration suggest formation of iron and sulfur phases which were detected in the XRD and XAS analyses conducted at the end of column's life. Different concentration of feed sulfate results in different sulfide biomineral formation in each individual column (Table 5.4).

It is known that microbial sulfate reduction significantly contributes to the biomineral formation under landfill conditions by forming sulfide minerals with much less specific surface area such as iron sulfide (FeS), and realgar (AsS), compare to the originally loaded iron sludge. The significant role of sulfate concentration in such system is confirmed by diverse mineralogy discovered in MS and HS columns. A geochemical reaction-path model, developed by O'Day et al. (2004), shows that in anoxic environments the ratio of reactive iron to sulfur determines the distribution of solid phases capable of sequestering arsenic. Therefore, sulfate concentration fed into the landfill simulated columns dictates solid phase end-product which in turn influence fate of released arsenic. FeS is the first sulfide phase forming in MS column. Realgar was also detected within the bottom three sections of MS column (Table 5.4). This model also

predicts Realgar as the first arsenic sulfide to precipitate in high-iron, reducing environments where H_2S activity is buffered by the coexistence of iron sulfide with ferric(hydr)oxide at circumneutral pH. Siderite and vivianite are present in all four sections of MS column with strongest peak in the upper section along with green rust.

Main sulfide phase detected in HS column is elemental sulfur throughout the column length except for section one (close to inlet) that consist of only poorly crystalline iron phase. There were no other sulfide mineral (Ferrous sulfide or Realgar) detected in this column. Vivianite was detected in the two middle sections but not close to inlet or outlet. Some traces of goethite were also detected by XRD but with low peak intensities. All of the biominerals in both columns have less specific surface area than the AFH initially presented.

The identification and quantification of secondary minerals produced following ferrihydrite reductive transformation was obtained by performing linear combinations fitting of k_3 weighted EXAFS spectra and was confirmed by XRD (Figure 5.7). Substantial mineral phase transformation is observed within the column, with ferrihydrite conversion to predominantly FeS in MS column and vivianite in HS column. The arsenic and iron oxidation state were measured by X-ray Absorption Near Edge Spectroscopy (XANES). As and Fe XANES analysis shows As(III) as the only oxidation state in all four solid sections of the column and Fe(II) as the only oxidation state in the three bottom sections of the column which changes to 50/50 Fe(II) and Fe(III) in the top section

(Figures 5.8 and 5.9). Formation of secondary sulfide minerals was also confirmed by XAS analysis which is discussed in detail in chapter 4.

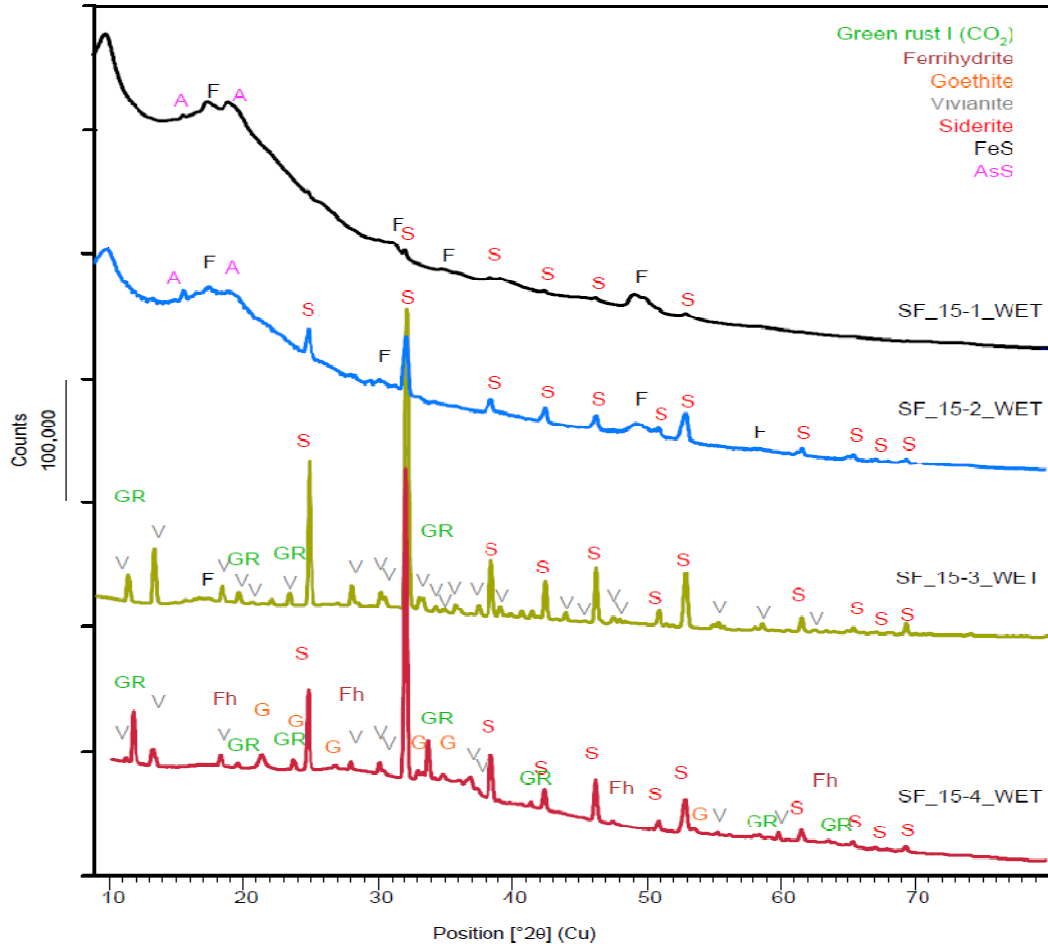


Figure 5.7. XRD patterns for biominerals formed in MS column. The XRD patterns compared to the database show FeS and siderite as the main species in the bottom and top sections of the column, respectively. Goethite was also detected but with weaker peaks than the reduced Fe minerals.

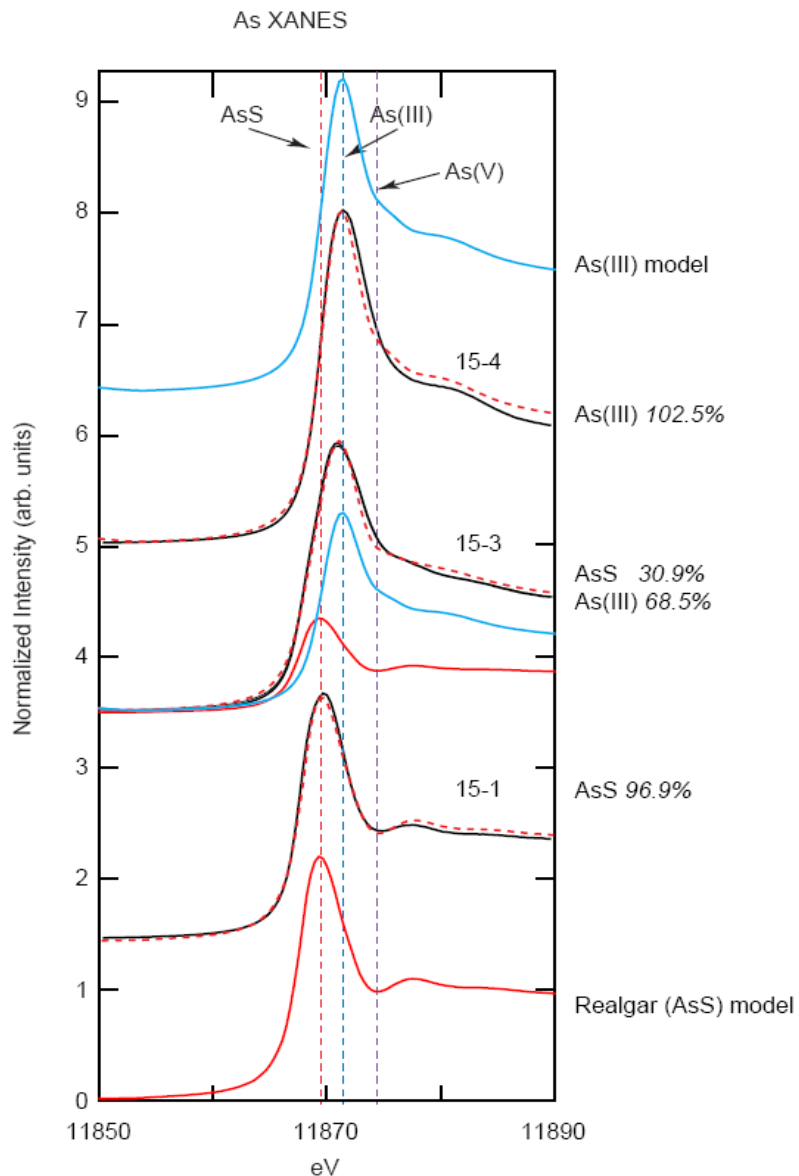


Figure 5.8. First derivative As XANES spectra for standard reference species compared to spectra for experimental samples collected from MS column at the completion of the 331 day advective flow experiment. The vertical dashed lines highlight the first-derivative peak energy of arsenite reference species. Mineral fit to samples from bottom and the top two sections confirm presence of As(III) as the only arsenic speciation in the solid phase.

Fe K-edge XANES

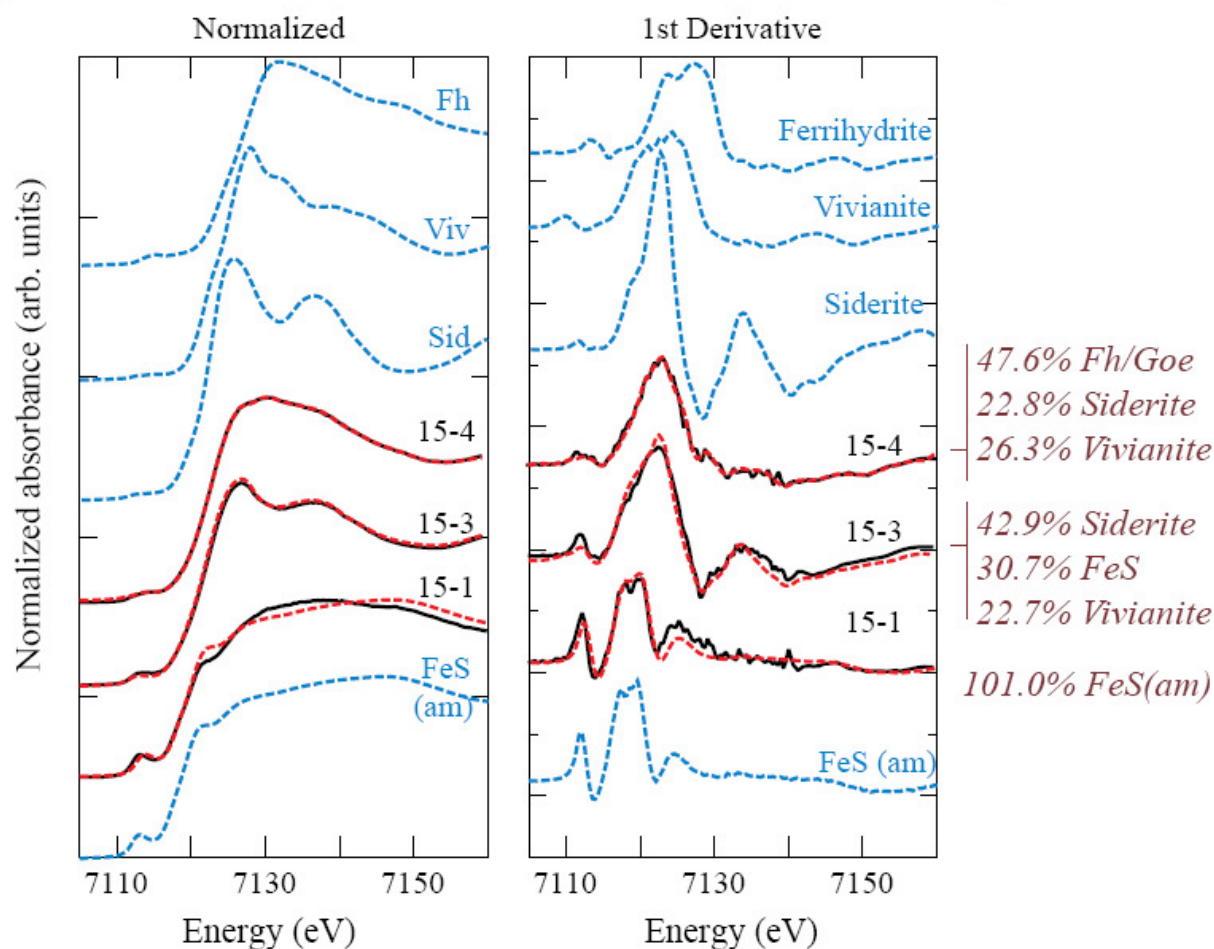


Figure 5.9. Normalized and First derivative Fe XANES spectra for standard reference species compared to spectra for experimental samples collected from MS column at the completion of the 331 day advective flow experiment. Mineral fit to samples from bottom and the top two sections confirm presence of ferrous solid phase as the main Fe oxidation state in the MS column.

Table 5.4. Biomineral transformation under the influence of different sulfate concentration

Column's Section (In the Direction of Flow)	MS Column (Sulfate Conc. 2.08 mM)	HS Column (Sulfate Conc. 20.8 mM)
IV	Siderite, Vivianite, Green rust, and Goethite	Sulfur and Goethite
III	FeS, AsS, Siderite and Vivianite	Sulfur, Vivianite and Goethite
II	FeS, AsS, Siderite and Vivianite	Sulfur*, Vivianite and Goethite**
I	FeS, AsS and Siderite	Poorly crystalline

*Elemental sulfur

**Goethite was detected as minor component in middle two sections

4.4. Electron Consumption Model

Diverse chemical composition and aqueous chemistry of our columns is driven by microbial oxidation of the only electron-donor source in the system, Lactate. However, formation of sulfide phases in both reactors are direct product of abiotic reactions between microbially reduced species. In this section, we discuss the biotic and abiotic reaction paths that could occur in our columns resulting in variation in solid phase characteristics.

To better understand possible pathways and mechanisms that cause such a diverse mineralogy and different speciation we developed a electron consumption model based on reactive components of each column. The standard state Gibbs free energy of reactions were adopted from Kocar et al. (2009) work on thermodynamic analysis of anaerobic sediments contaminated with arsenic using a range of Fe-(hydr)oxides and

lactate as electron donor. Knowing ΔG° for pertinent reactions and having the concentration of electrons available through lactate feed, we developed a model to predict the order of iron, arsenic, and sulfate reduction as a function of both time and depth of column. Solid Fe(III) and As(V) will be used by the biomass sequentially according to the energy yield of both reduction reactions.

Here in figures 5.10 and 5.11, we can observe the change of speciation (oxidation state) trend in the direction of flow and as a function of time. Lactate and sulfate are entering the reactors from the very beginning of the column operation. Following the injection of lactate, iron reduction starts immediately from day one and from section one and after a few days all the iron, sulfate, and arsenate at the bottom of the column got reduced. After about four days from the beginning of the experiment a mixture of both oxidation states for arsenic, sulfur, and iron are found in all four sections and after about three weeks everything in the column is reduced. The electron consumption trend in MS column represent a system with strong reducing power which provide a rich electron source to drive complete reduction reactions (Figure 5.10).

In HS column, however, we observed a very different speciation distribution because of much higher sulfate concentration, 10x higher than MS system, even though all the other parameters such as flow rate and electron concentration are exactly the same (Figure 5.11). In HS column also iron reduction in the first section, close to inlet, starts from the first day of operation as well as partial reduction of input sulfate that continues throughout the column's life. There is not enough reducing power though to completely

reduce all the sulfate which is continuously entering the column, neither it's sufficient for iron and arsenic reduction within all four sections of the column. Therefore, except for the iron close to the inlet and partially reduced sulfate that is moving up in the column in the direction of flow, none of the species are getting reduced completely due to lack of available electrons. High concentration of sulfate which is entering the reactor at the same time as electron source does, consumes all the reducing powers and leaves iron and arsenic in their original oxidation states.

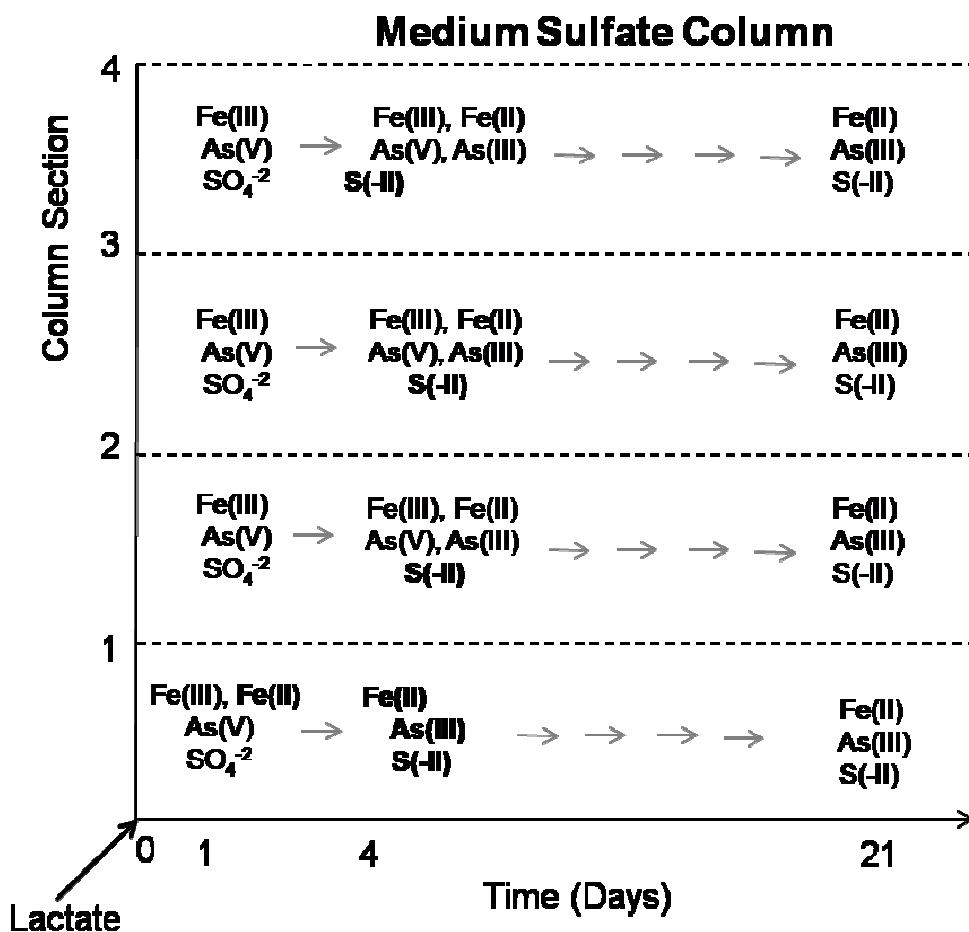


Figure 5.10. Electron consumption model for MS column. At sulfate concentration of 2.08 mM, lactate (5.5mM) provide sufficient reducing power to reduce sulfate, iron, and arsenic completely in the column in a period of less than a month.

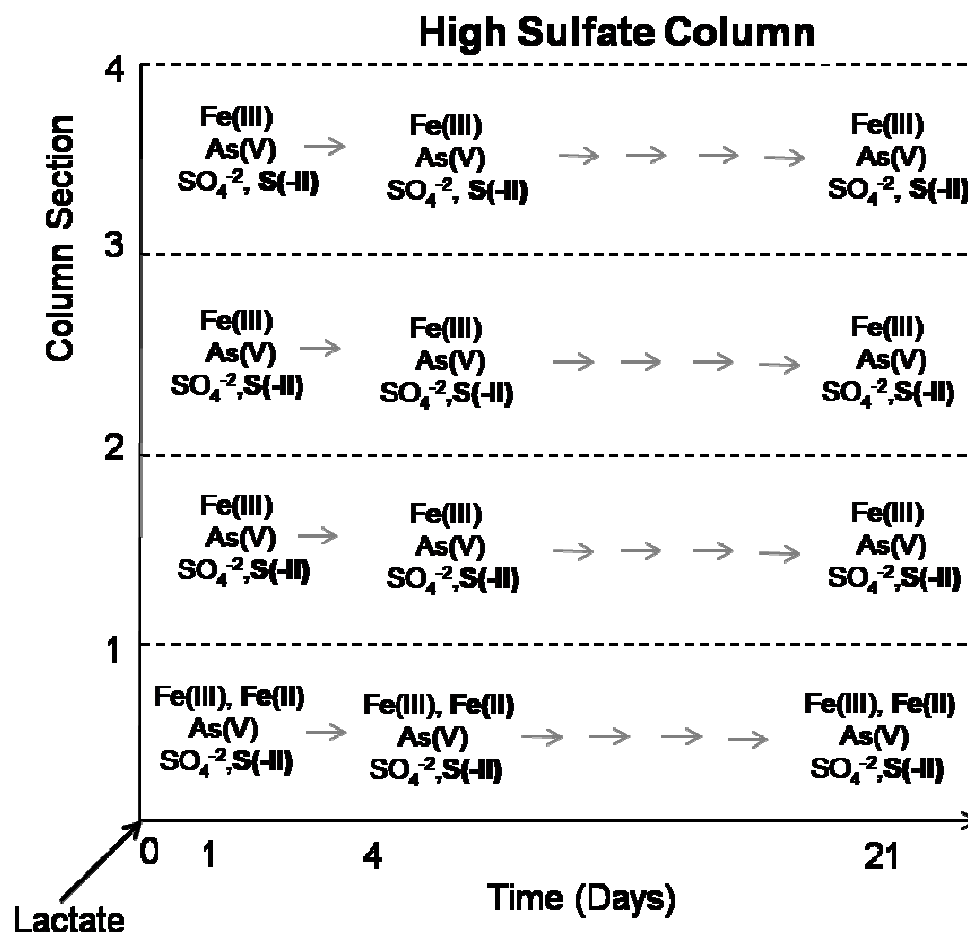


Figure 5.11. Electron consumption model for HS column. At sulfate concentration of 20.8 mM, lactate (5.5mM) is only able of partial reduction of sulfate and iron close to inlet. Reduced sulfur move up in the direction of flow where only oxidized state of iron and arsenic exist.

4.5. Possible Reaction Pathways and Mechanisms

Sulfate concentration dictates dominant redox reactions and pathways in our columns which will then determine arsenic fate under landfill conditions. The significance of sulfate role is on how it controls the availability of lactate for other species as the only source of electron for microbial reduction. Therefore, concentration of sulfate feed into

the column determines whether or not there is enough reducing power left to carry up with the flow to reduce iron and arsenic downstream.

In MS column close to the inlet, lactate is partially consumed by iron reducing bacteria to reduce Fe(III) on the surface of freshly loaded sludge to Fe(II), which then dissolves into the aqueous phase as a result of reductive dissolution. Arsenic reduces to arsenite through microbial reduction, and sulfate reducing bacteria (SRB) are reducing sulfate to sulfide which would react with aqueous ferrous and arsenite to form ferrous sulfide and realgar, as sulfide concentration favors formation of these biominerals in MS column. Under sulfate-reducing conditions, arsenic could be sequestered by the formation of AsS precipitates or strongly sorbed surface complexes (Gallegos et al., 2007). Sulfate reduction to sulfide, coupled to lactate oxidation, results in Fe(III) reduction by dissolved S(-II); where excess sulfide is generated (exceeding the removal rate by Fe(III)), formation of $\text{FeS}_{(s)}$ can also be expected (Kocar et al., 2010). The mechanism of ferric (hydr) oxide reduction by S(-II) involves ligand displacement of OH^- by HS^- and subsequent e^- transfer from S(-II) to Fe(III), forming a Fe(II) S' complex, followed by $\text{H}_2\text{O-S}^-$ ligand exchange and dissociation to form $\text{Fe(II)}_{(aq)}$ and S^0 (Afonso and Stumm, 1992; Poulton et al., 2004). Higher up in the column, close to the outlet, where lactate reducing power is diminishing, oxidation of sulfide could couple to reduction of Fe(III) to form elemental sulfur. In this reaction e^- transfers through surface complexation and results in the oxidation of dissolved sulfide to S^0 and dissolution Fe(II) (Poulton et al., 2004). Elemental sulfur could then undergo biologically mediated disproportionation (Reaction 2). Zero-valent sulfur can also oxidize arsenite to stable aqueous arsenate species that is

the dominant arsenic oxidation state continuously detected in our effluent measurements (Figure 5.1). Therefore, the speciation of As under reducing conditions is closely linked to that of sulfur.



Elemental sulfur could also react with dissolved sulfide to form aqueous polysulfides (Reaction 3)(Saalfeld et al., 2009);



Another possibility for oxidized arsenic speciation in this column could be the presence of green rust in the very top section close to outlet as it can inhibit arsenate reduction. Su's group conducted batch experiments on arsenate and arsenite sorption on carbonate green rust in an anaerobic glove box at pH ranging from 7.7 to 10.4. They found that sorbed arsenite was partially oxidized at the surface of carbonate green rust. Despite the low Eh reducing conditions, As(V) reduction in the presence of CGR did not occur even after reaction times of up to 60 days. As(V) reduction under such reducing conditions may be kinetically inhibited in the presence of CGR or is thermodynamically infeasible (Su et al., 2005). They also demonstrate in a batch experiment that As(III) oxidation occurred for the one day (pH 7.5) batch test resulting in conversion of about 20% of sorbed As(III) to As(V) on the surface of CGR. Because dissolved As(III) in water in the absence of CGR did not show any oxidation effect, it is concluded that As(III) oxidation

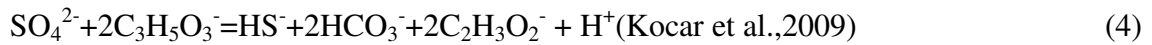
must be a solid-promoted process. Amstaetter et al. (2010) studied arsenic redox changes by goethite mineral suspension amended with Fe(II) under neutral pH. They discovered that goethite in the presence of Fe(II) is capable of As(III) oxidation under anoxic conditions. In contrast to thermodynamic predictions, Fe(II)-goethite systems did not reduce As(V), instead they observed rapid oxidation of As(III) to As(V) in Fe(II)-goethite systems. Their study indicates that in the simultaneous presence of Fe(III) oxyhydroxides and Fe(II), as commonly observed in environments inhabited by iron-reducing microorganisms, As(III) oxidation can occur.

In HS column, however, complete consumption of lactate by SRBs, close to inlet, which is the active zone of sulfidogenesis, leaves no more electron for microbial reduction of Fe(III) and As(V) and not even complete reduction of sulfate (Reaction 4).

Sulfate reduction significantly contributes to the oxidation of organic matter in anoxic environments (Finster et al., 2008). Therefore, in HS reactor concentration of $\text{Fe(II)}_{(\text{aq})}$ is low whereas dissolved sulfide concentration is high and is transported up in the direction of flow. High $\text{H}_2\text{S}_{(\text{aq})}$ concentration inhibits formation of Sulfide minerals and increases abundance of soluble thioarsenite species (Burton et al., 2011).

The results from Kirk et al. (2010) geochemical modeling calculations show that lower sulfide concentration promote orpiment (As_2S_3) and realgar (AsS) formation whereas higher sulfide concentration stimulates thioarsenic formation and enhance As solubility. H_2S is a strong reductant of iron oxides and arsenate in sulfidogenic environments.

Oxidation of sulfide, coupled to reduction of Fe (III) and As(V), in three top sections of the column produces dissolved As(III), Fe(II), and elemental sulfur (Reaction 5). Hence, top parts of HS column are zones of active abiotic redox reactions. A possible mechanism for the accumulation of elemental S in HS column is its precipitation from S^0 (aq) produced during the oxidation of sulfide by Fe oxyhydroxides (Couture et al., 2013).



Rapid reduction of Arsenate by sulfide allows for the formation of arsenic-sulfide complexes, lasting for several days in solution before dissociating and leading to the production of dissolved arsenite (Rochette et al., 2000).

Low-Fe environments inhibit FeS or pyrite precipitation and increase dissolved H_2S concentration, leading to orpiment formation. Dissolved H_2S concentration higher than 1 mM dissolves orpiment through formation of arsenic-sulfide complexes (O'Day et al., 2004). Therefore, low iron concentration could be the reason for absence of FeS and consequently realgar in HS column. Arsenic thioanions formation promotes arsenic solubility and keeps the free aqueous concentration below saturation for sulfide minerals (Bostick et al., 2005). For arsenic sulfide mineral to form, its solubility needs to be exceeded and also mineral precipitation rates need to be faster than the flow rate.

Kocar group conducted a column study of loaded As(V)-ferrihydrite coated sand inoculated with sulfate reducing bacteria and they observed that sulfidogenesis mainly occurs in zone of active Fe reductive dissolution and solid phase transformation which leads to changes in As partitioning; formation of As sulfide minerals, in particular, is inhibited by reactive Fe(III) or Fe(II) either through sulfide oxidation or complexation.

Another possible route for arsenic reduction is microbially driven. Under reducing conditions, chemoautotrophic dissimilatory As(V) reducers generate As(III) using sulfide as electron donor and through fixation of inorganic carbon that would oxidize back into CO₂ to transfer the electrons to Arsenate (Hoeft et al., 2010). Abiotic reduction of As(V) by dissolved sulfide is slow at neutral to basic pH, unlike abiotic Fe(III) reduction rate (Rochette et al., 2000), therefore, As(V) reduction is mainly microbially promoted downstream of the column. Hoeft's group calculation shows that sulfide and arsenate loss occurs at a 1:4 ratio, which indicates an eight-electron transfer reaction from the oxidation of 1 mol of sulfide with the reduction of 4 mol of arsenate. At high sulfide concentration, anoxygenic phototrophic bacteria favors elemental sulfur production over sulfate formation, but also hinders elemental sulfur disproportionation for thermodynamic reasons (Finster et al., 2008). As a result, in sulfide rich environments such as the HS column in this study, elemental sulfur remains as final solid sulfur phase (Figure 5.12).

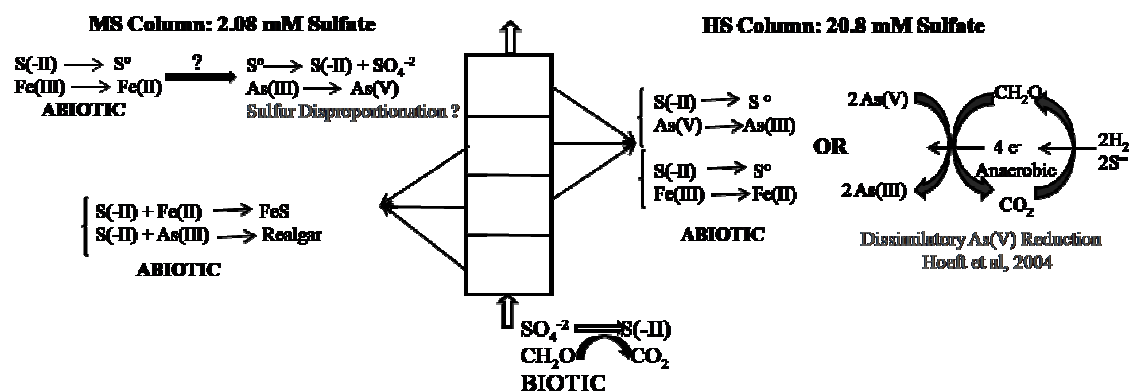


Figure 5.12. Influent sulfate concentration dictates possible biotic/abiotic reactions and pathways occurring in MS and HS reactors, resulting in diverse mineral phases and different arsenic speciation between the two columns.

4.6. Thermodynamic Favorability Diagram of Pertinent Reactions

In this work, we evaluate the behavior of ABSRs in a complex and multicomponents environment of municipal waste landfill. Understanding and mapping all the major reaction paths, involving more than one component (Fe, As, etc.) in a highly reducing, microbial rich environment with a range of phosphate, carbonate, organic carbon, and a wide range of sulfate concentration relies not only on kinetic factors, but even more importantly thermodynamic favorability of relevant redox reactions to determine whether a reaction can proceed and on energy yield for microbial respiration of processes representative of landfill conditions. Due to the significant impact that sulfate reduction and concentration has on the fate of Fe and subsequently As, thermodynamic favorability of its redox reaction is considered in our analysis. Kocar et al. (2009) has conducted a thermodynamic viability study using actual measurements from the sediments of a field site in Cambodia which is contaminated with arsenic. They determined standard state

Gibbs free energy for arsenate, ferrihydrite, and sulfate reduction using Lactate, acetate, or H_2 as electron donor (Figure 5.13). They found out that reduction of all three species are thermodynamically feasible over a wide range of electron donor, concentrations, and pH with ferrihydrite reduction being more favorable than arsenic at Fe^{2+} concentration of lower than 1.0×10^{-5} , which is the case in both HS and MS columns except for a few isolated higher Fe^{2+} concentration points. Biogeochemical reactions yielding the greatest Gibbs free energy will dominate until reactants are depleted, at which time the dominant process will cycle to the next most favorable energy yielding reaction (Stumm et al., 1996). However, the hierarchy of energy yielding redox couples also depends on the concentration gradient of the both reactants and products which influence the reduction rate of the relevant constituents in our columns. Based on the thermodynamic calculations, As reduction expected to occur regardless of the presence of reducible $Fe(III)_{(s)}$ or sulfate (Kocar et al., 2009). In this study, ΔG°_{rxn} from Kocar's group were adopted and effluent concentration from column experiments were used to develop a thermodynamic viability model for pertinent redox reaction favorability as a function of concentration (Figure 5.14). Arsenate/Arsenite redox zone was determined by bracketing the values in between the lowest and highest arsenite concentration of 1.28×10^{-2} mM and 0.262 mM measured in the effluent and therefore thermodynamic favorability of arsenate reduction by lactate is presented as two separate lines for the case of low and high arsenite concentration. Same strategy was adopted to plot the lines of redox favorability for $Fe(OH)_3$ and $FeOOH$. By knowing the concentration of the electron donor, Lactate, and ΔG°_{rxn} the order and extent of e^- consumption and species reduction in the columns could be also predicted as is explained in above section. Here in both HS

and MS columns phase transformation starts with reductive dissolution of ferrihydrite, follows by reduction of sulfate and then arsenate in the direction of the flow. Reduction of both As(V) and sulfate is favorable over a wide range of concentration in these columns.

Lactate Oxidation Reactions		$\Delta G^\circ_{\text{rxn}}$ (KJ/mol)
$4\text{Fe}(\text{OH})_3 + \text{C}_3\text{H}_5\text{O}_3^- + 7\text{H}^+ \Rightarrow 4\text{Fe}^{2+} + \text{CH}_3\text{COO}^- + \text{HCO}_3^- + 10\text{H}_2\text{O}$		-347.3
$2\text{HAsO}_4^{2-} + \text{C}_3\text{H}_5\text{O}_3^- + 3\text{H}^+ \Rightarrow 2\text{H}_2\text{AsO}_3 + \text{CH}_3\text{COO}^- + \text{HCO}_3^-$		-293.9
$4\text{FeOOH} + \text{C}_3\text{H}_5\text{O}_3^- + 7\text{H}^+ \Rightarrow 4\text{Fe}^{2+} + \text{CH}_3\text{COO}^- + \text{HCO}_3^- + 6\text{H}_2\text{O}$		-273.4
$4\text{Fe}_2\text{O}_3 + \text{C}_3\text{H}_5\text{O}_3^- + 7\text{H}^+ \Rightarrow 4\text{Fe}^{2+} + \text{CH}_3\text{COO}^- + \text{HCO}_3^- + 4\text{H}_2\text{O}$		-265.9
$2\text{H}_2\text{AsO}_4^- + \text{C}_3\text{H}_5\text{O}_3^- + \text{H}^+ \Rightarrow 2\text{H}_2\text{AsO}_3 + \text{CH}_3\text{COO}^- + \text{HCO}_3^-$		-216.7
$0.5\text{SO}_4^{2-} + \text{C}_3\text{H}_5\text{O}_3^- \Rightarrow 0.5\text{HS}^- + \text{CH}_3\text{COO}^- + \text{HCO}_3^- + 0.5\text{H}^+$		-65.4

Figure 5.13.Standard state Gibbs free energy for pertinent reactions using lactate as organic electron donor.Adopted from Kocar et al, 2009.

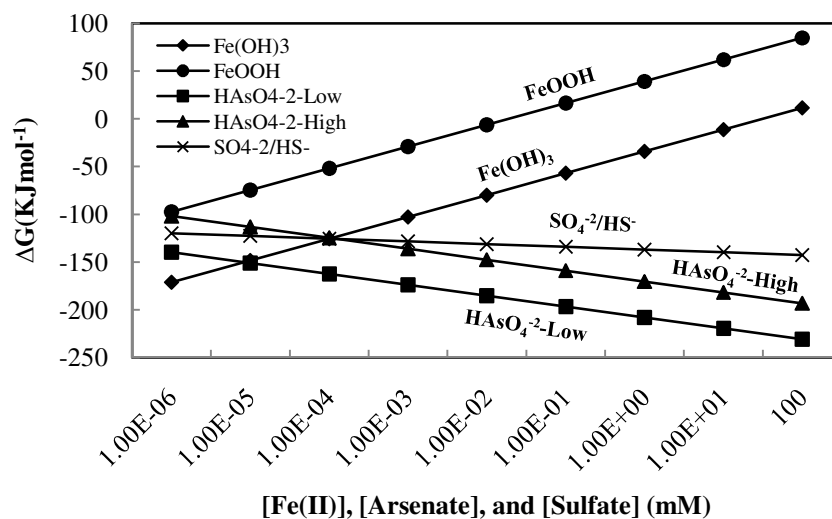


Figure 5.14.Thermodynamic favorability of pertinent redox reactions in a simulated landfill column. ΔG_{rxn} are calculated using concentration measured in the effluent of our columns.

6. Conclusions

In complex environments such as landfills with diverse microbial communities, complex composition and biogeochemical interactions sulfate plays a key role in fate of arsenic. Sulfate concentration dictates dominant redox reactions and pathways in our columns which will regulate arsenic sequestration/mobilization under reducing condition. The significance of sulfate role is on how it controls the availability of lactate for other species as the only source of electron for microbial reduction. Our electron consumption model predicts a different speciation distribution pattern for MS and HS mainly due to different input sulfate concentration. The electron consumption trend in MS column represents a system with strong reducing power which provides a rich electron source to drive complete reduction reactions for Fe, As, and Sulfate. Sulfide concentration favors formation of FeS and realgar in MS column. In HS column, however, higher sulfate concentration scavenges almost all the reducing power to reduce Fe(III) close to inlet and partially reduce sulfate. Major sulfide phase detected in HS column is elemental sulfur. Formation of sulfide phases in both reactors are direct products of abiotic reactions between microbially reduced species.

CHAPTER 6

CONCLUSIONS AND FUTURE WORK

The results presented in this study are useful in developing optimum processing conditions for arsenic stabilization to meet the arsenic waste disposal regulation and reduce the treatment cost.

The research effort undertaken in this project focused on the long-term behavior of arsenic bearing solid residuals (ABSRs) after municipal landfill disposal by conducting a series of continuous up-flow columns with conditions similar to those found in mature landfills. A primary focus was the generation of and role played by secondary minerals, derived from transformations of the amorphous ferric hydroxide (AFH) in the presence of sulfate under simulated landfill conditions.

Simulated landfill column experiments showed that biomineralization would naturally occur in typical mature municipal solid waste (MSW) landfills. Organic matter that is present in non-hazardous MSW landfills serves as a carbon source and electron donor to the diverse microbial community to reduce ABSRs.

The results of the simulated landfill column experiments render strong evidence that the TCLP does not accurately reflect the long-term As leaching that would occur under

landfill conditions and therefore is not a realistic test to evaluate arsenic release from ABSRs. Effluent arsenic concentration in all the columns was appreciably higher than the arsenic toxicity characteristic (TC) regulatory level of 5 mgL^{-1} for extended time periods tested. The maximum leaching concentration in the columns in this study ranged from 15 to $35 \text{ mgL}^{-1} \text{ As}$.

The mobilization of arsenic from the simulated landfill experiments follows a general trend that is reproduced over the whole range of conditions explored in this work; an asymmetric bell-shaped curve of arsenic effluent concentration vs. time consisting of the following stages: an initial lag phase (phase I) in which the effluent arsenic concentration is relatively low that coincides with microbial acclimatization, or/and the re-adsorption of released arsenic onto newly exposed AFH and re-precipitated iron surfaces, as Fe^{3+} undergoes reductive dissolution. Phase I is followed by a gradual but continuous increase of the effluent concentration (phase II) to reach a maximum, which is attributed to the depletion of sorption sites and formation of secondary mineral with less available active sites, resulting from continued iron reductive dissolution before tailing off (phase III) more slowly through the balance of the trial.

Despite other differences in arsenic leaching behavior between columns with different sulfate concentrations (0.064, 2.08, and 20.8 mM), and variation of total arsenic leaching over the duration of the run (30-100%), arsenic was released incongruently from iron in all columns. Incongruent dissolution means that the ratio of the concentration of iron to arsenic leached from the column is not congruent with that initially introduced in

the system in the co-precipitated ABSR. In all columns the iron to arsenic molar ratio of the ABSR was 22-27:1, whereas the column effluent ratios were never greater than 0.01. Non-stoichiometric dissolution occurs at the point when arsenic retention is no longer tied to iron retention which is the end of arsenic lag phase in these columns.

The mobilization of arsenic from arsenic-bearing solid residuals (ABSRs) in non-hazardous landfills is known to be a consequence of ABSR reductive dissolution and subsequent formation of secondary minerals. Iron and sulfur redox cycles have a considerable influence on arsenic cycling and its displacement in the landfill microcosm. The primary routes of iron and sulfate reduction in landfills are microbially mediated and biomineralization is a common by-product. Biomineralization may lead to formation of minerals such as siderite (FeCO_3), vivianite ($\text{Fe}_3(\text{PO}_4)_2$), iron sulfide (FeS), goethite (FeOOH), and realgar (AsS). Mineral transformation causes a significant decrease in the specific surface area and As adsorption capacity of secondary minerals, except under sulfidogenic environment where formation of arsenic sulfide may lead to greater arsenic retention.

Siderite and vivianite adsorption/co-precipitation studies indicate that co-precipitation is the favorable arsenic removal mechanism. Arsenic removal is greater via vivianite/siderite co-precipitation compared to adsorption. However, the Fe(II) minerals are not nearly as effective at sorbing arsenic as ferric(hydr)oxides.

The results of this study show that the concentration of sulfate fed into the system affects the biomineral formation, and that the relative amounts and sequence of precipitation of biominerals affect the free arsenic concentration. This suggests that biomineral formation and, consequently, arsenic stabilization, can be engineered by controlling the concentration of inflow sulfate to the system.

The solid phases inside one of the low inlet sulfate columns (0.064 mM) and a medium sulfate column (2.08 mM) were further studied using Micro-focused X-ray fluorescence (XRF) mapping and X-ray Absorption Spectroscopy (XAS), including extended X-Ray Absorption Fine Structure (EXAFS) and X-ray Absorption Near Edge Structure (XANES), to find out the nature of the Fe phases that are directly associated with As species. Iron XAS data show the reduction of AFH-derived Fe(III) to Fe(II) and secondary Fe (bio)mineralization.

As and Fe XAS showed that, in the low sulfate column, 75-81% of As(V) was reduced to As(III), and 53-68% of the Fe(III) sorbent was transformed, dominantly to siderite and green rust. In the high sulfate column, Fe(III) solids were reduced principally to amorphous FeS, whereas As(V) was reduced and integrated into a polymeric sulfide with local atomic structure similar to realgar. Multi-energy micro-X-ray fluorescence (ME- μ XRF) imaging at Fe and As K-edges showed that As formed surface complexes with ferrihydrite > siderite > green rust in the low sulfate column; while discrete realgar-like phases formed in the high sulfate systems. Results indicate that landfill sulfur chemistry exerts strong control over the potential mobilization of As from ferric sorbent residuals by controlling secondary As and Fe sulfide co-precipitate formation.

Much of the effort and significance of this project is about understanding the different means and mechanisms by which sulfate concentration and biomineralization influence arsenic fate under landfill conditions. Despite all the results of this study on formation of biominerals and the role these secondary phases play in fate of arsenic under landfill conditions, there is still a need for further investigation to compensate for the lack of knowledge that still exists on certain areas of long term effect of biogeochemical cycling of sulfur and iron on environmental arsenic mobility under reducing conditions, which are beyond the scope of this study. Here is the list of some of the areas that future research needs to focus on:

1) Design a research set-up to close the sulfur mass balance

a) Systematic measurement of dissolved $S^{\bullet}_{(aq)}$ in sulfidic environment as it plays a major role in arsenic redox cycle.

b) Arsenic thioanions are believed to comprise a major part of dissolved arsenic species under reducing condition which can persist in aqueous phase for weeks. There is not yet a well-defined method of measuring its concentration in solutions. Thioarsenic complex determination is currently only possible by XAS. Therefore, the formation, stability and sorption behavior of thioarsenic species should be considered in future research evaluating and predicting subsurface As mobility.

2) XAS analysis of arsenic species association with iron/sulfur

By combining X-ray absorption spectroscopy (XAS) and multiple energy micro X-ray fluorescence (ME- μ XRF) mapping (elemental and chemical), changes in sorbent and sorbate speciation, binding environments, and co-associations of the biominerals with arsenic species could be determined that enable improved prediction of As fate in mature landfills.

3) Column study on biotic vs. abiotic conditions

Operation of abiotic columns with medium sulfate (2.08 M) and high sulfate (20.8 mM) inflow, along with biotic columns, with different flow rate in both set is required to better evaluate the fate of arsenic under dynamic flow, sulfidic environments such as landfill.

APPENDIX A

CHAPTER 2 SUPPLEMENTARY INFORMATION

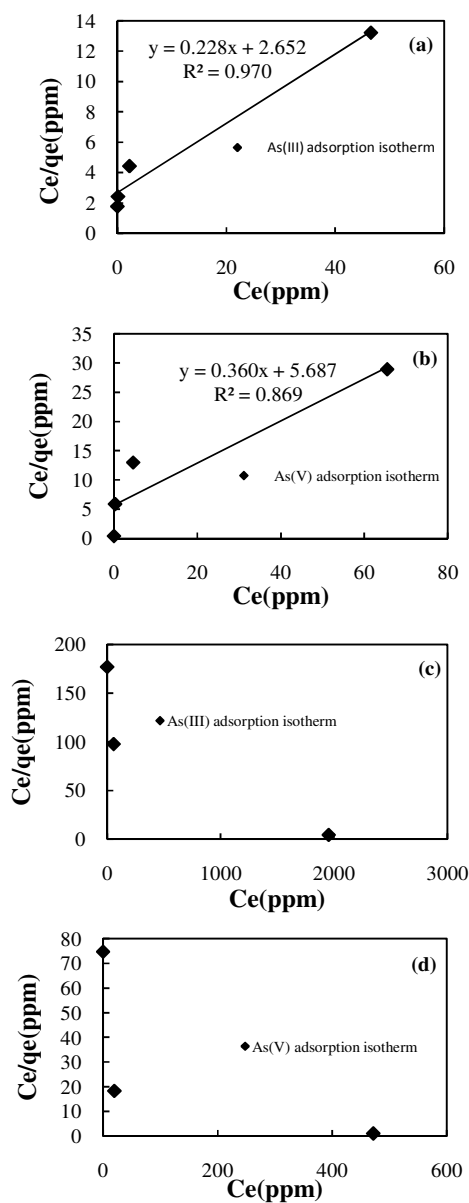


Figure 1. As(V) and As(III) adsorption (plots a and b) as well as co-precipitation (plots c and d) isotherms. Adsorption experiments were run at arsenic concentration: $0.2\text{-}100\text{ mg l}^{-1}$ and co-precipitation experiments were run at arsenic concentration: $0.2\text{-}3500\text{ mg L}^{-1}$

APPENDIX B

CHAPTER 4 SUPPLEMENTARY INFORMATION

1. XAS data collection and processing

The speciation and structural environment of Fe and As were determined using XAS at Stanford Synchrotron Radiation Lightsource (SSRL) on beamline (BL) 4-1 under dedicated conditions (3 GeV, 300 mA) using an unfocused beam with a dual crystal Si(220) monochromator for energy selection and a vertical beam size of 2 mm. Beam energy was calibrated on an iron foil (first edge inflection) at 7112 eV and arsenic foil (main edge inflection) at 11,867 eV, and calibration was monitored by periodic analysis of the foils. Fluorescence was monitored with a 13-element array solid-state Ge detector with a He cryostat sample holder (~ 8-15 K). Incident and transmitted intensities were measured with in-line 15 cm ionization chambers. Higher order harmonic frequencies were rejected by detuning the monochromator 40% from the maximum incident intensity. Isolation of backscattering contributions was accomplished by fitting a cubic spline function to the absorption envelope. The isolated function was then transformed from units of eV to \AA^{-1} to produce the EXAFS function ($\chi[k]$), where k (\AA^{-1}) is the photoelectron wave vector, which was then weighted by k^3 . Linear fitting routines were used to reconstruct the unknown sample spectra to determine the relative percentages of mineral phases within the samples (see (O'Day et al., 2004)). Spectra were fit by trial-and-error with 1 to 5 components from a reference library of ~30 spectra (O'Day et al., 2004). Standards were verified using X-ray diffraction (XRD). Fits were optimized by

allowing small energy shifts ($< 1\text{ eV}$), fits with up to 4 components were justified by XRD and μXANES . Accuracy of linear combination analysis was previously investigated by O'Day et al. (O'Day et al., 2004), where it was shown that fits were within $\pm 5\%$ of the actual mole percentages using the edge region $7100 - 7150\text{ eV}$. The detection limit for minor constituents was $\sim 5\%$.

1.1. Arsenic

Extended X-ray absorption fine structure (EXAFS) spectra were collected to $k = 13.5\text{ \AA}^{-1}$, with a 10 eV step from -200 eV to the near edge, 0.5 eV step across the edge and 0.05 k step in the EXAFS region. Fluorescence and transmission spectra were background subtracted and the atomic absorption was normalized to unity using the average post edge oscillation. Scans were averaged using the SIXPACK software package (Webb, 2006), normalized and background subtracted using PROCESS in EXAFSPAK, and fit by non-linear least-squares methods on individual atomic shells in k -space using OPT in EXAFSPAK (O'Day et al., 2004; George and Pickering, 2000; O'Day et al., 2004). Theoretical phase-shift and amplitude functions were calculated with the program FEFF (Rehr, 1993; Rehr, 1992). Based on empirical fits to known arsenic and iron reference compounds, estimated errors were $R \pm 0.01\text{ \AA}$, N or $\sigma^2 \pm 15\%$ for the first coordination shell, and $R \pm 0.02\text{ \AA}$, N or $\sigma^2 \pm 25\%$ for atoms beyond the first shell (see also (O'Day et al., 2004)). Beam induced oxidation or reduction was not observed, this was monitored by watching for changes in the relative amplitude of edge peaks.

1.2. Iron

X-ray absorption near edge structure (XANES) spectra were collected from -200 to + 400 eV about the K-edge with 0.35 eV fine energy steps from the pre-edge to near post-edge region. Reference samples were collected in fluorescence and transmission mode using the same procedures as for the AFH sludge samples. Spectra were processed as above for the As samples. The normalized first derivative of XANES spectra were compared to a set of reference standards for linear combination spectral fitting using the EXAFSPAK module DATFIT (George and Pickering, 2000).

2. XRF data collection

ME maps were collected by automated stage and monochromator control, scanning one row across the designated area at one pixel height for each energy position and repeating this process at each successive row until mapping of the entire area at each energy was completed (Mayhew et al., 2011). X-ray fluorescence imaging was carried out at Stanford Synchrotron Radiation Lightsource at beamline 2-3. Fluorescence at each pixel was measured at RT in a continuous scanning mode using a single-element SiLi Vortex detector with a multi-channel analyzer (MCA) system to bin and calibrate fluorescent counts from each element. Incident X-ray energy was tuned with a double crystal Si (111) monochromator with resolution of about 1 eV at the As edge. The accelerator ring operated at 300 mA and 3.0 GeV. The ME micro-(μ)XRF Fe and As maps were processed and fit using the micro-XRF analysis toolkit software package SMAK, a free software

program (http://home.comcast.net/~sam_webb/smak.html). Fluorescence data was normalized to the incoming incident x-ray (IOSTRM) to account for any fluctuations in the incoming x-ray intensity. Maps at each energy (5 for Fe, 4 for As) were imported into a single file processing in SMAK, where PCA and XANES processing is automated. The unique components highlighted with PCA were probed with μ XANES to confirm species or mineralogy and analyze the largest variety of different chemical species in the afforded beam time.

3. Details of column experiment

The iron-arsenic sludge was prepared to simulate the wastes generated from treatment technologies for removing arsenic from water (e.g., enhanced flocculation and precipitation with iron salts). Sodium arsenate heptahydrate ($\text{Na}_2\text{HAsO}_4 \cdot 7\text{H}_2\text{O}$, KR Grade, Sigma- Aldrich) was dissolved in lab deionized water (18.2 M Ω Milli-Q Water System by Millipore) in a 4L Erlenmeyer flask. Ferric chloride hexahydrate ($\text{FeCl}_3 \cdot 6\text{H}_2\text{O}$, ACS reagent, Sigma-Aldrich) was added to the As solution. The final volume was 1.00 L with 0.047 M as As and 0.935 M as Fe to give a Fe:As molar ratio of 20:1. This mixture was stirred on a reciprocating shaker table (Orbit, 100 rpm) for 1 hour. After mixing, the pH of the solution was adjusted to pH 7 by adding 295 mL of 10 M sodium hydroxide (NaOH, flakes, EMD Chemicals). The produced AFH sludge was equilibrated for 2 d while the pH was maintained at 7.0 ± 0.2 . The sludge was washed 5x to a supernatant EC < 1mS cm⁻¹, and concentrations of $[\text{As}_{(aq)}]$ and $[\text{Fe}_{(aq)}]$ were 74.2 μg

L⁻¹ and < detection limit, respectively. The sludge pH was checked during the washing process and was constant (7.0 ± 0.2) without further adjustment. After a final decanting, the remaining slurry was vacuum filtered through 0.45 μm (cellulose nitrate membrane filter, Whatman) and stored at 4° C until use within two weeks. Previous work in our lab using visual, SEM, and XRD analysis, has shown no evidence of phase changes under these conditions for 3 weeks, although changes are known to occur over longer time frames. The final sludge had a water-content of 79.4% wt/wt as measured by drying a sample at 70°C for 2 days. Full details are in the PhD Dissertation by Fernando Alday “*Iron Bio-mineralization: Implications on the Fate of Arsenic in Landfills*”, June 2010, University of Arizona (Alday, 2010).

Total Fe and As in the synthesized sludge was determined by digestion of a 1.0 g of dry sample using 70% by volume HNO₃ (J.T. Baker) in a CEM microwave digester, using SW 821-method 8051. The dry sludge As and Fe content was 25.52 mg g⁻¹ and 513.1 mg g⁻¹, respectively. Iron concentrations throughout were determined with 1,10 phenanthroline method (APHA,1998) using a spectrophotometer at 510 nm wavelength (Spectronic Genesys 5). Arsenic concentrations throughout were measured by inductively coupled plasma mass spectrometry (ICPMS, Agilent 7500a). All flasks and filters were weighed before and after sludge filtration to calculate sludge losses. The As and Fe retained in the sludge were 91.94% and 97.01% of the initial masses used to prepare the sludge.

Aqueous chromatography columns (Spectrum Chromatography; 2.5 cm inner-diameter x 30 cm length) were packed with the prepared iron/arsenic sludge (73.3 g of wet sludge with an equivalent of 15.1 g of dry sludge) mixed with glass beads (120 g; 0.8 mm diameter). Anaerobic digester sludge obtained from Ina Road Wastewater Treatment Plant, Tucson, Arizona (25 mL of slurry) was added as the microbial inoculum. The columns were fed with a synthetic landfill leachate containing minerals and nutrients necessary for growth of the microorganisms. This synthetic solution was adapted from Field et al. (2003) by replacing all the chloride salts with sulfate salts to avoid chloride peaks that can overlap other anion peaks in ion chromatography (IC) readings. The influent was purged with nitrogen gas to maintain anoxic conditions, and then it was fed continuously into the columns using a multi-syringe pump (BS-9000-6 programmable multi-syringe pump, Braintree Scientific). Table SI 2 summarizes the column conditions. Effluent samples, filtered through 0.22 μm cellulose acetate syringe filters, were analyzed to quantify arsenic, iron, and lactate (and its derivative, acetate). Ion chromatography (IC, Dionex, DX-500) was used to quantify lactate oxidation to acetate and the oxidation of the latter to bicarbonate. An inverted serum flask filled with a 2% (w/v) NaOH solution was used to collect methane gas that was analyzed using gas chromatography (Hewlett Packard, Series 5790A) with FID. Alkalinity was determined by acid titration with 0.1 M HCl solution. pH was measured with an Orion (Model 720) pH meter.

After completion of the column operation, the composition of the solids was analyzed. The column was opened in an oxygen free glove box (Terra Universal 100) to preserve redox-sensitive mineral species. The total content of the column was divided into four

sections, numbered from bottom to top in the direction of flow. The material from each layer was dried in the glove box at room temperature for 7 d. Once drying was completed, a 0.5 mm mesh was used to separate the beads (0.8 mm diameter) from the solids.

Table 1. Column Synthetic Landfill Leachate.

Organic Solution	(mM)
Lactate	5.5
2-bromoethanesulphonate (BES)	1.0 (LS only)
Inoculate	25 grams
Nutrient Solution	(mgL⁻¹)
KH ₂ PO ₄	37
Ca(OH) ₂	5
MgSO ₄ ·7H ₂ O	10
Mg	9
NH ₄ HCO ₃	987
NaHCO ₃	951
Trace Nutrient Solution	(µgL⁻¹)
H ₃ BO ₃	50
FeSO ₄ ·7H ₂ O	2800
ZnSO ₄ ·7H ₂ O	106
MnSO ₄ ·H ₂ O	415
(NH ₄) ₆ Mo ₇ O ₂₄ ·4H ₂ O	50
AlK(SO ₄) ₂ ·12H ₂ O	175
NiSO ₄ ·6H ₂ O	113
CoSO ₄ ·7H ₂ O	360
Na ₂ SeO ₃ ·5H ₂ O	100
CuSO ₄ ·5H ₂ O	157
EDTA	1000
Resazurin	200

(modified from (Sierra-Alvarez et al., 2005) to use of sulfate versus chloride salts)

Table 2. Column Design Specifications.

Dimensions	25 mm x 300 mm
Pore volume	61.36cm ³
Pore volumes per day	2.00
Flow	122.72 m day ⁻¹
Darcy's velocity	0.25 m day ⁻¹
Porewater velocity	0.5 m day ⁻¹
Residence time	12.00 hours

Table 3. Matrix for Fe XRF from mapped energy (eV) and the measured fluorescence for each reference mineral. The matrix is used at each pixel to assign a mineral phase.

Species	Formula	Energy (eV)				
Iron		7114	7121	7126	7130	7137
Mackinawite	FeS	0.13	0.80	0.95	1.01	1.08
Siderite	FeCO ₃	0.05	0.53	1.52	1.18	1.28
Green Rust	Fe ^{II} ₄ Fe ^{III} ₂ (OH) ₁₂ CO ₃	0.05	0.48	1.44	1.50	1.00
Ferrihydrite	Fe ₄ HO ₈ •4H ₂ O	0.09	0.14	0.68	1.21	1.20
Arsenic		11869	11872	11875	11880	
Sulfide	As ₄ S ₄	1.97	1.29	1.05	1.06	
Arsenite	As(III)	0.89	2.87	1.77	1.45	
Arsenate	As(V)	0.19	0.73	3.08	1.29	

Shaded boxes represent the diagnostic peak maximum for As speciation.

Table 4. Arsenic and Iron K-edge EXAFS fit results^a

<i>Arsenic</i>						
Sample	Atom	N	R	σ^2	ΔE_0	χ^2
LS-II	As-L		(Å)	(Å ²)	(eV)	
	O	2.43	1.77	0.006 ^b	-1.81	3.5
	O	1.39	1.69	0.006 ^b		
	MS	1.0 ^c	3.10 ^c	0.009 ^c		
	Fe	1	3.46	0.006 ^b		
	Fe	0.7	3.31	0.006 ^b		
HS-I	S	2.0 ^b	2.25	0.0025	-7.06	2.76
	As	1.0 ^b	2.58	0.0037		
	As	2.5 ^b	3.49	0.0054		
	As	0.75 ^b	3.62	0.0057		
HS-III	O	1.9	1.76	0.003 ^b	-3.94	1.16
	S	1.1	2.26	0.003 ^b		
	As	0.6 [/]	2.6	0.001		
	As	1.4 [/]	3.49	0.003		
HS-IV	O	3 ^b	1.78	0.0028	0.94	0.94
	Fe	1 ^b	3.49	0.0056		
Realgar (As ₄ S ₄)	As-S	2.0 ^b	2.24	0.0038	-10.9	0.42
	As-As	1.0 ^b	2.57	0.0052		
	As-As	2.5 ^b	3.47	0.0065		
	As-As	0.75 ^b	3.63	0.0071		
	As-S	2.5 ^b	3.67	0.0078		
<i>Iron</i>	Atom ^a	N	R	σ^2	ΔE_0	χ^2
Sample HS-I ^d	Fe-L		(Å)	(Å ²)	(eV)	
	S	2.84	2.27	0.0048 ^b	-0.406	1.38
	Fe	2.75	2.71	0.0073 ^b		
	Fe	2.11	3.62	0.0107 ^b		
	Fe	2.49	5.21	0.0040 ^{bc}		
	O	1.78	2.02	0.0040 ^b		
	Fe	1.42	3.26	0.0040 ^b		
Crystallographic values						
Mackinawite	Fe-S	4	2.255			
(FeS) ^e	Fe-Fe	4	2.598			
	Fe-Fe	4	3.674			
	Fe-Fe	4	5.200			
Green Rust ^f	Fe-O	6	2.090			
[Fe ^{II} _{6-x} Fe ^{III} _x (OH) ₁₂]	Fe-Fe	6	3.250 ^g			
An• nH ₂ O]						

^aAtom is the backscatter pair As-L contributing to the As EXAFS; N is the number of backscattering atoms at distance (R); σ^2 , the Debye-Waller term, is the absorber-backscatterer mean-square relative displacement; ΔE_0 is the threshold energy difference; χ^2 is a reduced least-squares goodness-of-fit parameter(= F-factor/(# of points - # of variables). Scale factor (S_0^2) = 1. ^bParameter fixed in least-squares fit using value from fits to reference compounds, CN and σ^2 cannot be covaried; ^c Spectrum fit with the sum of multiple scattering paths from As-O-O-As triangular path in arsenate tetrahedra, with N set to the degeneracy here assigned to 1. The Debye-Waller term σ^2 is fixed at 3/2 of the σ^2 for the As-O tetrahedra, “/” parameter linked in fit to the parameter above based on structural constraints. ^dThe inclusion of 6 scattering paths was justified by the recognition that the data were from a binary mixture and relevant paths from FeS and GR were included. The long backscattering Fe-Fe at 5.21 Å was included because it improved the fit parameter χ^2 from 1.50 to 1.39. ^eThe mackinawite structure is from [86] P4/n m m, a=3.6735, c=5.0328 cell volume 67.916; atom site x, y, z, Fe 0x,0y,0z; S 0x 0.5y 0.2602z. ^fGreen rust crystallographic structure from [46], An refers to the intercalated anion (e.g. CO₃²⁻, SO₄²⁻, etc.-), ^g 3.25 Å is the edge sharing iron octahedra distance. Shaded portions highlight the sulfide component in the fits.

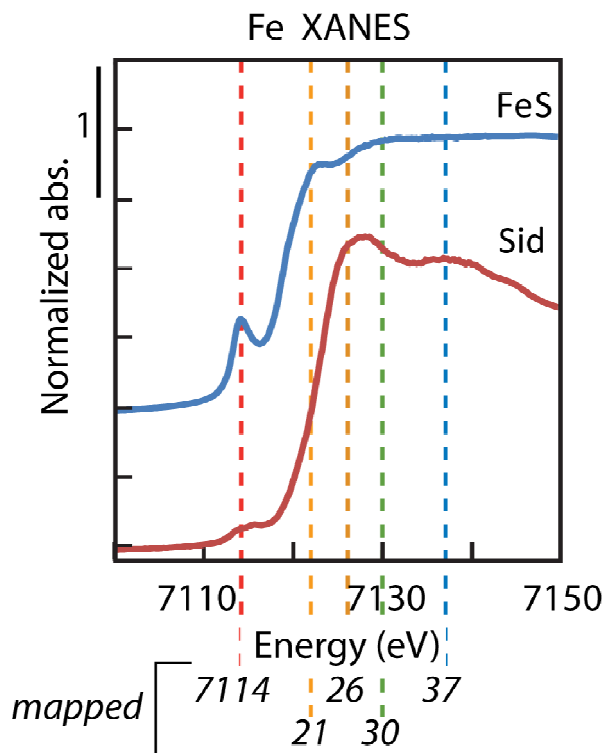


Figure 1. Schematic example of normalized Fe XANES intensity and selection of map energies.

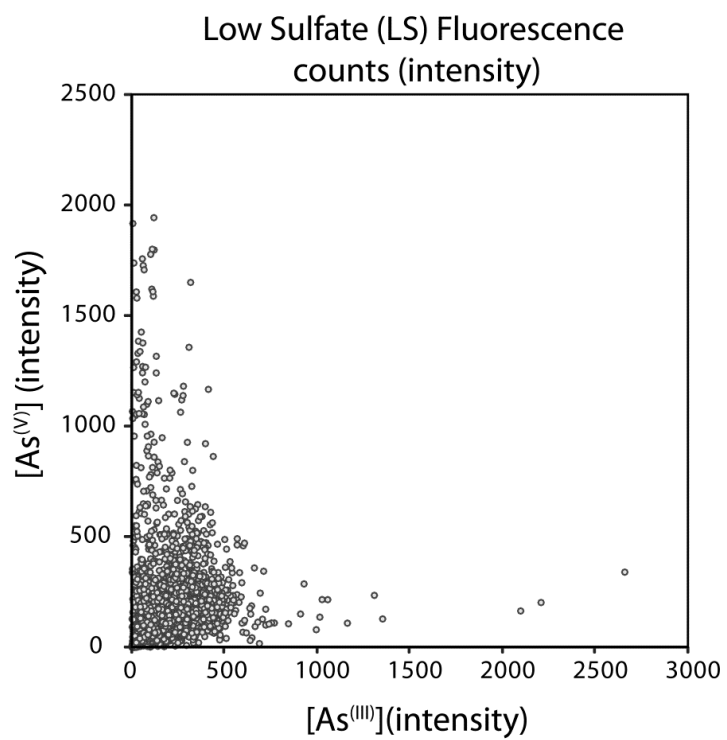


Figure 2. Pixel by pixel comparison from Fig. 3d (LS) of arsenic species in XRF image, showing intensity counts for AsIII and AsV.

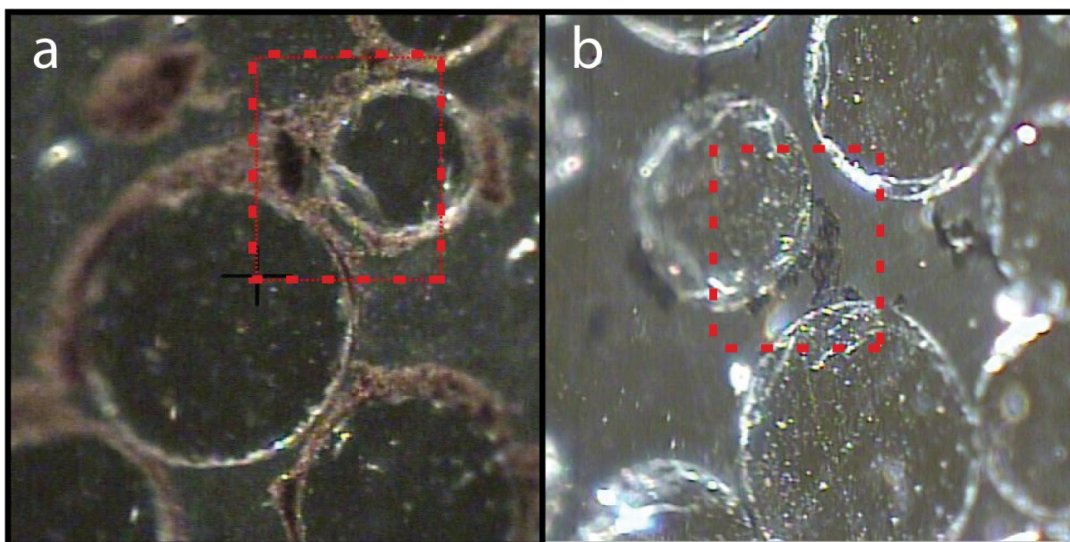


Figure 3. Light microscope micrographs of a) LS under backlit- transmitted light, and b) HS under reflected light with the mapped area by XRF indicated with the dashed box. The images show the reacted AFH solids in the space between glass beads with relatively more solids in the LS v HS column.

APPENDIX C

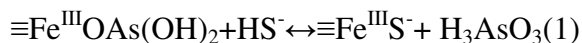
TIME DEPENDENT ARSENIC RELEASE FROM ARSENIC BEARING SOLID RESIDUALS UNDER SIMULATED LANDFILL CONDITIONS WITH DIFFERENT SULFATE CONCENTRATIONS

1. Introduction

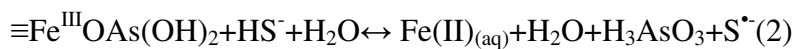
Despite the worldwide concern and extensive studies on chemical speciation of arsenic in sediments and aquifers, there is still a gap of knowledge on the long term effect of biogeochemical cycling of sulfur and iron on environmental arsenic mobility under reducing conditions. In complex environments with diverse microbial communities, such as landfills, sulfate and its redox transformation play a key role in arsenic speciation and fate of arsenic bearing solid residuals (ABSRs). Sulfate reducing bacteria (SRB) use either hydrogen or low molecular weight carbon compounds as electron donors for dissimilatory sulfate reduction to hydrogen sulfide (Maier et al., 2000). Microbially generated sulfide promotes aqueous As(III) and As(V) (oxy)thioanions complex formation. These complexes are persistent in solution in the range of pH from 5 to 10 and comprise a considerable portion of dissolved arsenic (Couture et al., 2011). Currently, the only method to determine presence of thioarsenic complex is by X-ray Absorption Spectroscopy (XAS) and, therefore, there is a gap of analytical data on arsenic thioanions complex in sulfidic environments.

Fate and speciation of arsenic and the extent of its mobilization into the landfill leachate is closely tied to the sulfate concentration in the aqueous phase, as well as to the rate of sulfate and iron reduction. In the zone of active sulfate reduction (sulfidogenesis), where the sulfate concentration is high, Fe(III) reduction to Fe(II)_(aq) depletes the solid phase of iron and enhances arsenic mobilization (Kocar et al., 2010). Microbial sulfidogenesis can strongly affect Fe geochemistry through a variety of processes. In the presence of iron(hydr)oxides, sulfidization promotes iron phase transformation through reductive dissolution. In Fe-rich, arsenic contaminated environments, any sulfidogenesis-induced Fe transformation can also cause changes in As behavior by promoting its partitioning into the aqueous phase. Reduction of As(V) to As(III) is rapid at the onset of sulfidogenesis, causing As(III) to be the dominant As oxidation state. Dissolved sulfide can displace sorbed As(III) via ligand exchange (Reaction 1) or during reductive dissolution of Fe (hydr)oxides(Reaction2)(Kocar et al., 2010; Poulton et al., 2004; dos Afonso and Stumm 1992):

Ligand exchange:



Reductive dissolution:



Sulfidogenesis can also sequester dissolved Fe by driving the precipitation of Fe sulfide minerals such as FeS or Fe₂S (pyrite). Rate of formation and precipitation of ferrous

sulfide is faster than As sulfide precipitation and is known to be the first to precipitate and to remove dissolved sulfide from Fe-rich, reducing environments (O'Day et al., 2004). However, in the presence of excess sulfide, arsenic mobilization could still result in precipitation of amorphous arsenic sulfide. However, detection of arsenic sulfide phases in reduced environments is difficult because they are often fine-grained and poorly crystalline (O'Day et al., 2004). Also, sulfide may react with ABSRs to produce oxidized S species such as elemental sulfur and polysulfides, as well as reduced $\text{Fe(II)}_{(\text{aq})}$. Couture et al. (2011), used thermodynamic databases for (oxy)thioarsenic complexes presented by Wilkin et al. (2003) and Helz and Tossell. (2008) to develop Eh-pH diagrams for the As-O-H-S systems. Their modeling results suggest that under sulfidic-reducing environments, dissolved arsenic(oxy)thioanions complexes are thermodynamically stable over a large pH range, from 5 to 10, thereby reducing the stability of As sulfide mineral phases and enhancing As partitioning into the solution.

Bio mineralization pathways under landfill conditions are controlled by flow-regulated, microbially reduced iron, arsenic, and sulfate, which determine mineral precipitation kinetics and selectivity (Hansel et al., 2003). Realizing the complexity of such environments and time dependent mineral phase transformation, which controls As mobilization rate, and considering the lack of research on time-dependent arsenic fate under landfill conditions, with diverse microbial communities, we have designed and operated a series of column experiments to illustrate the effect of both time and sulfate concentration on fate of arsenic.

This work evaluates the effect of liquid sulfate concentration on the evolution of arsenic mobilization over time, including formation of secondary biominerals, under simulated landfill conditions. Three flow-through columns loaded with a ferrihydrite-based ABSR were used to simulate landfill conditions in the laboratory. The columns were run simultaneously and in replicates for each sulfate concentration, and sequentially terminated at various times to observe the progression of ferrihydrite conversion and As mobilization following reductive dissolution. Changes in aqueous chemistry and solid phase distribution were considered over time to assess how arsenic leaching from arsenic-bearing wastes is influenced by time and by iron and sulfur biomineral formation in landfills.

2. Material and Methods

2.1. Ferrihydrite Sludge Preparation

Arsenic-bearing iron sludge was prepared to simulate the waste generated from the treatment of brines from arsenic removal ion exchange/membrane processes. Sodium arsenate heptahydrate ($\text{Na}_2\text{HAsO}_4 \cdot 7\text{H}_2\text{O}$, KR Grade, Sigma-Aldrich) was dissolved in purified water (Milli-Q Water System by Millipore) to prepare a 1 L solution with a concentration of 0.04 M as As. Ferric chloride hexahydrate ($\text{FeCl}_3 \cdot 6\text{H}_2\text{O}$, ACS reagent, Sigma-Aldrich) was added to the As solution to produce a supersaturated, 0.93 M as Fe solution with Fe:As molar ratio 21:1. This mixture was stirred on a reciprocating shaker table (Orbit, reciprocating speed 100 rpm) for 1 h before adjusting the pH to $\text{pH } 7.0 \pm 0.2$ with 10.0 M sodium hydroxide (prepared from NaOH, flakes, EMD Chemicals). The

produced amorphous ferric hydroxide (AFH) sludge was equilibrated for 2 days while the pH was maintained at 7.0 ± 0.2 . After equilibration and settling, a supernatant sample was filtered through a $0.45 \mu\text{m}$ cellulose acetate syringe filter (Whatman) for determination of concentration of dissolved As and Fe which yielded supernatant As concentration of about 78 ppb. Dissolved iron concentration was BDL. Subsequently, the residual salt content (sodium chloride) of the AFH was reduced by decanting off the supernatant and filling the 4 L flask to the top with Milli-Q water, mixing gently, and allowing the solid to resettle for 3-4 hours. This procedure was repeated until the conductivity of the supernatant was below 1.0 mScm^{-1} . During the process the pH remained constant (7.0 ± 0.2) without needing further adjustment. The final slurry was vacuum filtered through a $0.45 \mu\text{m}$ filter (cellulose nitrate, Whatman). The AFH water content was calculated by weight loss at 70°C after 2 days. The AFH water-content was 75% wt/wt. The sludge was stored in a capped-glass container for no more than three weeks at 4°C . Previous work in our lab (Alday 2010) using visual, SEM, and XRD analysis, has shown no evidence of phase changes under these conditions for 3 weeks, although changes are known to occur over longer time frames.

Total Fe and As in the AFH were determined by digestion of 1 g (dry wt.) samples, using 15 mL of 70% by volume HNO_3 (J.T. Baker) in a CEM microwave digester (method SW 821-8051). Iron was determined by the 1,10-phenanthroline method (APHA. 1998) using a spectrophotometer at 510 nm wavelength (Spectronic Genesys 5). Total and speciated arsenic concentrations were measured by Ion Coupled Plasma Mass Spectrometer (ICP-

MS, Agilent 7500a). The As and Fe per gram of dry AFH were 28.5 mg As and 456 mg Fe for all six columns (Table 1).

Table 1. Iron/Arsenic sludge characteristics.

pH	Supernatant As Concentration (ppb)	Supernatant Fe Concentration (ppb)	[mg As / g dry sludge]	[mg Fe / g dry sludge]	Fe:As Ratio	% Water Content
7.12	78.1	BDL	28.5	456.9	21.4	75.5

2.2. Column Characteristics

Chromatography-type Columns (Spectrum Chromatography; 2.5 cm ID × 30 cm length) were packed with about 80 g (wet wt.) of the prepared iron/arsenic sludge, mixed with 120 g of glass beads (0.8 mm diameter) used as inert support. Anaerobic digester sludge (25 mL of slurry) obtained from Ina Road Wastewater Treatment Plant, Tucson, Arizona, was added as the microbial source for the experiment. The column was fed with a synthetic landfill leachate adapted from Field et al. (2003) by replacing all chloride with sulfate salts to avoid chloride peaks overlapping other anion peaks in ion chromatography (IC). The column's influent sulfate concentrations were 2.08 mM for the low sulfate (LS) and 20.8 mM for the medium sulfate (MS) columns. The influent feed was made with de-gassed water and purged with nitrogen gas after mixing. Influent was fed continuously into the columns using a multi-syringe pump (BS-9000-6 programmable multi-syringe

pump, Braintree Scientific) at an average rate of 2 pore volumes d^{-1} (0.12 Ld^{-1}). Ion chromatography (IC, Dionex, DX-500) was used to quantify sulfate. Effluent sulfide was measured using colorimetric method adopted from Trueper et al. (1964), and pH was measured with an Orion (Model 720) pH meter.

2.3. Solid Phase Characterization

Low sulfate columns were terminated after operation times of 93, 226, and 476 days and medium sulfate columns were terminated after 93, 219, and 300 days. Effluent pH was measured every other week and it fluctuated between 7.5 and 8.5. After termination, the columns were opened in an oxygen free glove box (Terra Universal 100). The contents of each column (initially containing a mix of AFH, glass beads and anaerobic digester sludge) were divided into four approximately equal volume sections. Each section was dried in the glove box at room temperature for 7 days after which a 0.5 mm mesh was used to separate the glass beads from the solids. Solid phases were analyzed by Powder X-ray Diffraction (XRD). Powder XRD was by a Scintag XDS 2000 PTS Diffractometer with Cu-K α radiation ($\lambda = 1.54060 \text{ \AA}$) operated at a voltage of 40 kV and a current of 40 mA. Diffraction patterns were recorded by continuous scans from 10° to 70° at 2 degrees/minute. The mineral phases were identified using the instrument software and the International Centre for Diffraction Data (ICDD) database.

3. Results and Discussion

3.1. Arsenic and Iron Leaching Trends

The mobilization of arsenic from the simulated landfill experiments follows a general trend that is reproduced over the whole range of conditions explored in this work (Figure 1). An initial lag phase (I) of microbial acclimatization, in which the effluent arsenic concentration is relatively low. Phase I is followed by a gradual but continuous increase of the effluent Asconcentration to reach a maximum (phase II). Afterwards, As concentration decreases continuously and goes back to relatively low levels (phase III). Phase I lasts about 3 months for both low (2.08 mM) and high (20.8 mM) sulfate sets. Effluent arsenic concentration is continuously < 0.1 mM for the lag phase (phase I) (Figures 1 and 2).

Maximum arsenic concentration in phase II of LS and MS columns are ~ 0.27 mM and ~ 0.3 , respectively, indicating that in reducing environments with a higher sulfate concentration range (above 2 mM), arsenic release is independent of sulfate concentration (Figures 1 and 2), unlike what is observed in lower sulfate concentration range of 0.064-2.08 mM (Root et al., 2013).

Overall, the effluent arsenic concentration, for all 3 phases and for both sulfate concentrations, follows the same trend and are in close agreement with one another in terms of effluent concentration (Table 2). Almost 50% of the total loaded arsenic leached from both systems by the end of operation compare to columns with in-flow sulfate concentration of 0.064 mM in previous works which retained less than 20% of initial

arsenic. Arsenic results obtained in all the columns confirm As(III) as the dominant species in the effluent.

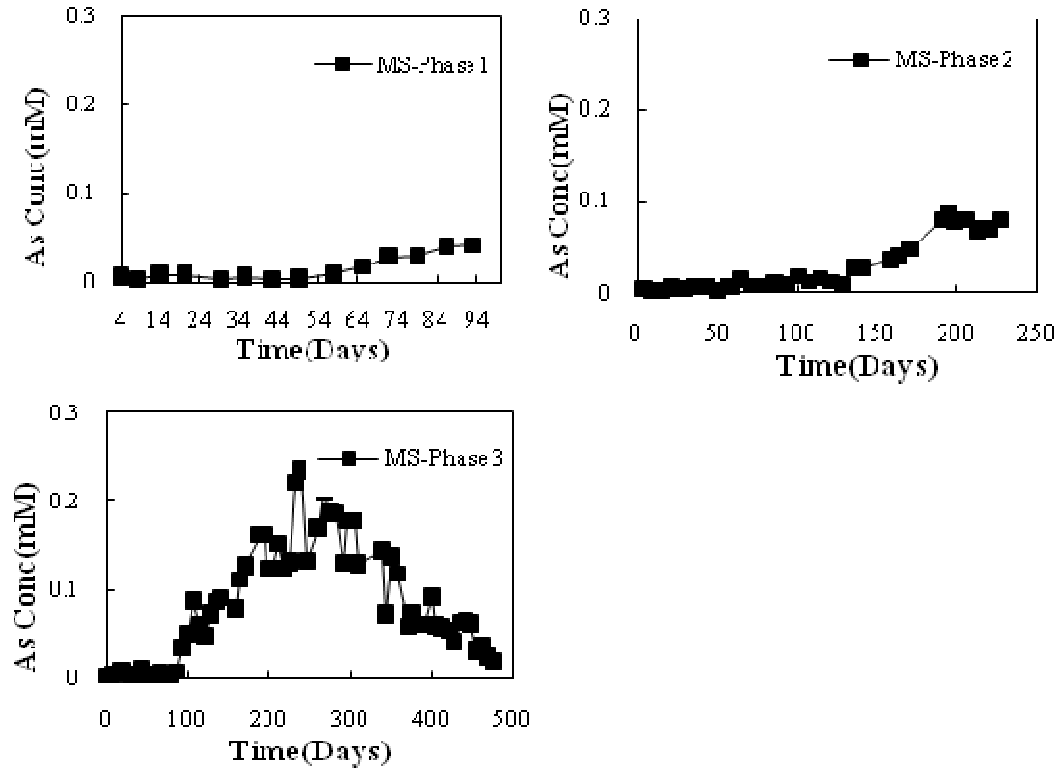


Figure 1. Effluent arsenic concentration profile at phase I, II, and III in LS set. Total arsenic leached at each phase is 1.45%, 3.48%, and 45.78% after 93, 226, and 476 days, respectively.

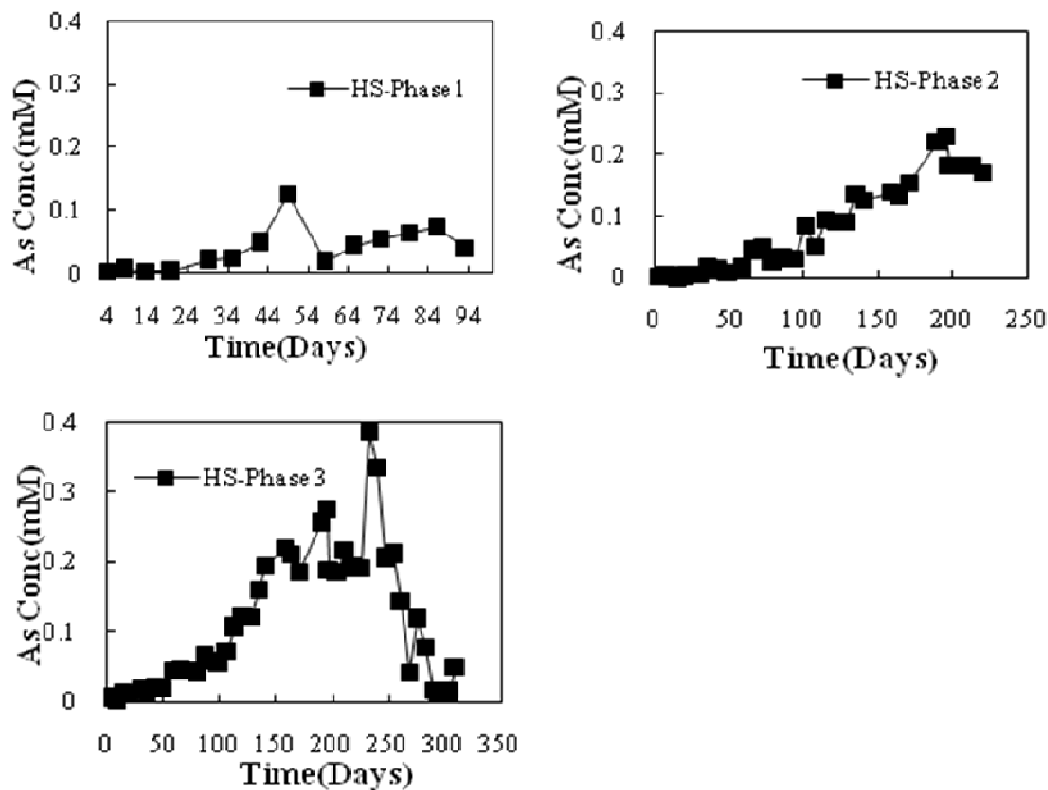


Figure 2. Effluent arsenic concentration profile at phase I, II, and III in MS set. Total arsenic leached at each phase is 4.07%, 21.64%, and 49.81% after 93, 219, and 300 days, respectively.

In the LS columns, the concentration of Fe in the effluent was below detection for almost the first 30 days of operation then remained at about 10 μM for the next 2 months and increased to an average concentration of $\sim 100 \mu\text{M}$ towards the end of operation. On the other hand, in MS column set, iron starts leaching at concentration about 50 μM for the first month, then increases to average concentration of $\sim 300 \mu\text{M}$ and tapers off to below 50 μM after about 200 days to the end of run. Although the Fe leaching behavior was different between the two column sets, it did not follow any clear trend and the effluent iron concentration oscillated between 100 μM and 300 μM for low and medium sulfate

columns set, respectively. The solids also showed the same change of coloration in both sets from dark orange to black and remained dark for the rest of the column's operation. Although Fe reducing activity was continuous throughout the operation, the fraction of initial iron load that leached out was <1 %, except for the phase III of MS set where 2 % of the loaded iron leached out after 300 days of operation (Table 2). The Fe^{3+} concentration during all the experiment was lower than that of Fe^{2+} . Iron reduction started from the very beginning of the run without any lag.

Table2.Total fraction of iron and arsenic leached out of LS and MS columns for all the 3 phases over time.

	Phase I			Phase II			Phase III		
	%As leached	%Fe leached	Time (Days)	%As leached	%Fe leached	Time (Days)	%As leached	%Fe leached	Time (Days)
LS Set	1.45	0.25	93	3.69	0.05	226	45.78	0.89	476
MS Set	4.07	0.91	93	21.65	0.92	219	49.81	1.86	300

The fate of As is tied to both S and Fe reduction, which is typically microbially mediated by the oxidation of organic carbon (e.g. lactate). Sulfate reduction can contribute significantly to secondary biomineral formation under landfill and natural environment conditions by motivating precipitation of sulfide minerals such as iron sulfides (FeS_x), and where arsenic is present, arsenic sulfides (e.g., realgar (AsS), and arsenopyrite (FeAsS)) (Bostick et al., 2003; O'Day et al., 2004; Kirk et al., 2010; and Burton et al., 2013). For all columns the organic carbon source was 5.5 mM lactate fed continuously.

The medium sulfate (MS) column's feed included 20.8 mM sulfate, while 3 low sulfate columns were fed a sulfate concentration of 2.08 mM.

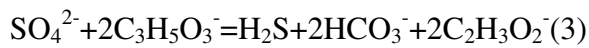
Influent and effluent sulfate was measured in both LS and MS columns to monitor sulfate reduction trend in the columns. In the LS set, lactate gets consumed to below detection level for the first 100 days of run after which its effluent concentration raised to about 35% of its input concentration, ~ 2 mM, for the next 100 days before it tapers off to below detection limit. Throughout the course of experiment, effluent sulfate concentration remained below 0.5 mM.

In MS column set, lactate consumption rate follows the same trend as in LS set, whereas only 50% of input sulfate gets removed, resulting in average effluent sulfate concentration of 15 mM throughout the run. This result shows that the input sulfate concentration in MS set exceeds the capacity of conversion (sulfate reduction) by the SRB existing in the columns.

The change in lactate consumption rate could be due to shift in dominant redox mechanism in the columns from biotic reduction (Fe reducers) to abiotic reduction of iron through electron transfer from dissolved sulfide. This conclusion is drawn based on the effluent lactate and sulfide results (Figure 3). Biotic sulfate reduction, which starts after the first 3 months of microbial acclimatization (phase I), produces a continued source of electron (dissolved sulfide) for iron reduction (Couture et al., 2011), which limits the activity of iron reducers and therefore increase the concentration of effluent lactate from

the columns until the depletion of easily accessed amorphous iron surface resulting from continued iron reductive dissolution and precipitation of secondary minerals (phase II) ceases abiotic iron reduction. From this point, around 250 d, concentration of dissolved sulfide increases in the effluent measurements (Figure 3) and effluent lactate concentration reduces to below 1 mM.

Microbial sulfate reduction coupled to lactate oxidation follows the stoichiometry (Kocar et al., 2010; Burton et al., 2011):



Therefore, it is expected the in-flow lactate to be consumed not only by SRB to reduce input sulfate, but also to be used by Fe and As reducing bacteria present in LS columns to support iron and arsenic reduction, with acetate being the alternative electron donor in the absence of lactate. Acetate is generated by the reduction of lactate with iron, arsenic, and sulfate. On the other hand, the effluent sulfate from MS columns indicates that the capacity for sulfidogenesis is limited by the supply of lactate, with a surplus of available sulfate. Therefore, a portion of the sulfate is probably reduced through microbial reduction of acetate knowing that effluent acetate concentration was low for the most part. It is also assumed that lactate was mainly consumed towards the in-flow end of columns, thereby limiting subsequent downstream sulfate reduction.

Microbial reduction of sulfate results in sulfide production, which is mainly retained in the reactor in the form of sulfide biominerals or gets oxidized by chemical reaction with $\text{Fe(III)}_{(s)}$ on the surface of ABSRs to release $\text{Fe(II)}_{(aq)}$. Only less than 20% of the sulfate input exited the column in low sulfate set over the whole operating period. Almost 100% of the sulfate retained in the column was reduced to sulfide (Figure 3). In the medium sulfate column, it seems that there is only enough electrons available, through lactate and acetate reduction, to reduce < 25% of input sulfate (~5 mM). It is unlikely that abiotic oxidation of dissolved sulfide contribute to the effluent sulfate as the common product of abiotic sulfide oxidation is elemental sulfur (Kocar et al., 2010; Poulton et al., 2004; Couture et al., 2011). For the first 200 days of operation, 100% of the reduced sulfur remained in the column, after which an average sulfide concentration of 0.05 mM was released through the rest of the operating period. Since sulfide is a strong reductant of Fe(III) in sulfate reducing environments, it may react with As-bearing iron oxides, originally packed in the columns, to produce oxidized S and dissolved Fe(II) , and results in low to undetectable sulfide concentration in effluent discharge from the reactors. Dissolved sulfide concentration can increase only after the supply of accessible reactive iron is exhausted via reductive dissolution processes and subsequent iron biomineral formation (Figure 3). Burton et al. (2011), developed a geochemical model in which they found that for As sulfide minerals to precipitate, pore-water sulfide must remain at moderately low levels, between ~0.4 mM to 1 mM, whereas the effluent sulfide concentration in our both LS and MS columns is noticeably lower than threshold concentration for sulfide mineral formation indicated in their model (Figure 3).

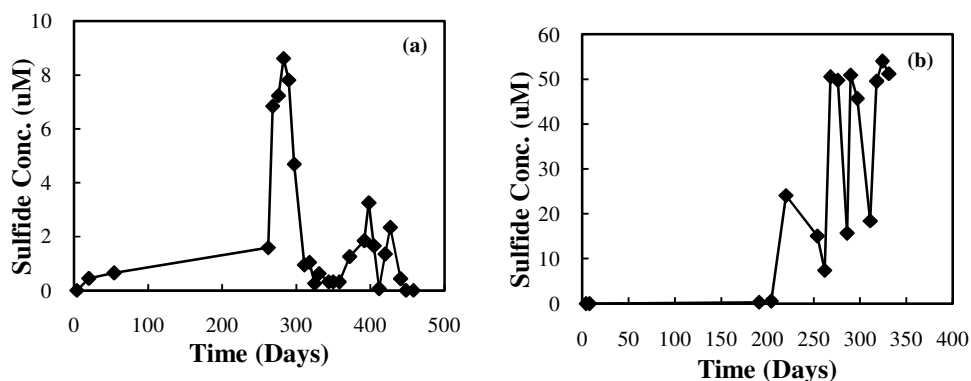


Figure 3. Effluent sulfide concentration profile from phase III of LS column (a), and MS column (b). After ~ 200 days of operation, with effluent sulfide concentration of $< 2 \mu\text{M}$ in both columns, out flowing sulfide from MS column increases to concentration 6x higher than the value measured in LS column effluent.

3.2. Incongruent Fe/As release Effect

In this work, the ratio of the concentration of iron to arsenic leached from the column is not congruent with that initially introduced in the system in the co-precipitated ABSR. Arsenic leaching occurred predominantly in its reduced arsenite form in both sets, and was during much of a column's operational period incongruently released from iron, except during the lag phase (Figure 4 and 5).

Fe/As non-stoichiometric release was evident in all experiments because a large fraction of arsenic was released (~ 50% of total loaded arsenic) in contrast to a small fraction of iron (<2% of total loaded iron). This meant the Fe/As molar ratio in the effluent was always much less than initial Fe/As loading ratio of 22:1. During the first few months of column operation, Fe/As ratio is about 5x than during the rest of the experiment before

arsenic concentration tappers off (1.25 vs. 0.25). This could be a result of arsenic re-adsorption onto freshly exposed ferrihydrite surface following iron reductive dissolution during phase I. At first, ferrihydrite reductive transformation increases arsenic retention back onto the iron solid surface, while prolonged reduction enhances arsenic desorption (Tufano et al., 2008). Incongruent arsenic release from iron becomes noticeable after 100 ad 150 days in both LS and MS columns, respectively. Looking at the incongruent release progress through the 3 phases, it could be concluded that entering the maximum As concentration phase, phase II, coincide with the iron retention phase (Figure 4 and 5).

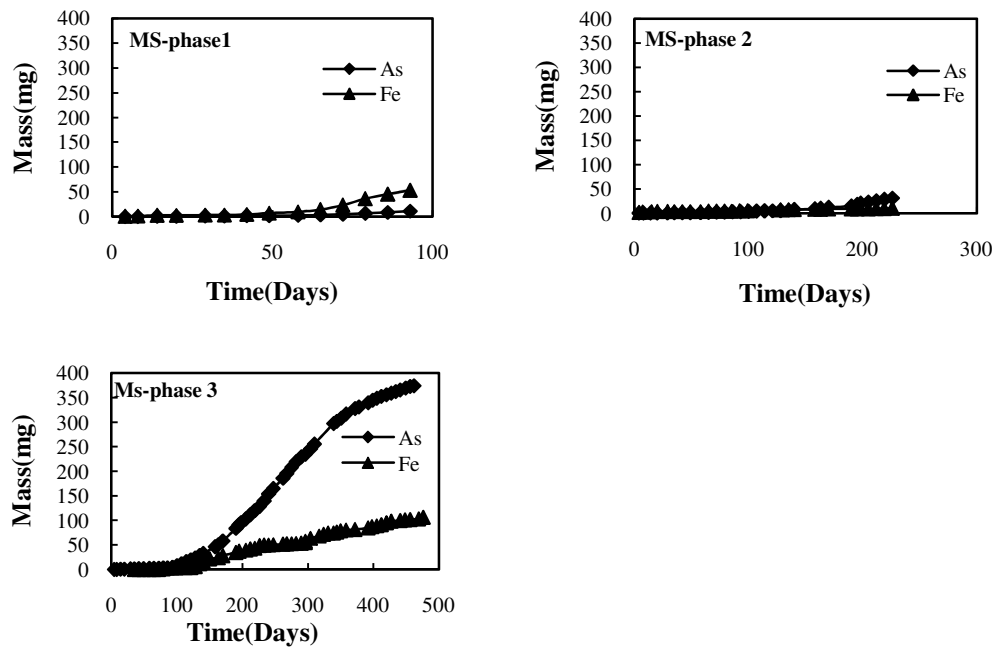


Figure 4. Evolution of incongruent Fe/As release is evident through three arsenic leaching regimes. As non-stoichiometric release from Fe starts in the transition from phase II to phase III.

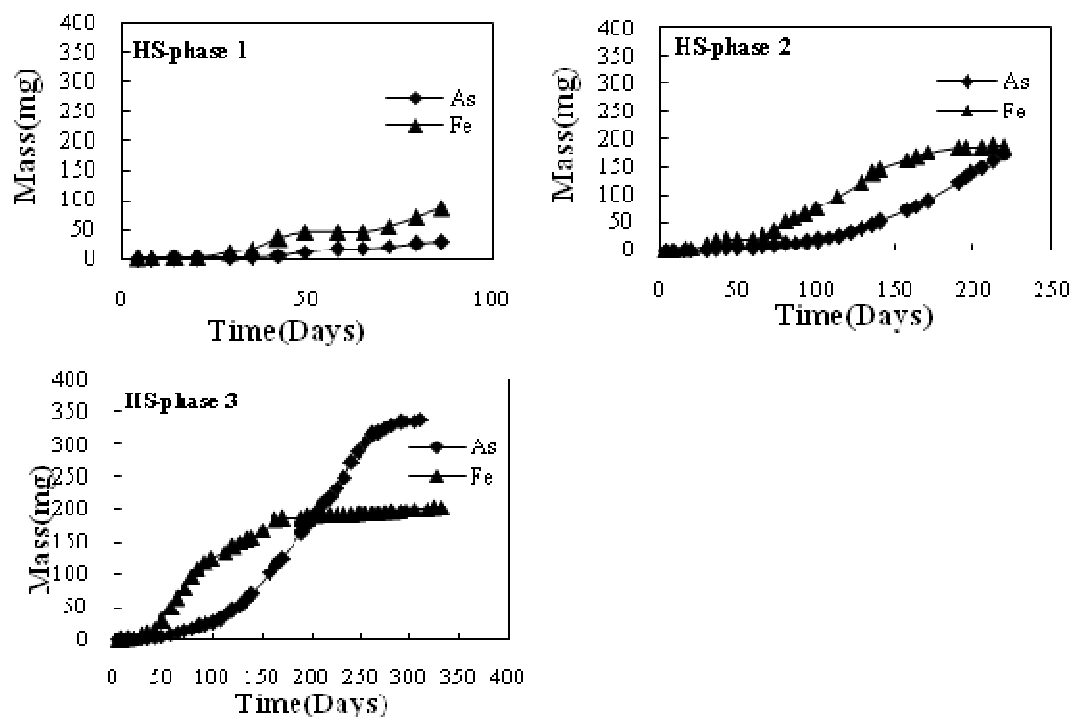


Figure 5. Evolution of incongruent Fe/As release is evident through three arsenic leaching regimes. Non-stoichiometric As release from Fe starts in the transition from phase II to phase III.

3.3. BiomineralTransformation/Characterization

Iron phase transformation into ferrous biominerals starts from the bottom section of all columns where the reducing power and therefore microbial activity is at its highest. These newly formed minerals gradually migrate in the direction of flow as time goes by, which results in mass depletion close to the column's inlet, leaving behind mainly amorphous iron phases. Transitioning from phase I through phase III, especially in MS set, biominerals formation and migration from the bottom of the column is evident. In section 1 of phase I column, after 3 months of operation, ferrous biominerals start forming close to the inlet, where there is the highest microbial activity in the column.

After a few months by staging through phase II and III, biomineral formation migrates up in the column, leaving behind only the amorphous phase, depleted from crystalline biominerals (Table 3). Ferrous biominerals, siderite and vivianite, are main crystalline phases detected with XRD in both column sets. The fact that there was no sulfide phase reported from XRD data collection does not mean that sulfide mineral did not form in the reactors but it could be in amorphous phase or small grain size and therefore not detectable with XRD. Reduction and release of arsenic in sulfidic environments could result in formation of arsenic sulfide. On the other hand, iron (hydr)oxides reductive dissolution consumes sulfide to reduce Fe(III) to Fe(II) and could prevent dissolved sulfide concentration from achieving levels sufficient for As sulfide precipitation (O'Day et al., 2004).

Table 3. Biomineral transformation over time under the influence of different sulfate concentration, detected by powder-XRD.

Column's Section	MS Phase 1	MS Phase 2	MS Phase 3	LS Phase 1	LS Phase 2	LS Phase 3
IV	Goethite	Siderite, Vivianite, Goethite	Siderite	Siderite, Goethite	Siderite, Goethite	Siderite, Vivianite
III	Goethite	Siderite, Vivianite, Goethite	Siderite	Siderite, Goethite	Siderite, Vivianite, Goethite	Siderite, Vivianite
II	Goethite	Amorphous	Amorphous	Siderite, Vivianite	Siderite, Goethite	Siderite
I	Siderite, Vivianite	Amorphous	Amorphous	Vivianite	Siderite, Vivianite, Goethite	Amorphous

After each column was stopped, the column was divided into four sections from bottom to top, which was the direction of the flow, to characterize the remaining solids. During the first month of column operation, change in color was noticeable in all sections, suggesting solid phase transformations on the surface of the original amorphous iron. The solids transform from orange(ferrihydrite) to brown at first, and then continue to darken to black over the course of the experiment. Although these changes in coloration suggested the formation of magnetite, and ferrous sulfide, these mineral were not found in the XRD analyses conducted at the termination of each column. After 3 months of operation, almost all the solid phase in the column turned black. Although XRD is more a qualitative technique than quantitative, both siderite and vivianite show strong peaks confirming an important presence in the total solids content. Some traces of goethite were also detected in phase I and II of both column sets, but with low peak intensities except for phase I of MS set where goethite was detected as the only transformed iron phase. Even though a quantification study was not realized, the amounts of the mineral phases in the solid samples trended with the direction of the flow; vivianite showed a decrease of the peak intensities in the direction of the flow, which suggests a decrease of its quantity from bottom (layer I) to top (layer IV) of the column; whereas siderite showed the opposite trend, which suggests an increase of its quantity from bottom (layer I) to top (layer IV) of the column. Downstream migration of the pore-water Fe(II) front was evident over time, especially in MS set. There is evidence for movement of Fe within the columns over time that causestransport of dissolved Fe(II)and precipitation of secondary Fe mineral phases down gradient. During phase II and IIIof operation, secondary iron

minerals are removed from the inflow end of the columns and redistribute mainly along the top two sections, leaving amorphous iron phase behind close to inlet (Table2).

Iron phase transformation from the original amorphous ferric hydroxide phase to either mixed ferric and ferrous or ferrous-only phases causes a significant decrease in the specific surface area and As adsorption capacity of the Fe minerals. The decrease in sorption sites from the initial AFH to the final ferrous minerals, siderite and vivianite, is significant. Distinct arsenic minerals such as realgar (AsS) and orpiment (As_2S_3) are not detected within column solids despite sulfidization of iron phases inside each column. Dissolved sulfide produced from microbial sulfate reduction drives reductive dissolution and transformation of amorphous iron hydroxide to secondary iron minerals in the column which causes arsenic mobilization and partitioning into the aqueous phase. Consumption of sulfide as a chemical reductant of Fe(III) probably maintains dissolved sulfide concentration in pore-water below the level required for Fe/As sulfide precipitation. Advective flow in the column transports released arsenic downstream, preventing As sulfide precipitation. However, amorphous As sulfide can form and precipitate at higher sulfide concentration which is not detectable by XRD technique.

4. Conclusions

In this work, time dependent arsenic leaching regime in three distinct phases are illustrated through series of column experiments. Non-stoichiometric arsenic release from iron is clearly observed to happen within the transition from effluent arsenic lag phase to

phase of rapid arsenic increase in the effluent. Sulfate concentration does not seem to have a significant impact on incongruent dissolution trend as in both set of columns, with different sulfate concentration, incongruent dissolution starts at about the same time. Also, over all arsenic leaching pattern in both sets of columns and within all three phases are similar. Non-stoichiometric arsenic release from iron becomes noticeable after 100 and 150 days in both LS and MS columns, respectively. Looking at the incongruent dissolution progress through the 3 phases, it could be concluded that entering the maximum As concentration phase, phase II, coincide with the iron retention phase. Also, it seems that siderite and vivianite are the main phase transformed products in both sulfate concentration sets. The fact that Fe/As sulfide phase were not detected with XRD does not mean that those phases are not present in our systems as sulfide minerals could precipitate in amorphous form or in low abundance, relative to ferrous minerals, and hence not detectable with XRD.

REFERENCES

- Afonso, M., D.; Stumm, W. Reductive dissolution of iron(III) (hydr)oxides by hydrogen-sulfide. *Langmuir* **1992**, 8(6), 1671–1675.
- Alday, F. J. Iron Biomineralization: Implications on the fate of arsenic in landfills. Ph.D. Dissertation, **2010**, University of Arizona, Tucson, AZ.
- Amstaetter, K.; Borch, T.; Larese-Casanova, P.; Kappler, A. Redox transformation of arsenic by Fe(II)-activated goethite (α -FeOOH). *Environ. Sci. Technol.* **2010**, 44, 102–108.
- Amy, G.; Edwards, M.; Brandhuber, P.; McNeill, L.; Benjamin, M.; Vagliasindi, F.; Carlson, K.; Chwirka, J. **2000**. *Arsenic Treatability Options and Evaluation of Residuals Management Issues*. AWWA Research Foundation, Denver, CO.
- Appelo, C. A. J.; Van der Weiden, M. J. J.; Tournassat, C.; Charlet, L. Surface complexation of ferrous iron and carbonate on ferrihydrite and the mobilization of arsenic. *Environ. Sci. Technol.* **2002**, 36, 3096-3103.
- Beaulieu, B. T.; Savage, K. S. Arsenate adsorption structures on aluminum oxide and phyllosilicate mineral surfaces in smelter-impacted soils. *Environ. Sci. Technol.* **2005**, 39, (10), 3571-3579.
- Benner, S.G.; Hansel, C.M.; Wielinga, B.W.; Barber, T.M.; Fendorf, S. Reductive dissolution and biomineralization of iron hydroxide under dynamic flow conditions. *Environ. Sci. Technol.* **2002**, 36, 1705-1711.
- Blanchard, M.; Alfredsson, M.; Brodholt, J.; Wright, K.; Catlow, C.R.A. Arsenic incorporation into FeS₂ pyrite and its influence on dissolution: A DFT study. *Geochim. Cosmo. Acta* **2007**, 71: 624-630.
- Bose, P.; and Sharma, A. Role of iron in controlling speciation and mobilization of arsenic in subsurface environment. *Water Research*, **2002**, 36, 4916-4926.
- Bostick, B. C.; Fendorf, S. Arsenite sorption on troilite (FeS) and pyrite (FeS₂). *Geochim. Cosmochim. Acta* **2003**, 67, (5), 909-921.
- Bostick, B., C.; Chen, C.; Fendorf, S. Arsenite retention mechanisms within estuarine sediments of pescadero, CA. *Environ. Sci. Technol.* **2004**, 38, 3299–3304.
- Bostick, B. C.; Fendorf, S.; Brown, G. E. In situ analysis of thioarsenite complexes in neutral to alkaline arsenic sulphide solutions. *Mineralogical Magazine* **2005**, 5, (5), 781-795.

- Bruno, J.; Wersin, P.; and Stumm W. On the influence of carbonate in mineral dissolution:
- II. The solubility of $\text{FeCO}_3(\text{s})$ at 25°C and 1 atm total pressure. *Geochim. Cosmochim. Acta.* **1992**, 56, 1149-1155.
- Burnol, A.; Garrido, F.; Baranger, P.; Joulain, C.; Dictor, M.C.; Bodenan, F.; Morin, G.; Charlet, L. Decoupling of arsenic and iron release from ferrihydrite suspension under reducing conditions: a biogeochemical model. *Geochemical transactions.* **2007**, 8 12.
- Burton, E. D.; Johnston, S. G. Impact of silica on the reductive transformation of schwertmannite and the mobility of arsenic. *Geochim. Cosmochim. Acta.* **2012**, 96, 134–153.
- Burton, E. D.; Johnston, S. G.; Bush, R. T. Microbial sulfidogenesis in ferrihydrite rich environments: effects on iron mineralogy and arsenic mobility. *Geochemical transactions.* **2011b**, 75, 3072-3087.
- Burton, E. D.; Johnston, S.; G.; and Planer-Friedrich, B. Coupling of arsenic mobility to sulfur transformations during microbial sulfate reduction in the presence and absence of humic acid. *Chemical Geology*, **2013**, 343 12-24.
- Burton, E. D.; Bush, R. T.; Sullivan, L. A.; Mitchell, D. R. G. Reductive transformation of iron and sulfur in schwertmannite-rich accumulations associated with acidified coastal lowlands. *Geochim. Cosmochim. Acta* **2007**, 71, 4456–4473.
- Burton, E. D.; Johnston, S. G.; Kraal, P.; Bush, R.; Claff, S. R. Sulfate availability drives divergent evolution of arsenic speciation during microbially-mediated reductive transformation of schwertmannite. *Environ. Sci. Technol.* **2013**, 47, (5), 2221-2229.
- Cances, B.; Juillot, F.; Morin, G.; Laperche, V.; Polya, D.; Vaughan, D.J.; Hazemann, J.L.; Proux, O.; Brown, G.E.; Jr. and Calas, G. Changes in arsenic speciation through a contaminated soil profile: a XAS based study. *The Science of the total environment* **2008**, 397, 178-189.
- Canfield, D. E.; Raiswell, R.; Bottrell, S. The Reactivity of sedimentary iron minerals towards sulfide. *American Journal of Science*, **1992**, Vol. 292, 1992, P. 659-683.
- Canfield, D., E.; Thamdrup, B.; and Kristensen, E. The Sulfur Cycle. *Aquatic Geochemistry* **2005**, Elsevier Academic Press, San Diego.
- Charlet, L.; Polya, D. A. Arsenic in shallow, reducing groundwaters in southern asia: An Environmental Health Disaster. *Elements*, **2006**, 1811-5209.
- Childs, C.W. Ferrihydrite: a review of structure, properties, and occurrence in relation to soils. *Z PflanzenernhrBodenk*, **1992**, 155:441–448.

- Chow, S.S.; Taillefert, M. Effect of arsenic concentration on microbial iron reduction and arsenic speciation in an iron-rich freshwater sediment. *Geochim. Cosmochim. Acta* **2009**, *73*, 6008–6021.
- Christensen, T. H.; Kjeldsen, P.; Bjerg, P. L.; Jensen, D. L.; Christensen, J. B.; Baun, A.; Albrechtsen, H.J.; Heron, G. Biogeochemistry of landfill leachate plumes. *Applied Geochemistry* **2001**, *16*, (7-8), 659-718.
- Clancy, T.; Hayes, K.F. and Raskin, L. Arsenic waste management: A critical review of testing and disposal of arsenic-bearing wastes generated during arsenic removal from drinking water, *Environ. Sci. Technol.* **2013**, *47*(19): 10799-10812.
- Clifford, D. A.; Ghurye, G. L. Metal-oxide adsorption, iron exchange, and coagulation-microfiltration for arsenic removal from water. In *Environmental Chemistry of Arsenic*, Frankenberger, W. T. J., Ed. Marcel Dekker, Inc.: New York, **2002**; pp 217-245.
- Cortinas, I, Sierra-Alvarez, R., Field, J.A. Biologically Mediated Mobilization of Arsenic from Granular Ferric Hydroxide in Anaerobic Columns Fed Landfill Leachate. *Biotechnology and Bioengineering*, vol. 101, no. 6, pp 1205-1213, 2008.
- Cortinas, I.; Field, J. A.; Kopplin, M.; Garbarino, J. R.; Gandolfi, A. J.; Sierra-Alvarez, R., Anaerobic Biotransformation of Roxarsone and Related N-Substituted Phenylarsonic Acids. *Environ. Sci. Technol.* **2006**, *40*, (9), 2951-2957.
- Couture, R.-M.; Van Cappellen, P., Reassessing the role of sulfur geochemistry on arsenic speciation in reducing environments. *Journal of Hazardous Materials* **2011**, *189*, (3), 647-652.
- Couture, R. M.; Gobeil, C.; Tessier, A. Arsenic, iron and sulfur co-diagenesis in lake sediments. *Geochim. Cosmochim. Acta* **2010**, *74*, 1238-1255.
- Couture, R. M.; Wallschlager, D.; Rose, J.; and Van Cappellen, P. Arsenic binding to organic and inorganic sulfur species during microbial sulfate reduction: a sediment flow-through reactor experiment. *Environ. Chem.* **2013**, *10*, 285–294.
- Couture, R. M.; Rose, J.; Kumar, N.; Mitchell, K.; Wallschlager, D.; and Van Cappellen, P. Sorption of arsenite, arsenate, and thioarsenates to iron oxides and iron sulfides: A kinetic and spectroscopic investigation. *Environ. Sci. Technol.* **2013**, *47*, 5652–5659.
- Cullen, W.R.; and Reimer, K.J. Arsenic speciation in the environment. *Chem. Rev* **1989**, *89*: 713-764.
- Cummings, D. E.; Caccavo, F.; Fendorf, S.; Rosenzweig, R. F. Arsenic mobilization by the dissimilatory Fe(III)-reducing bacterium *Shewanella alga* BrY. *Environ. Sci. Technol.* **1999**, *33*: 723-729.

- deLemos, J. L.; Bostick, B. C.; Renshaw, C. E.; Stürup, S.; Feng, X. Landfill-stimulated iron reduction and arsenic release at the Coakley Superfund Site (NH). *Environ. Sci. Technol.* **2005**, *40*, (1), 67-73.
- deLemos, J. L.; Bostick, B.C.; Renshaw, C. E.; Sturup, S.; and Feng, X. H. Landfill stimulated iron reduction and arsenic release at the Coakley Superfund Site (NH). *Environ. Sci. Technol.* **2006**, *40*:67-73.
- Demergasso, C. S.; Ching, G. D.; Escudero, L. G.; Mur, J. J. P.; Alio, C. P. Microbial precipitation of arsenic sulfides in Andean salt flats. *Geomicrobiology Journal* **2007**, *24*, (2), 111-123.
- Dixit, S.; Hering, J.G. Comparison of arsenic(V) and arsenic (III) sorption onto iron oxide minerals: Implications for arsenic mobility. *Environ. Sci. Technol.* **2003**, *37*, 4182-4189.
- Dixon, J.B.; Weed, S.B. Minerals in soil environments. *Soil Science Society of America, Inc.* **1989**, 380-427.
- Dos Santos, A. M.; Stumm, W. The reductive dissolution of iron(III) (hydr)oxides by hydrogen sulfide. *Langmuir* **1992**, *8*, 1671-1675.
- Drissi, S. H.; Refait, P.; Abdelmoula, M.; Génin, J. M. R. The preparation and thermodynamic properties of Fe(II)—Fe(III) hydroxide-carbonate (green rust 1); Pourbaix diagram of iron in carbonate-containing aqueous media. *Corrosion Science* **1995**, *37*, (12), 2025-2041.
- Eynard, A.; del Campillo, M. C.; Barrón, V.; Torrent, J., Use of vivianite ($\text{Fe}_3(\text{PO}_4)_2 \cdot 8\text{H}_2\text{O}$) to prevent iron chlorosis in calcareous soils. *Fertilizer Research* **1992**, *31*, (61-67).
- Farquhar, M. L.; Charnock, J. M.; Livens, F. R.; Vaughan, D. J. Mechanisms of arsenic uptake from aqueous solution by interaction with goethite, lepidocrocite, mackinawite, and pyrite: An x-ray absorption spectroscopy study. *Environ. Sci. Technol.* **2002**, *36*, (8), 1757-176.
- Fendorf, S. M.; Van Geen, H. A. Spatial and temporal variation of groundwater arsenic in south and southeast Asia. *Science*, **2010**, *328*, 1123-1127.
- Finster, K. Microbiological disproportionation of inorganic sulfur compounds. *Journal of Sulfur Chemistry* Vol. 29, Nos. 3-4, June-August **2008**, 281-292.
- Ford, R.G.; Fendorf, S.; Wilkin, R.T. Introduction: controls on arsenic transport in near-surface aquatic systems. *Chemical Geology* **2006**, *228*:1-5.
- Fredrickson, J.K.; Zachara, J.M.; Kennedy, D.W.; Dong, H.; Onstott, T.C.; Hinman, N.W.; Li, S. Bionogenic iron mineralization accompanying the

- dissimilatory reduction of hydrous ferric oxide by a groundwater bacterium. *Geochim. Cosmochim. Acta* **1998**, Vol. 62, No. 19/20, 3239-3257.
- Frenkel, A. I.; Hills, C. W.; Nuzzo, R. G. A view from the inside: Complexity in the atomic scale ordering of supported metal nanoparticles. *The Journal of Physical Chemistry B* **2001**, *105*, (51), 12689-12703.
- Gallegos, T. J.; Hyun, S. P.; Hayes, K. F. Spectroscopic investigation of the uptake of arsenite from solution by synthetic mackinawite. *Environ. Sci. Technol.* **2007**, *41*, (22), 7781-7786.
- Gallegos, T. J.; Han, Y. S.; Hayes, K. F. Model predictions of realgar precipitation by reaction of as(III) with synthetic mackinawite under anoxic conditions. *Environ. Sci. Technol.* **2008**, *42*, (24), 9338-9343.
- Gao, X.; Root, R.; Farrell, J.; Ela, W.; Chorover, J. Effect of silicic acid on arsenate and arsenite retention mechanisms on 6-L ferrihydrite: A spectroscopic and batch adsorption approach. *Applied Geochemistry (in press)* **2013**.
- Genin, J. M. R.; Ruby, C.; Upadhyay, C. Structure and thermodynamics of ferrous, stoichiometric and ferric oxyhydroxycarbonate green rusts; redox flexibility and fougurite mineral. *Solid State Sciences* **2006**, *8*, (11), 1330-1343.
- Ghosh, A.; Mukiibi, M.; Ela, W. TCLP Underestimates leaching of arsenic from solid residuals under landfill conditions. *Environ. Sci. Technol.* **2004**, *38*, (17), 4677-4682.
- Ghosh, A.; Sáez, A. E.; Ela, W. Effect of pH, competitive anions and NOM on the leaching of arsenic from solid residuals. *Science of the Total Environment* **2006**, *363*, (1-3), 46-59.
- Ghosh, A.; Mukiibi, M.; Saez, A. E.; Ela, W. leaching of arsenic from granular ferric hydroxide residuals under mature landfill. *Environ. Sci. Technol.* conditions, **2006**, *40*(19): 6070-6075.
- Guo, H.; Stüben, D.; and Berner, Z. Removal of arsenic from aqueous solution by natural siderite and hematite, *Appl. Geochem.* **2007**, *22* 1039–1051.
- Guo, H.; Stüben, D.; and Berner, Z. Arsenic removal from water using natural iron mineral–quartz sand columns, *Science of the Total Environment* **2007**, *377* 142–151.
- Guo, H.; Stüben, D.; and Berner, Z. Adsorption of arsenic(III) and arsenic(V) from groundwater using natural siderite as the adsorbent. *Journal of Colloid and Interface Science.* **2007**, *315* 47–53.
- Guo, H.; Li, Y.; and Zhao, K. Arsenate removal from aqueous solution using synthetic siderite, *J. Hazard. Mater.* **2009** doi:10.1016/j.jhazmat.

- Han, Y.S.; Jeong, H. Y.; Demond, A. H.; Hayes, K. F. X-ray absorption and photoelectron spectroscopic study of the association of As(III) with nanoparticulate FeS and FeS-coated sand. *Water Research* **2011**, 45, (17), 5727-5735.
- Hansel, C.M.; Benner, S.B.; Fendorf, S. Competing Fe(II)-induced mineralization pathways of ferrihydrite. *Environ. Sci. Technol.* **2005**, 39(18):7147-7153.
- Hansel, C.M.; Benner, S.B.; Nico, P.; Fendorf, S. Secondary mineralization pathways induced by dissimilatory iron reduction of ferrihydrite under advective flow. *Geochim. Cosmochim. Acta* **2003**, Vol. 67, No. 16, 2977-2992.
- Hansel, C.M.; Benner, S.B.; Nico, P.; Fendorf, S. Structural constraints of ferric (Hydr)oxides on dissimilatory iron reduction and the fate of Fe(II). *Geochim. Cosmochim. Acta* **2004**, 68(15), 3217-3229.
- Harrington, J.M.; Fendorf, S.E.; and Rosenzweig, R.F. Biotic generation of arsenic(III) in metal(loid)-contaminated freshwater lake sediments. *Environ. Sci. Technol.* **1998**, 32, 2425-2430.
- Helz, G., R.; Tossell, J., A. Thermodynamic model for arsenic speciation in sulfidic waters: a novel use of ab initio computations. *Geochim. Cosmochim. Acta*, **2008** 72, 4457-4468.
- Herbel, M.; and Fendorf, S. Biogeochemical processes controlling the speciation and transport of arsenic within iron coated sands, *Chem. Geol.* **2006**, 228, 16-32.
- Hering, J. G.; Chen, P.-Y.; Wilkie, J. A.; Elimelech, M.; Liang, S. Arsenic removal by ferric chloride. *J. Am. Water Works Assoc.* **1996**, 88, 155-167.
- Hoef, S. E.; Lucas, F.; Hollibaugh, J. T.; and Oremland, R. S. Characterization of microbial arsenate reduction in the anoxic bottom waters of Mono Lake, California. *Geomicrobiology Journal*, **2002**, 19(1), 23-40.
- Hoef, S. E.; Kulp, T. R.; Stolz, J. F.; Hollibaugh, J. T.; Oremland, R. S. Dissimilatory arsenate reduction with sulfide as electron donor: experiments with Mono Lake water and isolation of strain MLMS-1, a chemoautotrophic arsenate respirer. *Appl Environ Microbiol* **2004**, 70, (5), 2741-2747.
- Hoef, S. E.; Kulp, T. R.; Han, S.; Lanoil, B.; Oremland, R. S. Coupled arsenotrophy in a hot spring photosynthetic biofilm at Mono Lake, California. *Applied and Environmental Microbiology* **2010**, 76(14):4633. DOI:10.1128/AEM.00545-10.
- Hooper, K.; Iskander, G.; Sivia, F.; Hussein, J.; Hsu, M.; Deguzman, Z.; Odion, Z.; Iley, F.; Sy, M.; Petreas, and Simmons, B. Toxicity characteristic leaching procedure fails to extract oxoanion-forming elements that are extracted by municipal solid waste Leachates, *Environ. Sci. Technol.* **1998**, 32, 3825-3830.

- Horneman, A.; van Geen, A.; Kent, D.V.; Mathe, P.E.; Zheng, Y.; Dhar, R.K.; O'Connell, S.; Hoque, M.A.; Aziz, Z.; Shamsudduha, M.; Seddique, A.A.; Ahmed, K.M. Decoupling of As and Fe release to Bangladesh groundwater under reducing conditions. Part I: Evidence from sediment profiles. *Geochim.Cosmochim.Acta***2004**, 68(17), 3459-3473.
- Illes, E.; and Tombacz, E. The effect of humic acid adsorption on pH-dependent surface changing and aggregation of magnetite nanoparticles. *Journal of colloid and Interface Science*, **2005**, 295 (2006) 115-123.
- Impellitteri, C. A.; and Scheckel, K. G. The distribution, solid-phase speciation, and desorption/dissolution of As in waste iron-based drinking water treatment residuals. *Chemosphere*, **2006**, 64 875–880.
- Jeong, H. Y.; Hanb, Y. S.; Parkc, S. W.; Hayes, K. F. Aerobic oxidation of mackinawite (FeS) and its environmental implication for arsenic mobilization. *Geochim.Cosmochim.Acta*,**2010**, 74- 3182–3198.
- Jing, C.; Liu, S.; Patel, M.; Meng, X. Arsenic leachability in water treatment adsorbents. *Environ. Sci. Technol.* **2005**, 39: 5481–5487.
- Jing, C.; Liu, S.; and Meng, X. Arsenic remobilization in water treatment adsorbents under reducing conditions: Part 1. Incubation study, *Sci. Total Environ.***2008**, 389: 188-194.
- Johnston, S. G.; Keene, A. F.; Burton, E. D.; Bush, R. T.; Sullivan, L. A.; McElnea, A. E.; Ahern, C. R.; Smith, C. D.; and Powell B. Arsenic mobilisation in a seawater inundated acid sulfate. soil. *Environ. Sci. Technol.***2010**,44, 2016–2021.
- Jönsson, J.; Sherman, D. M. Sorption of As(III) and As(V) to siderite, green rust (fougerite) and magnetite: Implications for arsenic release in anoxic groundwaters. *Chemical Geology* **2008**,255, (1:2), 173-181.
- Karhadkar, P.P.; Audic, J.M.; Faup, G.M.; and Khanna, P. Sulfide and sulfate inhibition of methanogenesis. *Water Research*, **1987**, 21(9), 1061-1066.
- Keimowitz, A.R.; Mailloux, B.J.; Cole P.; Stute, M.; Simpson, H.J.; Chilrud, S.N. Laboratory investigations of enhanced sulfate reduction as a groundwater arsenic remediation strategy. *Environ. Sci. Technol.***2007**, 41, 6718-6724.
- Kirk, M. F.; Roden, E. E.; Crossey, L. J.; Brealey, A. J.; Spilde, M. N. Experimental analysis of arsenic precipitation during microbial sulfate and iron reduction in model aquifer sediment reactors. *Geochim.Cosmochim.Acta*,**2010**,74, (9), 2538-2555.
- Kneebone, P. E.; O'Day, P. A.; Jones, N.; Hering, J. G. Deposition and fate of arsenic in iron- and arsenic-enriched reservoir sediments. *Environ. Sci. Technol.***2002**,36, (3), 381-386.

- Kjeldsen, P.; Barlaž M. A.; Rooker, A. P.; Baun, A.; Ledin A.; Christensen, T. H. Present and long-term composition of MSW landfill leachate: A Review. 2002, Critical Reviews in . *Sci.Technol***2002**, Volume 32, Issue 4.
- Kocar, B., D.; Fendorf, S. Thermodynamic constraints on reductive reactions influencing the biogeochemistry of arsenic in soils and sediments. *Environ. Sci.Technol.***2009**, 43, 4871-4877.
- Kocar, B, D.; Borch, T.; Fendorf, S. Arsenic repartitioning during biogenic sulfidization and transformation of ferrihydrite. *Geochim.Cosmochim.Acta*,**2010**, 74 980-994.
- Kocar, B.D.; Herbel, M.J.; and Tufano, K.J.; Fendorf, S. Contrasting effects of dissimilatory iron(III) and arsenic(V) reduction on arsenic retention and transport. *Environ. Sci.Technol.***2006**, 40(21), 6715-6721.
- Kukkadapu, R. K.; Zachara, J. M.; Fredrickson, J. K.; Kennedy, D. W. Biotransformation of two-line silica-ferrihydrite by a dissimilatory Fe(III)-reducing bacterium: formation of carbonate green rust in the presence of phosphate. *Geochim.Cosmochim.Acta***2004**,68, (13), 2799-2814.
- Laloui-Carpentier, W.; Li, T.; Vigneron, V.; Mazeas, L.; Bouchez, T. Methanogenic diversity and activity in municipal solid waste landfill leachates. *Antonie Van Leeuwenhoek International Journal of General and Molecular Microbiology*, **2006**, 89(3-4), 423-434.
- Langner, H.W.; Inskeep, W.P. Microbial reduction of arsenate in the presence of ferrihydrite. *Environ. Sci. Technol.* **2000**,34, 3131-3136.
- Lennie, A. R.; England, K. E. R.; Vaughn, D. J. Transformation of synthetic mackinawite to hexagonal pyrrhotite: A kinetic study. *American Mineralogist* **1995**,80, 960-967.
- Lerotic, M.; Jacobsen, C.; Schäfer, T.; Vogt, S. Cluster analysis of soft X-ray spectromicroscopy data. *Ultramicroscopy* **2004**,100, (1:2), 35-57.
- Lindsay, W. L. *Chemical Equilibria in Soils*; John Wiley & Sons: New York, **1979**; p 450.
- Lloyd, J.R. Microbial reduction of metals and radionuclides. *FEMS Microbiology Reviews*.**2003**, 27, 411-425.
- Liu, S.; Jing, C.; Meng, X. Arsenic re-mobilization in water treatment adsorbents under reducing conditions: Part II. XAS and modeling study. *Science of The Total Environment* **2008**,392, (1), 137-144.
- Lovley, D.R. Dissimilatory Fe(III) and Mn(IV) reduction. *Microbiological Reviews***1991**, 55 (2), 259–287.

- Lovley, D. R.; Phillips, E.J.P.; and Lonergan, D.J. Enzymatic versus nonenzymatic mechanisms for Fe³C reduction in aquatic sediments. *Environ. Sci. Technol.* **1991**, 25:1062–1067.
- Ludvigsen, L.; Albrechtsen, H.J.; Ringelberg, D.B.; Ekelund, F.; and Christensen T.H. Distribution and composition of microbial populations in landfill leachate contaminated aquifer (Grindsted, Denmark) *Microbial Ecology* **1999**, 37(3): 197.
- Maier, R.M.; Pepper, I.L.; and Gerba, C.P. Methanogenesis. *Environmental Microbiology*, **2000**, 340-345.
- Manceau, A. The mechanism of anion adsorption on iron oxides: Evidence for the bonding of arsenate tetrahedra on free Fe(O,OH)₆ edges. *Geochim. Cosmochim. Acta*, **1995**, 59, (17), 3647-3653.
- Majzlan, J. B.; Lalinska, M.; Chovan, L.; Jurkovic, S.; Milovska and Gottlicher, J. The formation, structure, and ageing of As-rich hydrous ferric oxide at the abandoned Sb deposit Pezinok (Slovakia). *Geochim. Cosmochim. Acta*, **2007**, 71(17): 4206-4220.
- Mayhew, L. E.; Webb, S. M.; Templeton, A. S. Microscale imaging and identification of Fe speciation and distribution during fluid-mineral reactions under highly reducing conditions. *Environ. Sci. Technol.* **2011**, 45, (10), 4468-4474.
- McCormick, M.L.; Bouwer, E.J.; Adriaens, P. Carbon tetrachloride transformation in a model iron-reducing culture: Relative kinetics of biotic and abiotic reactions. *Environ. Sci. Technol.* **2002**, 36(3), 403-410.
- Meng, X.; Korfiatis, G. P.; Jing, C.; Christodoulatos, C. Redox transformations of arsenic and iron in water treatment sludge during aging and TCLP extraction. *Environ. Sci. Technol.* **2001**, 35, (17), 3476-3481.
- Millero, F.J. M.; Gonzalez-Davila, and Santana-Casiano, J. M. The reduction of Fe(III) with sulfite in natural waters, *J. Geophys. Sci.* **1995**, 100, 7235-7244.
- Mohan, D.; Pittman, C. U. J. Arsenic removal from water/wastewater using adsorbents: A critical review. *Journal of Hazardous Materials* **2007**, 142, (1:2), 1-53.
- Mukiibi, M.; Sáez A.E. ; and Ela, W.P. Effect of ferrous iron on arsenate sorption to amorphous ferric hydroxide, *Annals of the New York Academy of Science*, **2008** 1140(1): 335.
- Muramatsu, C.; Sakata, M.; and Mitsunobu, S. Immobilization of arsenic(V) during the transformation of ferrihydrite: A direct speciation study using synchrotron-based XAFS spectroscopy. *Chemistry Letters*, **2012**, 41, 270-271.
- Nealson, K. H.; and Myers, C.R. Microbial reduction of manganese and iron: new approaches to carbon cycling. *Appl Environ Microbiol.* **1992**, 58(2): 439–443.

- Newman, D. K.; Kennedy, E. K.; Coates, J. D., Ahmann, D.; Ellis, D. J.; Lovley, D. R.; and Morel, F. M. M. Dissimilatory arsenate and sulfate reduction in *desulfotomaculum auripigmentum* sp. nov. *Archives of Microbiology*, **1997**, 168(5), 380-388.
- Nickson, R. T.; McArthur, J. M.; Ravenscroft, P.; Burgess, W. G.; Ahmed, K. M. Mechanism of arsenic release to groundwater, Bangladesh and West Bengal. *Applied Geochemistry* **2000**, 15, (4), 403-413.
- Nordstrom, D.K. Worldwide occurrences of arsenic in groundwater. *Science* **2002**, 296(5576), 2143-2145.
- O'Day, P. A. Chemistry and mineralogy of arsenic. *Elements* **2006**, 2, (2), 77-83.
- O'Day, P. A.; Vlassopoulos, D.; Root, R.; Rivera, N. The influence of sulfur and iron on dissolved arsenic concentrations in the shallow subsurface under changing redox conditions. *Proceedings of the National Academy of Sciences of the United States of America* **2004**, 101, (38), 13703-13708.
- O'Day, P. A.; Rivera, N.; Root, R.; Carroll, S. A. X-ray absorption spectroscopic study of Fe reference compounds for the analysis of natural sediments. *American Mineralogist* **2004**, 89, (4), 572-585.
- Ona-Nguema, G.; Morin, G.; Juillot, F.; Calas, G.; Brown, G. E. EXAFS analysis of Arsenite adsorption onto two-line ferrihydrite, hematite, goethite, and lepidocrocite. *Environ. Sci. Technol.* **2005**, 39, (23), 9147-9155.
- Ona-Nguema, G.; Morin, G.; Wang, Y.; Menguy, N.; Juillot, F.; Olivi, L.; Aquilanti, G.; Abdelmoula, M.; Ruby, C.; Bargar, J. R.; Guyot, F.; Calas, G.; and Brown Jr. G. E. Arsenite sequestration at the surface of nano-Fe(OH)₂, ferrous-carbonate hydroxide, and green-rust after bioreduction of arsenic-sorbed lepidocrocite by *Shewanella putrefaciens*. *Geochim. Cosmochim. Acta*, **2009**, 73 1359–1381.
- Osanna, A.; Jacobsen, C. In *Principal Component Analysis for Soft X-ray Spectromicroscopy, X-ray Microscopy* Melville, 2000; American Institute of Physics: Melville, **2000**; pp350-355.
- Pedersen, H.; Postma, D.; and Jakobsen, R. Release of arsenic associated with the reduction and transformation of iron oxides. *Geochim. Cosmochim. Acta*, **2006**, 70 4116–4129.
- Pierce, M. L.; Moore, C. B. Adsorption of arsenite and arsenate on amorphous iron hydroxide. *Water Research* **1982**, 16, (7), 1247-1253.
- Pigna, M.; Krishnamurti, G.S.R.; and Violante, A. Kinetics of arsenate sorption-desorption from metal oxides: Effect of residence time, *Soil Sci. Soc. Am. J.* **2006**, 70:2017-2027.

- Polizzotto, M. L.; Harvey, C. F.; Sutton, S. R.; Fendorf, S. Processes conducive to the release and transport of arsenic into aquifers of Bangladesh. *P. Natl. Acad. Sci. U. S. A.* **2005**, 102, 18819–18823.
- Polizzotto, M. L.; Harvey, C. F.; Li, G.; Badruzzaman, B.; Ali, A.; Newville, M.; Sutton, S.; Fendorf, S. Solid-phases and desorption processes of arsenic within Bangladesh sediments. *Chemical Geology* **2006**, 228, (1:3), 97-111.
- Postma, D.; and Jakobsen, R. Redox Zonation: Equilibrium constraints on the Fe(III)/SO₄-reduction interface, *Geochim. Cosmochim. Acta*, **1996**, 60(17):3169-3175.
- Poulton, S. W. Sulfide oxidation and iron dissolution kinetics during the reaction of dissolved sulfide with ferrihydrite. *Chemical Geology* **2003**, 202, (1:2), 79-94.
- Poulton, S. W.; Krom, M. D.; Raiswell, R., A revised scheme for the reactivity of iron (oxyhydr)oxide minerals towards dissolved sulfide. *Geochim. Cosmochim. Acta*, **2004**, Vol. 68, No. 18, pp. 3703–3715.
- Raghav, M.; Sáez, A. E.; Ela, W.; P. Understanding abiotic ferrihydrite re-mineralization by ferrous ions. *International Journal of Environ. Sci. Technol.* **2014**. ISSN: 1735-1472.
- Randall, S. R.; Sherman, D.M.; Ragnarsdottir, K. V. *Geochim. Cosmochim. Acta*, **2001**, 65, 1015-1023.
- Renock, D.; Gallegos, T.; Utsunomiya, S.; Hayes, K.; Ewing, R. C.; Becker, U. Chemical and structural characterization of As immobilization by nanoparticles of mackinawite (FeS_m). *Chemical Geology* **2009**, 268, (1:2), 116-125.
- Rickard, D. Kinetics and mechanism of the sulphidation of goethite. *Am. J. Sci.* **1974** 274, 941–952.
- Rochette, E. A.; Bostick, B. C.; Li, G.; Fendorf, S. Kinetics of arsenate reduction by dissolved sulfide. *Environ. Sci. Technol.* **2000**, 34, 4714-4720.
- Roden, E.E.; Zachara, J.M. Microbial reduction of crystalline iron(III) oxides: Influence of oxide surface area and potential for cell growth. *Environ. Sci. Technol.* **1996**, 30(5), 1618-28.
- Roh, Y.; Zhang, C.L.; Vali, H.; Lauf, R.J.; Zhou, J.; Phelps, T.J. Biogeochemical and environmental factors in ferri-mineralization: Magnetite and siderite formation. *Clays and Clay Minerals*, **2003**, Vol. 51, No. 1, 83-95.
- Root, R. A.; Fathardoobadi, S.; Alday, F.; Ela, W.; and Chorover, J. Microscale speciation of arsenic and iron in ferric-based sorbents subjected to simulated landfill conditions. *Environ. Sci. Technol.* **2013**, 47 (22), pp 12992–13000.

- Root, R. A.; Dixit, S.; Campbell, K. M.; Jew, A. D.; Hering, J. G.; O'Day, P. A. Arsenic sequestration by sorption processes in high-iron sediments. *Geochim.Cosmochim.Acta*,**2007**,*71*, (23), 5782-5803.
- Root, R. A.; Vlassopoulos, D.; Rivera, N. A.; Rafferty, M. T.; Andrews, C.; O'Day, P. A. Speciation and natural attenuation of arsenic and iron in a tidally influenced shallow aquifer. *Geochim.Cosmochim.Acta*,**2009**,*73*, (19), 5528-5553.
- Rosado, R.; del Campillo¹, M.C.; Martinez, M. A.; Barron, V.; Torrent, J.Long-term effectiveness of vivianite in reducing iron chlorosis in olive trees. *Plant and Soil*.**2001**, 241: 139–144, 2002.
- Royer, R. A.; Burgos, W, D.; Fisher, A. S.; Unz, R. F.; and Dempsey, D. Enhancement of biological reduction of hematite by electron shuttling and fe(II) complexation. *Environ. Sci.Technol*.**2002**, 36, 1939-1946.
- Saalfeld, S. L.; Bostick, B. C. Changes in iron, sulfur, and arsenic speciation associated with bacterial sulfate reduction in ferrihydrite-rich systems. *Environ.Sci. Technol*.**2009**,*43*, (23), 8787-8793.
- Sadiq, M. Arsenic chemistry in marine environments: a comparison between theoretical and field observations. *Marine Chemistry* **1990**, *31*, (1:3), 285-297.
- Schwertmann, U.; Cornell, R. M. Ferrihydrite. In *Iron Oxides in the Laboratory*, Wiley-VCH Verlag GmbH: **2007**; pp 103-112.
- Scott, D. T.; McKnight, D. M.; Blunt-Harris, E. L.; Kolesar, S. E.; and lovely, D. R. Quinone moieties act as electron acceptor in the humic substances by humics-reducing microorganisms.*Environ. Sci.Technol*.**1998**, 32, 2984-2989.
- Silva, J.; Vargas de Mello, J. W.; Gasparon, M.; and Pereira Abrahão, W. A. Effects of competing anions and iron bioreduction on arsenic desorption.*Water Air Soil Pollut*, **2012**, 223:5707–5717.
- Singer, P.C.; and Stumm, W. The solubility of ferrous iron in carbonate-bearing waters.*J. Amer. Water Works Assoc.* **1970**, 62,198-202.
- Smedley, P.L.; Kinniburgh, D.G.A review of the source, behavior and distribution of arsenic in natural waters.*Appl. Geochem.* **2002**, 17 (5), 517-568.
- Smith, E.; Naidu, R.; Alston, A. M. Arsenic in the soil environment: A review. *AdvAgron***1998**, 64, 149–195.
- Smith, A. H.; Lingas, E. O.; Rahman, M. Contamination of drinking-water by arsenic in Bangladesh: a public health emergency. *Bulletin of the World Health Organization* **2000**,*78*, (9), 1093-1103.

- Stumm, W.; Morgan, J. J. Aquatic chemistry: *Chemical Equilibria and Rates in Natural Waters*, 3rd ed.; John Wiley and Sons, Inc.: New York, **1996**.
- Sturm, A.; Crowe, S.A.; Fowle, D.A. Trace lead impacts biomineralization pathways during bacterial iron reduction. *Chemical Geology* **2008**, 249 282–293.
- Suess, E.; Scheinost, A. C.; Bostick, B. C.; Merkel, B. J.; Wallischlaeger, D.; Planer-Friedrich, B. Discrimination of thioarsenites and thioarsenates by x-ray absorption spectroscopy. *Analytical Chemistry* **2009**, 81, (20), 8318-8326.
- Su, C. M.; Wilkin R. T. Arsenate and arsenite sorption on and arsenite oxidation by iron(II,III) hydroxycarbonate green rust. *Advances in Arsenic Research*, 2005, vol. 915 (eds. P. A.O'Day, D. Vlassopoulos, X. Meng and L. G. Benning). Oxford University Press, pp. 25–40.
- Tadanier, C.J.; Schreiber, M.E.; Roller, J.W. *Environ. Sci. Technol.* **2005**, 39 (9), 3061-3068.
- Thinnappan, V.; Merrifield, C. M.; Islam, F. S.; Polya, D. A.; Wincott, P.; Wogelius, R. A. A combined experimental study of vivianite and As (V) reactivity in the pH range 2–11. *Appl. Geochem.* **2008**, 23, 3187-3204.
- Thoral, S.; Rose, J.; Garnier, J. M.; Van Geen, A.; Refait, P.; Traverse, A.; Fonda, E.; Nahon, D.; Bottero, J. Y. XAS study of iron and arsenic speciation during Fe(II) oxidation in the presence of As(III). *Environ. Sci. Technol.* **2005**, 39, 9478-9485.
- Trueper, H. G.; Schlegel, H. G.; and Van Leeuwenhoek, A. 30:225-238 NEN **1964**, 3235.8.3.
- Tufano, K.; Fendorf, S.T. Confounding impacts of iron reduction on arsenic retention. *Environ. Sci. Technol.* **2008**, 42(13), 4777-4783.
- Tufano, K. J.; Reyes, C.; Saltikov, C. W.; Fendorf, S. Reductive processes controlling arsenic retention: Revealing the relative importance of iron and arsenic reduction. *Environ. Sci. Technol.* **2008**, 42(22), 8283-8289.
- Turpeinen, R.; Pääntas-Kallio, M.; and Kairesalo, T. Role of microbes in controlling the speciation of arsenic and production of arsines in contaminated soils. *The Science of the Total Environment*, **2002**, 285 133_145.
- Upadhyaya, G.; Jackson, J.; Clancy, T. M.; Hyun, S. P.; Brown, J.; Hayes, K. F.; Raskin, L. Simultaneous removal of nitrate and arsenic from drinking water sources utilizing a fixed-bed bioreactor system. *Water Research* **2010**, 44, (17), 4958-4969.
- U.S. Environmental Protection Agency (US EPA). Regulations on the disposal of arsenic residuals from drinking water treatment plants. **2000**, 600/R-00/025.

- U.S. Environmental Protection Agency (US EPA). Fact Sheet: Drinking water standard for arsenic. **2001**, 815-F-00-015.
- U.S. Environmental Protection Agency (US EPA). Arsenic treatment technology. Evaluation handbook for small systems. **2003**, 816-R-03-014.
- US EPA *Health effects from exposure to high levels of sulfate in drinking water study*. EPA 815-R-99-001; US Environmental Protection Agency, Office of Water: Washington, DC, **1999**.
- USEPA, National Primary Drinking Water Regulations; Arsenic and clarifications to compliance and new source contaminants monitoring; Final Rule. In *66 (14), Federal Register*, **2001**; pp 6976-7066.
- Vance, D.B.; Iron: The Environmental impact of a universal element. *Environmental Technology*, **2003**.
- van Geen, A.; Rose, J.; Thorai, S.; Garnier, J. M.; Zheng, Y.; Bottero, J. Y. Decoupling of As and Fe release to Bangladesh groundwater under reducing conditions. Part II: Evidence from sediment incubations. *Geochim. Cosmochim. Acta*, **2004**, 68(17), 3475-3486.
- Veselska, V.; Majzlan, J.; Hiller, E.; Petkova, K.; Jurkovic, L.; Durza, O.; and Volekova-Lalinska, B. Geochemical characterization of arsenic-rich coal-combustion ashes buried under agricultural soils and the release of arsenic. *Applied Geochemistry*, **2013**, 33, 153-164.
- Waychunas, G. A.; Rea, B. A.; Fuller, C. C.; Davis, J. A. Surface chemistry of ferrihydrite: Part 1. EXAFS studies of the geometry of coprecipitated and adsorbed arsenate. *Geochim. Cosmochim. Acta*, **1993**, 57, (10), 2251-2269.
- Wiesli, R. A.; Beard, B. L.; Johnson, C.M. Experimental determination of Fe isotope fractionation between aqueous Fe(II), siderite and green rust in abiotic systems. *Chem. Geol.* **2004**, 211, 343-362.
- Wilkin, R. T.; Ford, R. G.; Arsenic solid-phase partitioning in reducing sediments of a contaminated wetland. *Chemical Geology* **2006**, 228, (1:3), 156-174.
- Wilkin, R. T.; Wallschläger, D.; Ford, R. G. Speciation of arsenic in sulfidic waters. *Geochem. Trans.*, **2003**, 4(1), 1-7.
- Wolthers, M.; Charlet, L.; Van der Weijden, C. H. Arsenic sorption onto disordered mackinawite as a control on the mobility of arsenic in the ambient sulphidic environment. *Journal De Physique* **2003**, (107), 1377-1380.
- Wolthers, M.; Charlet, L.; Van der Weijden, C. H.; Van der Linde, P. R.; Rickard, D. Arsenic mobility in the ambient sulfidic environment: Sorption of arsenic(V) and

- arsenic(III) onto disordered mackinawite. *Geochim.Cosmochim.Acta*,**2005**,*69*, (14), 3483-3492.
- Yan, S.; Hua, B.; Bao, Z.; Yang, J.; Liu, C.; and Deng, B. Uranium(VI) removal by nanoscale zerovalent iron in anoxic batch systems.*Environ. Sci. Technol.* **2010**, *44*, 7783–7789.
- Xinjun, A.;Xueping, C.; Jing, Y.; Zhaosu, W.; Guoxin, S. Effect of microbial mediated iron plaque reduction on arsenic mobility in paddy soil. *Environ. Sci. Technol.***2009**,*21*1562–156.
- Zachara, J.M.; Kukkadapu, R.K.; Fredrickson, J.K.; Gorby, Y.A.; and Smith, S. C. Biomineralization of poorly crystalline Fe(III) oxides by dissimilatory metal reducing bacteria (DMRB). *Geomicrobiology Journal*, **2002**, *19*:2, 179 – 207.
- Zayed, G.; Winter, J. Inhibition of methane production from whey by heavy metals - protective effect of sulfide. *Applied Microbiology and Biotechnology*, **2000**, *53*(6), 726-731.
- Zobrist, J.; Dowdle, P.R.; Davis, J.A.; Oremland, R.S. Mobilization of arsenite by dissimilatory reduction of adsorbed arsenate, *Environ. Sci. Technol.* **2000**, *34*, 4747-4753.